



THE UNIVERSITY *of* EDINBURGH  
School of GeoSciences

# Confirmation Report

Investigating geothermal heat resources of legacy mine workings, why  
are some mine waters hotter than others?

**Mylene Receveur**

Christopher McDermott, Stuart Gilfillan, Andrew Fraser-Harris, Ian Watson



PhD in Geology

School of Geosciences  
University of Edinburgh, Scotland  
May 27, 2020

# Abstract

This confirmation report has been realized as part of the confirmation process for the PhD in Geology at the university of Edinburgh, taking place with the 6-9th month from the start of the PhD. This PhD consists in investigating the geothermal heat resources of legacy mine workings in the UK and understand why waters from different mines have different temperatures.

Abandoned flooded coal mines in the UK represent low-temperature geothermal reservoirs that can potentially be used for heat storage or production (Adams and Younger, 2001). The presence of mining voids inherited from the extraction of coal seams in e.g. the Carboniferous layers of the Midland Valley of Scotland, has led to the formation of high-permeability reservoirs in which large volume of water are stored. Hot mine water therefore constitutes a low carbon heat source from which heat can be extracted using open-loop ground source heat pump systems.

However, a little is known about the heat potential, the heat sources and the recharge mechanisms in mine systems (Coal Authority, Pers. Com., 2019). Temperature measurements in several shafts in the UK have shown the lack of correlation between the depth of the measurement and the temperature of the mine water (Gillespie et al., 2013). In addition to the regional geothermal gradient, it is suggested that other factors might contribute to defining the mine water temperature. The complexity of the interconnections between mine workings represents one of the most challenging barriers in understanding mines hydro-geology.

The conducted PhD research will therefore aim to understand the temperature distribution in the mines by identifying the main factors controlling heat recharge. A key outcome of this work will be the development of a predictive tool, model or conceptual approach that enables the scientific estimation of the extent and nature of the heat available over the long term in abandoned flooded coal mines.

# Executive summary

This report consist of a review of the literature and of the initial results for each of the three chapters that will structure the PhD research work entitled "Investigating geothermal heat resources of legacy mine workings - why are some mine waters hotter than other?". It also contains the data management plan, a GANTT chart, the supervisory arrangements and a summary of the resources available for the organisation of the PhD.

The PhD work will be organized in three main research axis defining three different chapters, whose research questions have been defined as followed:

## **Chapter 1: What are the key heat recharge mechanisms and heat sources controlling the water temperature in flooded coal mines?**

- What are the main heat sources in coal mines?
- What is the relative contribution of heat diffusion and advection during production (i.e. heat/water extraction) and recovery?
- Can thermal steady state (energy balance between heat extracted and heat recharge) be reached, and what is the footprint area of the heat extracted for a typical single house energy consumption?

The suggested hypothesis to answer those questions are:

- H0 – Pyrite oxidation only slightly contribute to heat renewal in mines
- H1 – During production, heat is mainly sourced from advective mine-water in tunnels and horizontal conduction in goaf, with limited depletion from surrounding rock (i.e. vertical conductive heat flux).
- H2 – During recharge, vertical heat flux are dominant, but solar recharge is negligible relative to the geothermal heat flux. Groundwater advection and deep warm water upflow enhance heat recovery rate.
- H3 – Thermal balance can be reached for low extraction rate, and the footprint area is mainly dependent on the thermal conductivity of the host rock and/or on the hydraulic gradient.

## **Chapter 2: What is the impact of past mining activities on the thermal state in mines?**

- Does the temperature gradient in mines re-equilibrate with the undisturbed regional gradient after periods of mining with ventilation/dewatering and a subsequent period of flooding?
- How does water advection in large voids impact the temperature distribution in mines?
  - Are the mine waters at equilibrium with the host rock temperature?
  - What is the rate of heat exchange between the recharge mine-water and the surrounding host rock in mined areas and in tunnels, depending on the origin/temperature of recharge water, on its flow rate, on the flow path length and on the properties of the host rock.

- Can we reproduce temperature profiles in shafts during flooding, heat/water recovery and during production, using numerical modelling?

The research questions for chapter 2 will be validated or refuted by verifying the following hypothesis:

- H0 - The geothermal gradient in the flooded mine reaches a state of "partial equilibrium" within 20 years after flooding is completed.
- H1 – The temperature gradient in mines follow the regional trend, with a dominant conductive heat profile in the host rock and isothermal conditions in tunnels/shafts.
- H2 - The temperature of mine water is in equilibrium with the rock temperature in goaf materials, but mainly depends on the source/depth of water recharge and on the residence time of water in tunnels.
- H3 – It is possible to simulate both recovery rate and temperature profiles in shaft during flooding, heat recovery and production to fit existing data when appropriate boundary conditions are set.

### **Chapter 3: What are the key mine features allowing to assess the sustainable heat potential of coal mines at the scale of a mine?**

- Can 3D processes (i.e. overall heat capacity/change in heat storage) can faithfully be scaled up in 2D?
  - What is the effect of lateral connectivity of roadways on the extent of the heat sink and on the heat exhaustion/recharge rate?
  - How does the density and/or absolute volume of mining void contribute to define the total energy content of the mine?
- Can homogeneous hydraulic and thermal properties accounting for both galleries and induced fractures be attributed to all mined areas?
  - Does the geometry of the voids resulting from different mining approaches (i.e. pillar-and-stall, longwall mining) impact the heat exchange rate between the host rock and the mine-water and the recharge rate at the scale of the mine?
  - How does the relative permeability contrasts between roadway/tunnels, the mined area and unaffected host rock contribute to the rate and overall change in energy content in the system?
- What is the effect of the distribution, density and inter-connectivity of the roadway network and the coal seams on the direction/amplitude of the induced heat fluxes during production/recovery, and on the temperature distribution within the mine?
  - Can we simulate the water recovery rate/temperature measured in shafts in the Midlothian coalfield ?
  - Can the extracted water temperature and the evolution of the temperature profiles within the shafts in Dawdon-Horden be reproduced?

The hypothesis suggested to answer the research questions for Chapter 3 are:

- H0 - The larger the areal extent of the mine, the greater the recharge rate (i.e. the faster thermal balance is reached).
- H1 - The total residual void volume (i.e. water content) can be used to derived a heat depletion rate factor.
- H2 - The geometry of the voids resulting from different mining approaches (i.e. pillar-and-stall, longwall mining) does not impact the heat exchange rate between the host rock and the mine-water and the recharge rate at the scale of the mine.
- H3 - The relative permeability contrasts between roadway/tunnels, the mined area and unaffected host rock is a key feature to assess the overall change in energy content in the system and the rate of energy transfer.
- H4 - An "equivalent porosity" and "equivalent heat capacity" parameter can be defined to scale up 3D processes in 2D models.
- H5 - The number/geometry of interconnections between tunnels and the model boundary conditions highly affect the temperature distribution and long term production temperature.

For each of these three chapter, we aim at publishing one scientific paper on selected ideas, findings or modeling approach. While a topic for the first paper (Chapter 1) has to date already been discussed with the supervisory team, the problematic for the papers from Chapter 2 and Chapter 3 still need to be defined.

# Contents

	<b>Page</b>
<b>1 Context</b>	<b>7</b>
1.1 Background . . . . .	7
1.2 Abandonned mines geothermal resources . . . . .	7
1.3 Knowledge gap and research area . . . . .	8
<b>2 Research design</b>	<b>10</b>
2.1 Research questions . . . . .	10
2.2 Research objectives . . . . .	10
2.3 Method . . . . .	11
2.4 Modeling code . . . . .	11
2.5 Data . . . . .	12
<b>3 Case study</b>	<b>19</b>
3.1 Midlothian Coalfield . . . . .	20
3.2 Dawdon-Horden Mining Block . . . . .	26
<b>4 Conceptual models of mines</b>	<b>27</b>
4.1 Hydrology of mine aquifers . . . . .	27
4.2 Thermal system . . . . .	28
<b>5 Chapter 1 : Heat extraction Model</b>	<b>35</b>
5.1 Background . . . . .	35
5.2 Research Gaps . . . . .	38
5.3 Aims and methods . . . . .	39
5.4 Research questions . . . . .	39
5.5 Hypothesis . . . . .	39
5.6 Preliminary results . . . . .	40
5.7 Conclusion and research outputs . . . . .	52
<b>6 Chapter 2: Thermal state of the mine</b>	<b>53</b>
6.1 Background . . . . .	53
6.2 Research Gaps . . . . .	54
6.3 Aims and methods . . . . .	54
6.4 Research questions . . . . .	54
6.5 Hypothesis . . . . .	55

6.6 Preliminary results . . . . .	55
6.7 Results and research outputs . . . . .	57
<b>7 Chapter 3: Recharge potential of the Midlothian and Dawdon-Horden coalfields: an investigation of the key features for thermal modeling of flooded coal mines</b>	<b>61</b>
7.1 Background . . . . .	61
7.2 Research Gaps . . . . .	64
7.3 Aims and methods . . . . .	64
7.4 Research questions . . . . .	65
7.5 Hypothesis . . . . .	65
7.6 Preliminary results . . . . .	66
7.7 Conclusion and research outputs . . . . .	67
<b>8 Data management plan</b>	<b>68</b>
8.1 Data repositories . . . . .	68
8.2 Version control management plan . . . . .	68
<b>9 Time plan</b>	<b>69</b>
<b>10 Supervisory arrangements</b>	<b>71</b>
<b>11 Resources and Training</b>	<b>72</b>
11.1 Training need analysis . . . . .	72
11.2 Teaching experience . . . . .	72
11.3 Resources available . . . . .	72
11.4 Resources needed . . . . .	73
11.5 Conferences . . . . .	74
<b>12 Ethical and Health and safety considerations</b>	<b>75</b>
<b>13 Take home message</b>	<b>76</b>
<b>A Appendix</b>	<b>77</b>
A.1 Rock properties . . . . .	77
A.2 Radiogenic heat production . . . . .	77
A.3 Heat related equations . . . . .	77
A.4 Analytical solutions . . . . .	81
A.5 Figures Benchmarks Chapter 1 . . . . .	83
<b>References</b>	<b>102</b>

# 1 Context

## 1.1 Background

Heat demand for domestic and commercial space heating and hot water heating accounts for more than 1/3 of the energy consumption in the UK, and for more than 50% in Scotland. Most of the heat consumption is currently covered by natural gas, accounting for a large proportion of the Greenhouse Gas emissions in the country. Through the 2019 UK's Climate Change Act, both the UK Government and Scotland agreed to reach neutral carbon emissions by 2050 and 2045, respectively (Stark, 2019).

To achieve this goal, the decarbonization of residential heat became one of the main preoccupation of both governments. Scotland targets to replace all gas boilers by low-carbon heating systems in all new homes by 2025 (*Clean Growth - Transforming Heating* 2018). By 2032, the objective is to supply 35% of cool/heat for domestic heating and 70% for non-domestic heating, from low-carbon energy sources, against only 7.7% in 2017. Using mine-water as a heat energy source has therefore been of growing interest as it could partly contribute to this ambitious project (Banks et al., 2004). Todd et al., 2019 showed that about 7% of Scotland's heat requirement could indeed be sourced from abandoned flooded mine workings, lying just below populated areas.

## 1.2 Abandoned mines geothermal resources

Abandoned flooded mines constitute potential low-temperature geothermal reservoirs that can be used for energy storage and production (Adams and Younger, 2001). Coal has been mined in Scotland since the 12th century, but only emerged during the 16th Century and significantly increased in number during the 17th Century. In the early times of mining, coal was mostly extracted from shallow mines using the pillar-and-stall method. In the early 18th, the invention of the Newcomen steam engine enabled pumping water more efficiently, allowing the access to deeper part of the mines. This engine was first installed in the UK at Dudley Castle in Staffordshire in 1712. From the 1950's, longwall mining was the main method of extraction of coal in deep mines, and many areas initially mined by the room-and-pillar method were latterly reworked using this method (Atkinson, 1966). However, the commitment of the government to increase shares of oil and nuclear for electricity generation progressively led to a drop in the demand for coal. Hundreds of collieries closed between 1958 and 1959, and 23 additional mines closed following the 1984 miners' strike. Only 50 mines were still opened in 1992. The last underground coal mine, the Kellingley Colliery, closed in 2015.

After the closure of deep mines and the cessation of dewatering, water generally rebounds back to natural levels and fills the voids inherited from the mining activities (Younger and Adams, 1999). This interconnected network of open voids (i.e. mine workings, shafts and roadways) tends to form highly transmissive 'anthropogenic aquifers' (Adams and Younger, 2001) from which important volume of water can be stored and extracted (Banks et al., 1997). Besides, a compilation of mine water temperatures in the Midland Valley of Scotland showed that mine-waters are generally hotter than natural groundwater, which is generally around 10 to 12 °C in UK

(Gillespie et al., 2013). This can be explained by the existence of processes typically occurring in worked coal mines, such as pyrite oxidation, or heat advection through artificial large-scale transmissive pathway (Bailey et al., 2016).

Not only is mine-water heat attractive for its geothermal potential, but also for its proximity to the consumer and its broad accessibility (Watzlaf and Ackman, 2006). Indeed, most of the mines are located near densely populated area, giving the opportunity to provide local population (i.e. both single household or district heating) with a low-carbon energy source for space heating or cooling (Farr et al., 2016). Energy can be extracted from mine-water using open loop or closed loop Ground Source Heat Pump (GSHP) systems (Małolepszy, 2003). Such system have already been implemented worldwide, such as Heerlen in the Netherlands (Ferket et al., 2011) or Mieres in Spain (Andrés et al., 2017; Loredo et al., 2017). In the UK, the first systems were implemented in Shettleston and Lumphinnans in Scotland in 1999-2000, providing heat to 16 and 18 dwellings, respectively (Banks et al., 2009). The existence of infrastructures such as mine shafts moreover gives the opportunity to access mine-water while avoiding costs associated to the drilling of new boreholes, making of mine-water based heat systems cost-effective solutions relative to conventional GSHP systems (Ghoreishi-Madiseh et al., 2012). In addition, to mitigate the discharge of contaminated mine water to the surface environment, the Coal Authority has been responsible for the implementation of mine water treatment systems across the UK (Younger, 2004). About 3000 L/s of mine water are pumped from more than 50 abandoned coal mines, representing about 100 MW of potential low enthalpy heat energy (Banks et al., 2009). Where pumping schemes are already implemented to maintain mine-water level below ground surface, using it as a source of energy could therefore give the opportunity to decrease costs associated to the maintenance of treatment systems by selling heating or cooling services (Loredo et al., 2016).

In addition to their heat source capacities, mines could on the other hands be used for their energy storage potential. Industries, data centers or sport facilities are examples of buildings that have cooling demands that could be meet by reversing the heat pump system. Cyclical heating/cooling could indeed be performed by injecting excess heat from those buildings into the ground, and store it for future heating usage. Seasonal production has already been implemented worldwide (i.e. Heerlen' project) and has been proved to increase the overall efficiency and sustainability of mine-water based heat pump systems, by balancing heat recharge and discharge (Banks, 2008).

### 1.3 Knowledge gap and research area

The geothermal potential of flooded mines depends both on the temperature of the mine-water and the rate at which that water can be extracted without significantly depleting the resource (Watzlaf and Ackman, 2006). Previous publications about geothermal resources assessment in abandoned coal mines have used either numerical or analytical models to estimate the sustainability of heat extraction from flooded mine workings. Despite the existence of diverse worldwide studies, no standard procedure has emerged yet in mine modeling (Renz et al., 2009). This can mostly be attributed to the important complexity and the potential highly case-specific hydraulic character of such system. In addition, it appears that there is no clear understanding of the main heat sources and key heat transfer mechanisms in mines, and of their contribution on the heat recharge rate. Most of the past studies indeed only considered the local geothermal gradient as the main contributor to the thermal state of the

mines, but only a few of them investigated the impact of previous mining activities on the geothermal gradient.

To promote the development of heat extraction schemes, the Coal Authority however wish to get a better understanding of the geothermal resources in mines, including their storage capacity and the sustainability of heat extraction. Knowing the lateral extent of the area affected by heat extraction around a production well and the recovery rate (i.e. time for a mine system to recover its initial temperature when production stops) is also of primary interest as it could support the development of a methodology to guide the licensing of heat (Ian Watson, Coal Authority, Pers. Com. 2019).

The present study therefore aims at getting a better understanding of the contribution from different heat sources on the heat recharge rate in mines and key heat transfer processes controlling the mine water temperatures. We will investigate the amplitude/direction of the heat fluxes induced by heat extraction from the mine and during recovery, but also the temperature distribution resulting from its complex production and flooding history. All those elements are critical to assess realistically the heat resource in mines, their renewability, the long-term energy balances, and thus the sustainability of heat extraction from mine. This project finally aims at developing a reproducible strategy for mine modeling while simplifying their geometrical and hydraulic complexity, in order to create a tool able to guide the licensing of heat.

## 2 Research design

### 2.1 Research questions

The topic of this PhD can be defined as the "conceptualization of mine water temperatures", aiming at answering the general question: "why do different mines have different temperatures?". The aim of the research project is to get a better understanding of the key factors controlling the mine-water temperature as well as the temperature distribution in flooded abandoned mines, with a focus on UK coal mines.

To achieve this goal, the project has been divided in three main objectives that will be used to answer the following key research questions:

- What are the key heat recharge mechanisms and heat sources controlling the water temperature in flooded coal mines?
- What is the impact of past mining activities on the thermal state and temperature distribution in mines?
- What are the key mine features allowing to assess the sustainable heat potential of coal mines at the scale of a mine?

### 2.2 Research objectives

To answer those questions, the first objective is to create hydrological/thermal conceptual model(s) of flooded coal mines to identify the main controls on mines temperatures. We also want to develop a numerical approaches able to discriminate between the contribution from different types of heat fluxes induced by heat extraction and heat/water recovery.

The second objective is to determine the thermal state of a mine after a period of mining and flooding. The aim is to assess the initial temperature distribution within a mine to evaluate its original heat potential.

The third objective is to assess the key features in mine plans having significant impact on the heat depletion and rate of energy recharge at the scale of a mine or network of interconnected mines. An approach to create representative but simplified model of mine workings will be developed in order to assess the potential of mines, in terms of energy storage/heat capacity. This analysis will be based on a comparative study between mines of different structures in two different coalfields: the Midlothian Coalfield in Scotland and the Horden-Dawdon Coalfield in NE England. Based on the knowledge acquired from previous research axis, this will be used to define the extent of the area impacted by heat extraction around the production well, depending on the mine structure.

Ultimately, the goal of the PhD will be to develop an analytical or numerical tool able to predict the long-term temperature change of the mine-water extracted for geothermal utilization.

## 2.3 Method

The research project will be divided in two part. The first part will be focused on developing modelling approaches, studying general processes and perform sensitivity analysis using simple conceptual representations of mine workings. In a second phase, we will implement and verify the findings and hypothesis based on available data from two study areas.

First, hydrogeological conceptual model(s) will be created considering different heat sources (i.e. natural heat flow, solar/surface heat, radiogenic heat production, pyrite oxidation, groundwater inflow from depth) and heat transfer mechanisms (i.e. heat convection / diffusion) depending on the geological context (i.e. horizontal layers, dipping layers, syncline). Numerical models will subsequently be used to assess the relative contribution of those heat sources on the heat recharge rates in mines (i.e. sensitivity analysis) and calculate energy balances. Of particular interest will be to identify the nature of the fluxes induced by water and/or heat extraction from flooded mine workings and their evolution throughout a production and recovery period. This will be done using 1D models of heat extraction and 2D models representing mines of simple geometries with different thermal/hydraulic boundary conditions and heat source/sinks. Results will be validated against analytical solutions.

Then, special attention will be paid to the perturbations caused by mining activities on the geothermal gradient, through long-term simulations of water extraction and recovery. A series of 2D finite-element models of mine workings with different geometries, boundary conditions and/or material properties will be developed to assess the impact of long-term water extraction and rebound on the resulting thermal state of a mine and expected heat recovery time (i.e. return to initial undisturbed temperature equilibrium). Results will be calibrated and validated using existing temperature profiles and recovery data.

Findings related both to the main heat sources/recharge mechanisms and key geometrical features will finally be applied to the selected case studies. A method will be developed to extract important geometrical features from the mine plans and create representative and computationally cost-effective mesh. After verifying the applicability of 2D models to simulate 3D mechanisms, an optimal mine modeling strategy will be developed using available geometrical/monitoring data in each area. A comprehensive comparative study between those two mining areas will be performed based on numerical simulations of flooding, heat extraction and heat recovery. Results will be used to estimate the area impacted by the extraction of heat, the time necessary for recovery, but also to assess their overall heat capacity. Based on the local energy demand, those elements will be used to predict the changes in the production temperature with time and evaluate the long-term sustainable heat recovery/storage potential of the mine reservoir.

## 2.4 Modeling code

Previous researches on the geothermal potential of flooded coal mines used modeling approach to predict both the absolute thermal capacity of mines and the temperature changes of the extracted fluid over time (Renz et al., 2009). Different methods have been used in the literature to solve for heat transfers and fluid flow equations in mine systems, going from analytical models (Rodríguez and Díaz, 2009) to 1D/2D/3D numerical models (Loredo et al., 2016), or using a combination of both (Renz et al., 2009; Ferket et al., 2011).

Analytical models solve for the exact mathematical solutions of flow and heat transport by considering ho-

mogeneous systems, and therefore require geometrical simplifications (Banks et al., 2009; Loredo et al., 2017). They have been described as a useful tool at an early stage of a feasibility study to get a first insight into heat transfers and the sustainability of heat abstraction from geothermal systems. Numerical codes used to model heat and flow transport processes in mines include Finite Difference simulators (FDM) such as SHEMAT (Ferket et al., 2011), Finite Element modeling software (FEM) such as TOUGH2 (Małolepszy, 2003; Guo et al., 2017), FEFLOW (Renz et al., 2009; Diersch et al., 2010; Andrés et al., 2017), HydroGeosphere (Raymond and Therrien, 2008), or Finite Volume algorithm (FVM), such as MARTHE, FLUENT (Hamm and Bazargan Sabet, 2010), THEMUT (Ghoreishi-Madiseh et al., 2012) or OpenFOAM (Bao and Liu, 2019). Numerical models allow creating more realistic representations of mining scenarios but require more data and computational time. In addition, such complex model might be subjected to numerical instabilities, limiting their reliability (Renz et al., 2009). Numerical approaches are developed in more details in Chapter 6. Here we use OpenGeoSys, an open-source FEM modeling code which was developed to solve for coupled thermo-hydro-geomechanical-chemical (THMC) processes in porous and fractured media (Kolditz et al., 2012).

## 2.5 Data

Available data from diverse sources will be used to build and verify both conceptual and numerical models of mines. The data includes information from in situ sensors acquired by the Coal Authority, legacy data available in various archives (i.e. historical temperature data from Burley et al., 1984, pumping data from former private Coal Mining Companies), geological data from the British Geological Survey (BGS) database... The Glasgow Geothermal Energy Research Field Site and related published papers moreover constitute since 2018 an additional source of data (i.e. stratigraphy, rock properties, pumping tests results, temperature profiles), specifically acquired to improve the understanding of the geothermal potential of abandoned flooded mine workings below Glasgow. An inventory of the data available from the Coal authority has been made in January 2020 and is subjected to the academic license. Those data include:

- Monitoring data, including manual logging, continuous logging from temperature and water logger, punctual surveys, pumping tests... Depending on the nature of the site (i.e. naturally gravity-driven discharge area, pumped shaft/borehole, pumped discharge), different data set can be available.
  - Time series of pumping rate/discharge rate and/or groundwater levels (i.e. flooding rate) in shafts
  - Time series of temperature change in the shafts (at the logger depth)
  - Temperature and conductivity profiles with location of the seams intersected by the shafts
- GIS data
  - Mine data: shaft, workings (deep, shallow and probable workings), roadway, mining blocks, seam levels, outcrop location, geological disturbances... Plans for under-sea mines of the Dawdon-Horden area have not been digitalised, therefore no GIS shapefiles are available for under-sea workings.
  - Monitoring sites, discharge site, temperature sites
  - Water data: Contour of minewater block, rivers

- Mine abandonment Plans. Mine plans are more detailed than GIS shapefiles and can be used to identify the exact location of mine features (i.e. depth, interconnections between the mine workings, roadways and shafts). In the UK, the record of mine abandonment only started with the Mines Inspection and Regulation Act 1870, while the acquisition of accurate mine plans only became mandatory in 1872 (Brown et al., 2002). Even though, data often showed only the extent of the workings, but not their depth or any geological information. The acquisition of reliable data and maps only started with the nationalization of the coal industry in 1947, hence most of shallow early workings are unknown and unmapped (Henton, 1974). Moreover, mine plans do generally not inform on the current state of the mines and some information such as areas of extensive collapse are generally not known (Sgambat et al., 1980).

Tables 2.1 and 2.2 summarizes the data available for the two study areas, described in the following chapter, that will be used for the calibration and validation of the models.

Name	Location type	Data Type	Hydro		Thermal	
			Calibration	Validation	Calibration	Validation
Bilston Glen	shaft	T-EC profile			2012 profiles	2016 and 2019 profiles
Bilston Glen	monitoring point	Water level, temperature TS	2000 - 2018	2019 -2023	-	-
Easthouse	shaft	T-EC profile			2016 profile	2019 profile
Easthouse	monitoring point	Water level, temperature TS	2013 - 2018	2019 -2023	2016 - 2018	2019 -2023
Junckie's discharge	monitoring point	Flow, temperature TS	2015 - 2018	2019 -2023	2016 - 2019	2020-2023
Elginhaugh discharge	monitoring point	Flow	(1996 - 2011)	-	-	-
Elginhaugh discharge	monitoring point	On-site temperature	-	-	-	-

Figure 2.1: Data available for model calibration and validation in the Midlothian Coalfield (Bilston Glen and Easthouses mines)

Name	Location type	Data Type	Hydro		Thermal	
			Calibration	Validation	Calibration	Validation
Hawthorn	shaft	T-EC profile			2000, 2003 profiles	2005, 2006, 2008 profiles
Hawthorn	monitoring point	Water level, temperature TS	2016-2018	2019 -2023	2016-2018	?
Dawdon	shaft	T-EC profile			2000, 2003, 2004 profiles	2005, 2006, 2008 profiles
Dawdon	monitoring point	Water level, temperature TS	2016 - 2018	2019 -2023	2016 - 2018	2019 -2023
Easington	shaft	T-EC profile			2000 profile	2005, 2006, 2008 profiles
Easington	monitoring point	Water level, temperature TS	2016-2018	2019 -2023	2016-2018	2019 -2023
Horden	shaft	T-EC profile			2003, 2004 profiles	2005, 2006, 2008 profiles
Horden	monitoring point	Water level, temperature TS	2016-2018	2019 -2023	2016-2018	2019 -2023

Figure 2.2: Data available for model calibration and validation in the Dawdon-Horden Coalfields

Figures 2.3 to 2.6 and Figures 2.7 to 2.8 are maps showing the available data for the Midlothian Coalfield and Dawdon-Horden mining blocks, respectively.

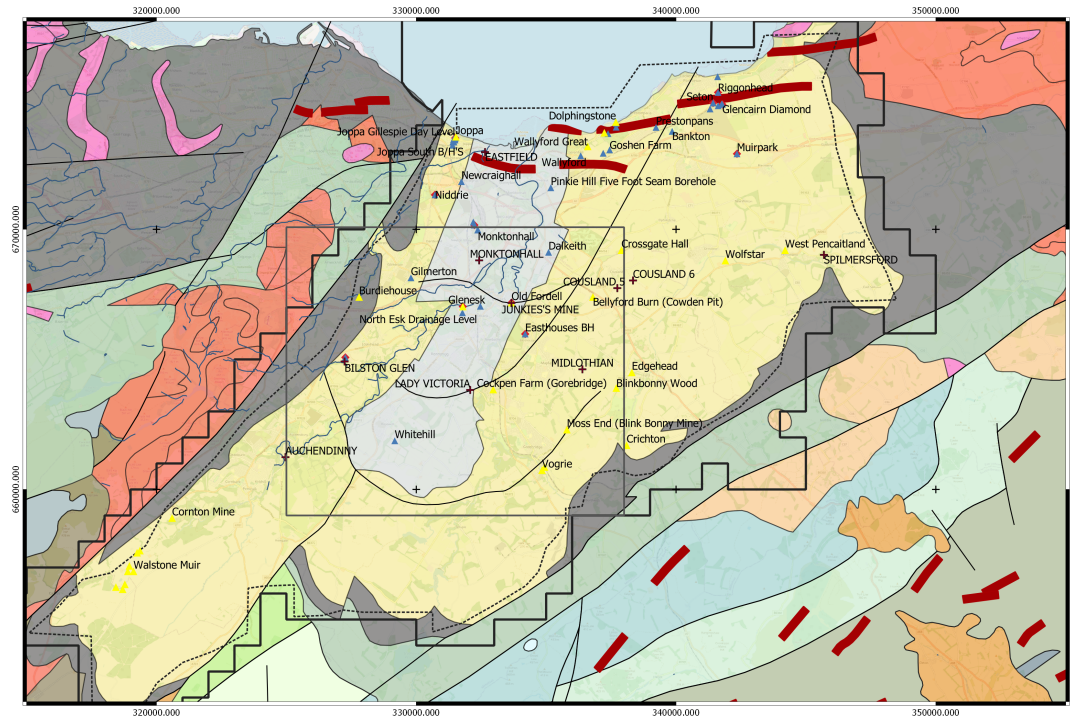


Figure 2.3: Geological map of the Midlothian Coalfield

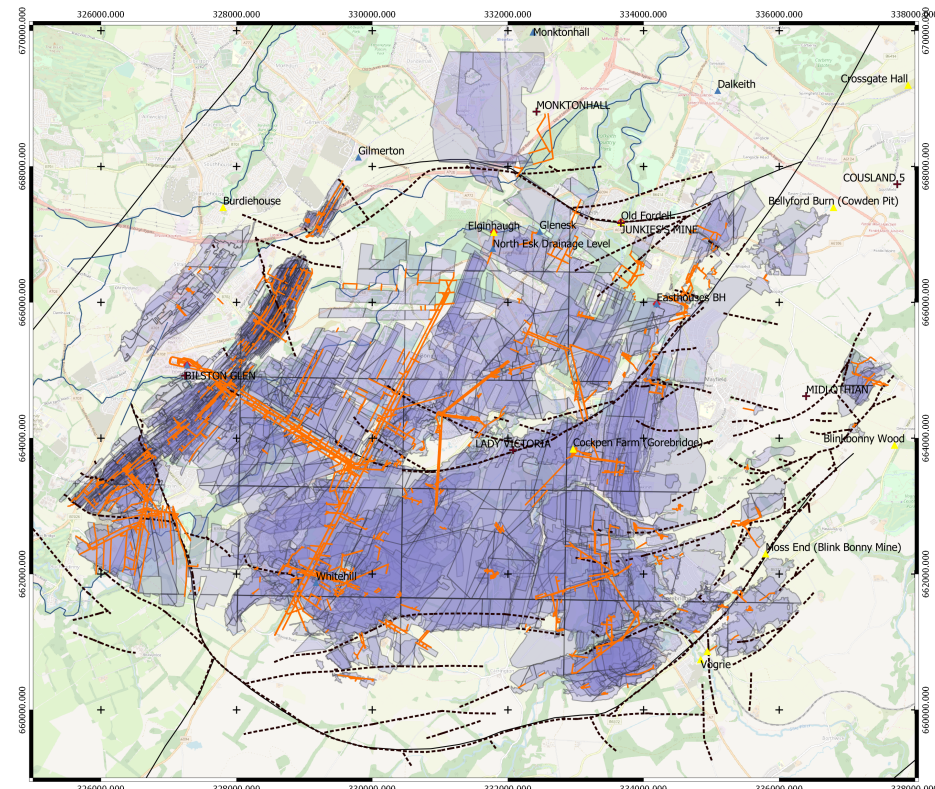


Figure 2.4: Underground mine workings and roadways in the Midlothian Coalfield

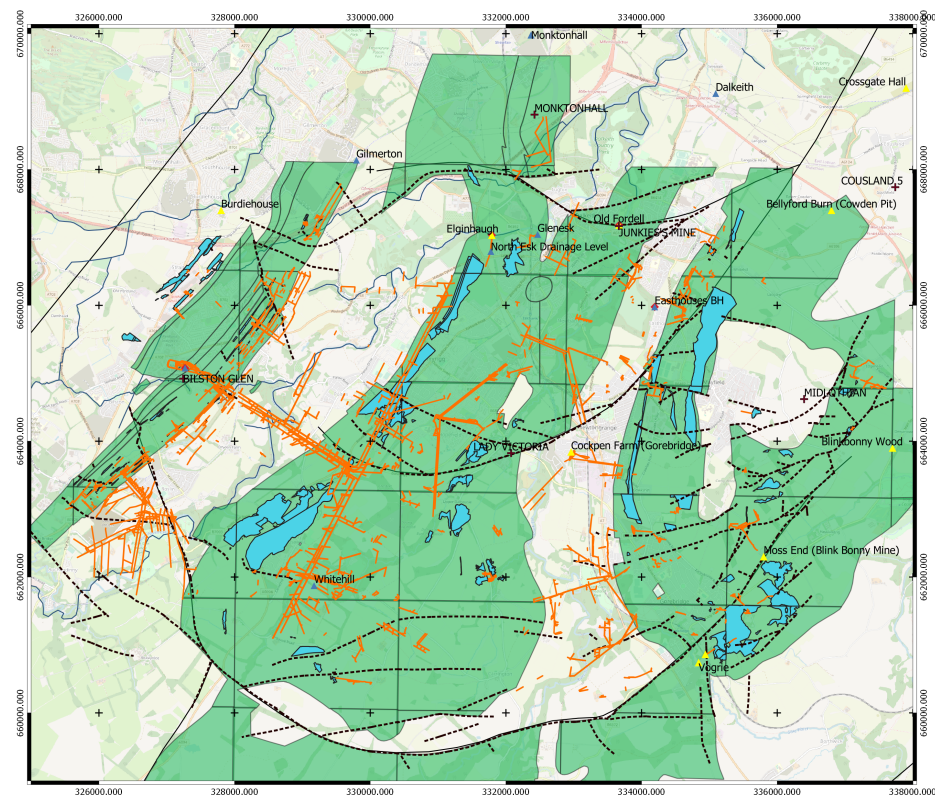
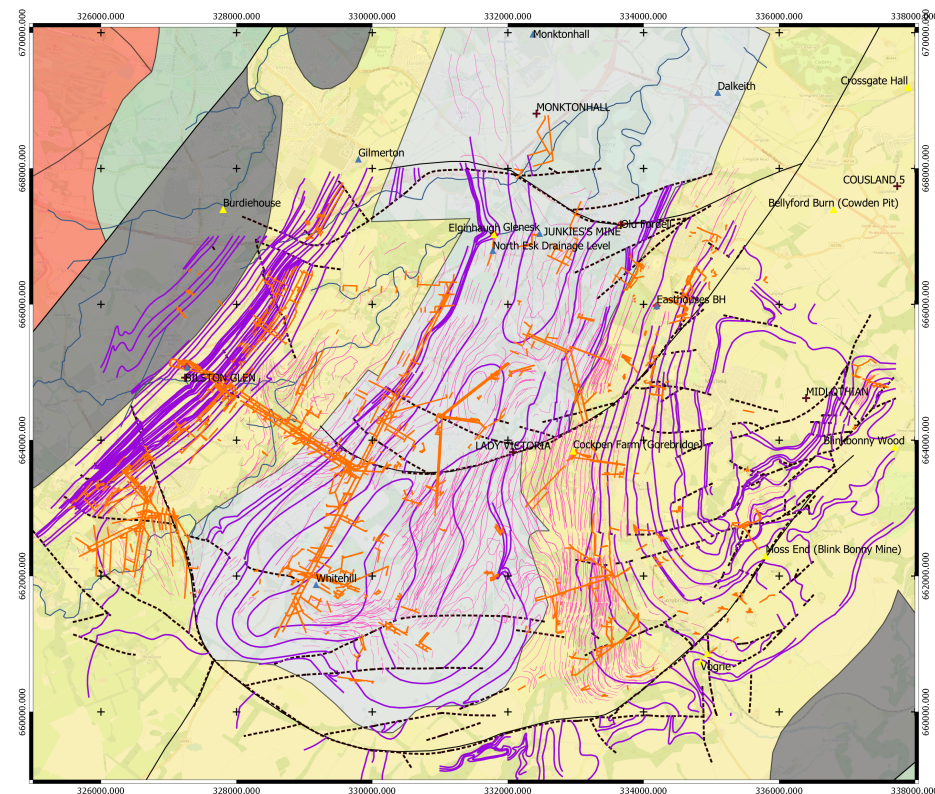


Figure 2.5: Probable and shallow mine workings in the Midlothian Coalfield



### Legend

Sites	Faults
+	Boreholes
▲	Discharges
△	Monitoring site
◆	Temperature sites
Mine Data	
Orange line	Spine Roadway
Purple line	Outcrops
Pink line	In Seam Level Contours
Dashed line	Geological Disturbances
Blue line	Shallow Working
Green line	Probable Working
Light blue line	Underground Working
Blue line	Waterways
Water Data	
Dashed box	Water Blocks 2019
White box	Coalfield Consultation Area
Geology	
Red line	Dykes
	Bedrock Geology Midlothian
	Clackmannan Group
	Scottish Coal Measures Group
	Crawford Group
	Gala Group
	Inverclyde Group
	Kirkcolm Group
	Lanark Group
	Portpatrick Formation
	Reston Group (Lower Old Red Sandstone)
	Stratheden Group (Old Red Sandstone)
	Shinnel Formation
	Silurian rocks
	Strathclyde Group
	Tappins Group
	Extrusive rocks 1
	Extrusive rocks 2
	Igneous intrusions

Figure 2.6: Outcrop of coal seams in the Midlothian Coalfield

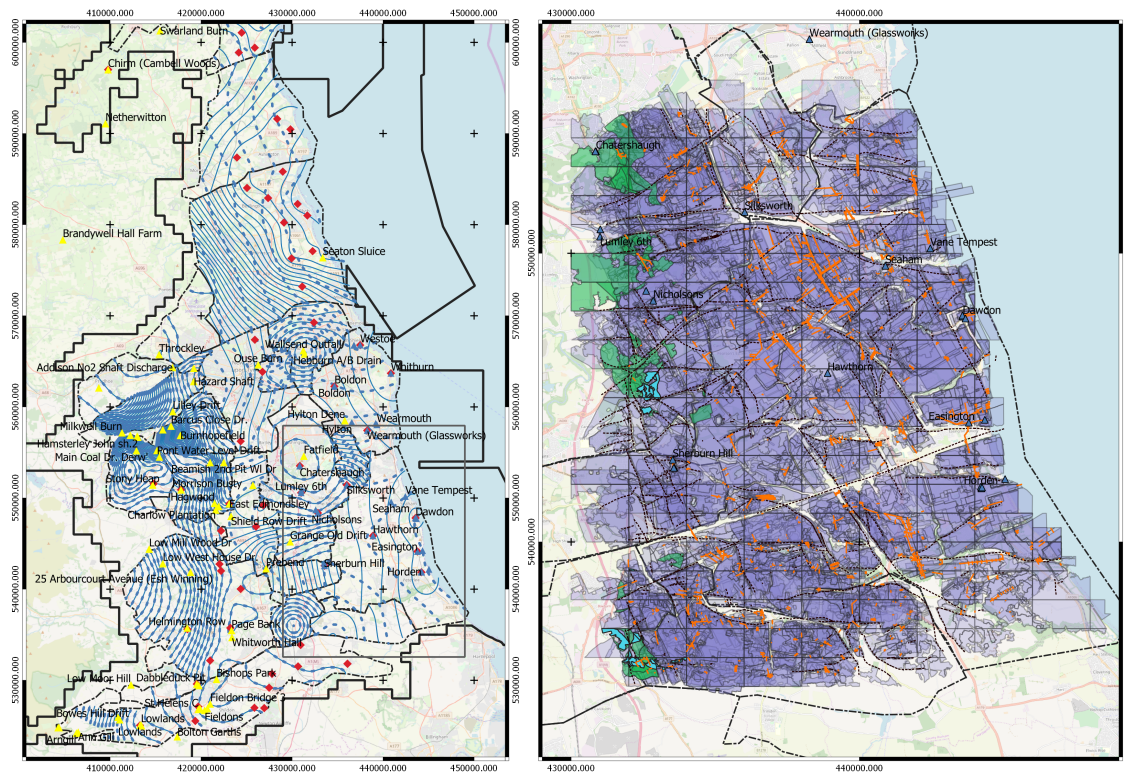
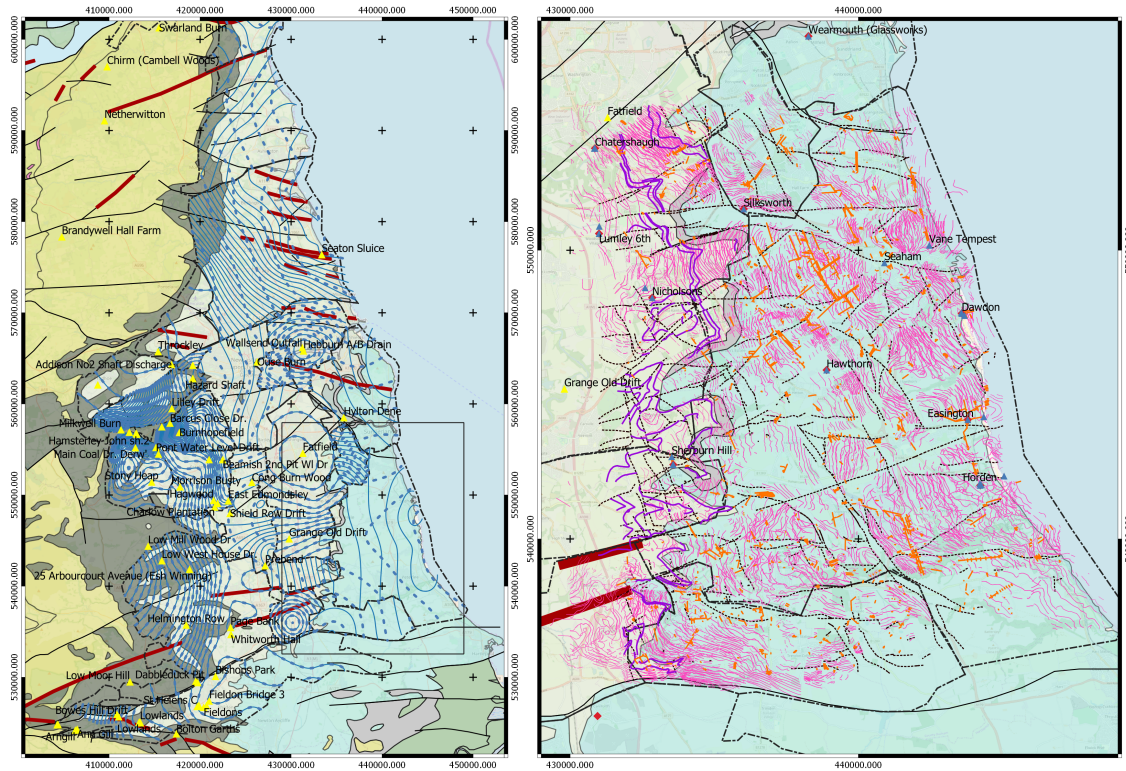


Figure 2.7: a) Water level data and location for monitoring sites, and b) Onshore underground, probable and shallow mine workings and roadways in the Horden-Dawdon mining block



## Legend North East England

Sites		Current contours
+	Boreholes	Water Blocks 2019
▲	Discharges	Coalfield Consultation Area
△	Monitoring site	
◆	Temperature sites	
Mine Data		Geology
Orange line	Spine Roadway	Dykes
Purple line	Outcrops	Faults
Pink line	In Seam Level Contours	North East Bedrock Geology
Dash-dot line	Geological Disturbances	Pennine Lower Coal Measures
Cyan line	Shallow Working	Pennine Middle Coal Measurers
Green line	Probable Working	Pennine Upper Coal Measures
Light purple line	Underground Working	Permain rocks
		Yoredale Group
		Zeichstein Group
Water Data		
- - -	Future contours	

Figure 2.8: a) Geological map, and b) Seam levels with location of outcrops in the Horden-Dawdon mining block

### 3 Case study

The Bilston Glen area, situated in the Midlothian Coalfield in Scotland, and the Dawdon-Horden Mining Block, situated in NE-England have been selected as case studies for the PhD research work, as both coalfields are or could be of geothermal interest for the authorities (Fig. 3.1). While the Scottish coalfield is still at a post-mining water recovery stage, the Dawdon-Horden Coalfield is being pumped to avoid surface discharge since 2004 (source: The Coal Authority). For both area, the significant quantity and variability of the data type available (i.e. temperature and water level time series, depth-profiles) will therefore allow a proper calibration and validation of the numerical models. Moreover, the Midlothian Coalfield is located in a syncline structure, while the Dawdon-Horden Coalfield lies within slightly dipping layers extending under the sea, which would allow performing a comparative study based on the geometry of the mine workings. The present chapter consists of a literature review of the geological context and structure of the mines for both coalfields.

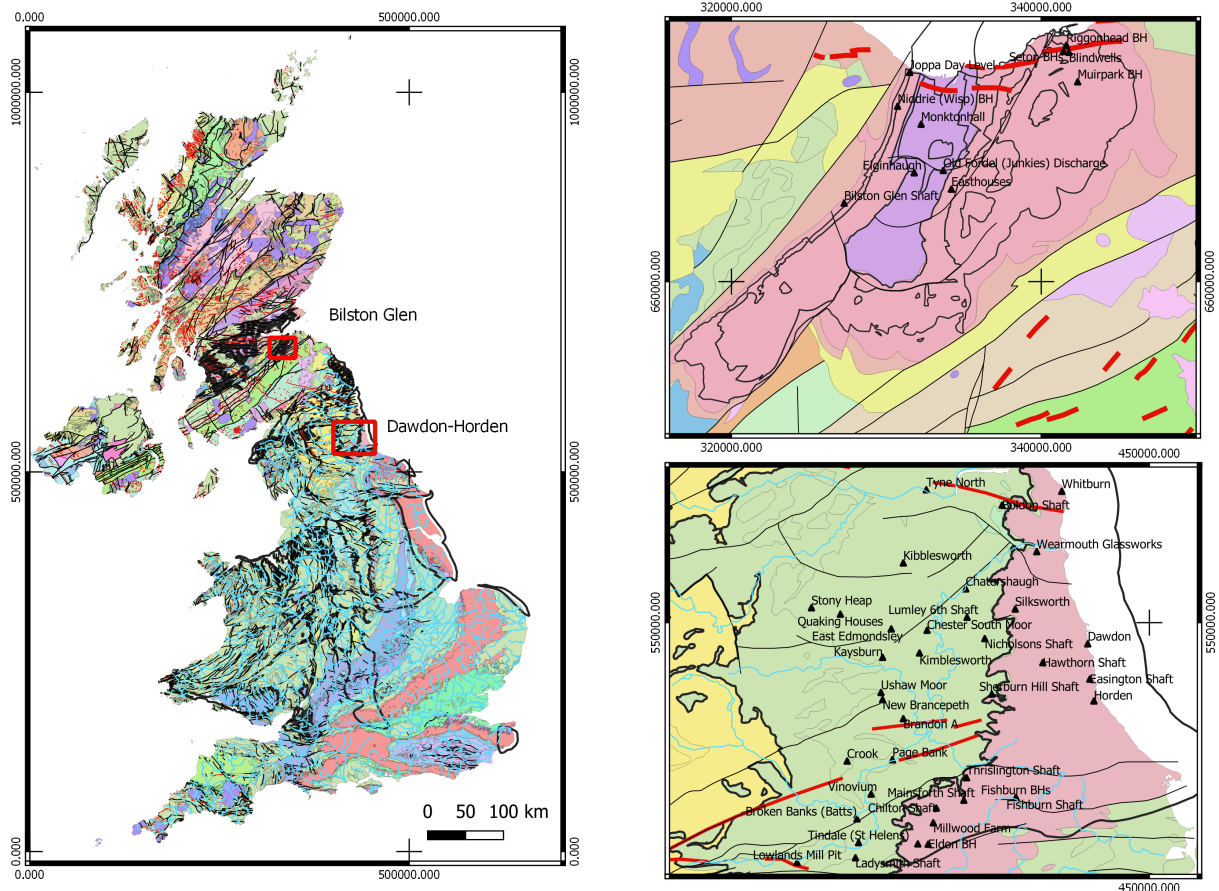


Figure 3.1: Location of the study areas (i.e. the Midlothian and Dawdon-Horden coalfields) over a geological map background. The black triangles represent the main mine shafts

### 3.1 Midlothian Coalfield

The Midlothian Coalfield is located in the south east of the Midland Valley of Scotland (MVS), a 80 km wide, 150 km long WSW-ENE trending Carboniferous graben that developed on the eroded and deformed remnant of the Caledonian Mountains in Scotland (Browne et al., 1999; Underhill et al., 2008; Cameron and Stephenson, 1985; Read et al., 2002). It is located within the Midlothian-Leven Syncline, bounded on the north by the reverse NE-trending Pentland Fault and on the south by the Dunbar-Gifford and the Lammermuir faults (Fig. 3.2).

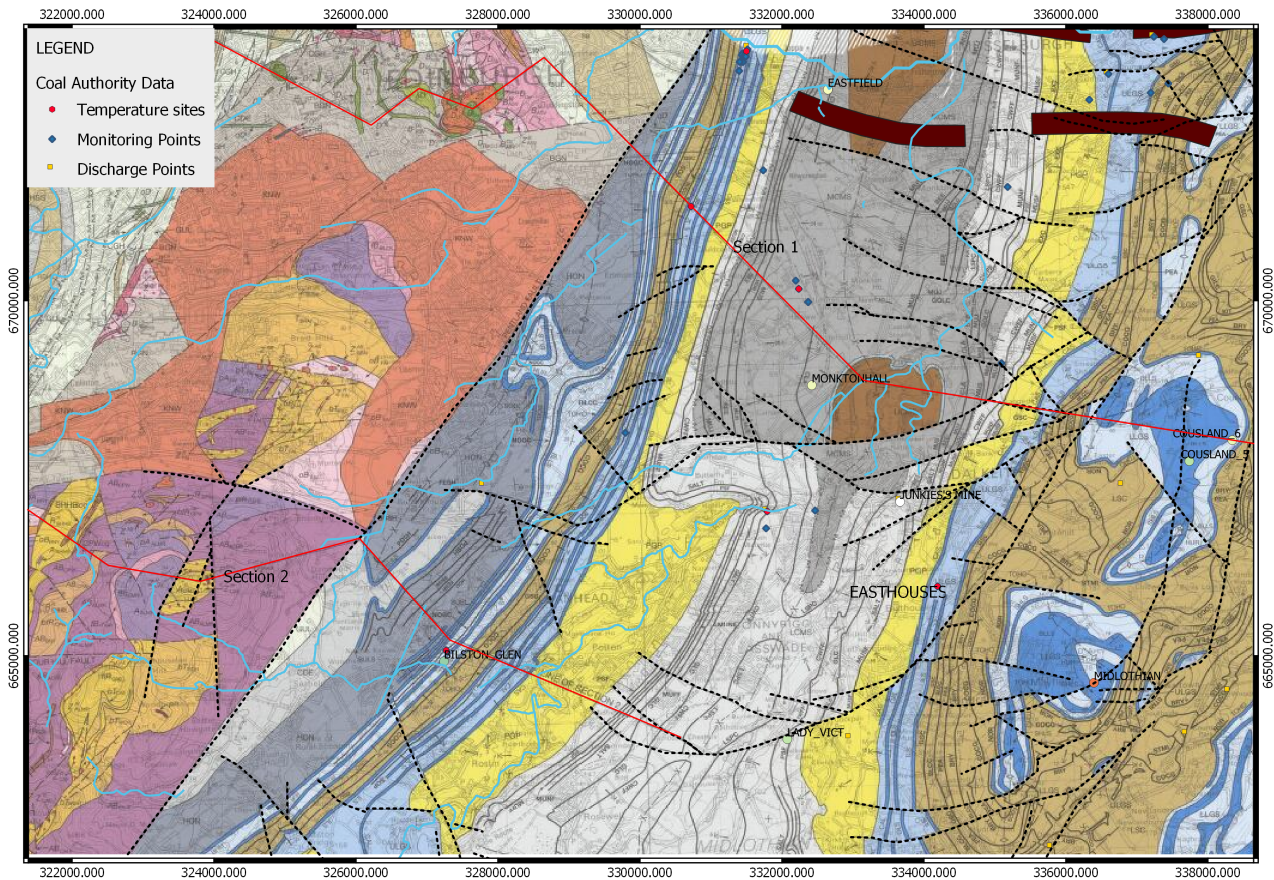


Figure 3.2: Geological map of the Midlothian Coalfield area (source: BGS database), with location of monitoring points (source: The Coal Authority)

The Midlothian-Leven Syncline is suggested to have been formed by syn-sedimentary growth during the Early Carboniferous followed by a Late Carboniferous fold tightening and reverse faulting that affected rocks from the Coal Measures Group (Underhill et al., 2008). While most of the faults became inactive after the early Carboniferous, the truncation of some structures by E-W striking Latest Carboniferous-Early Permian normal faults, quartz-dolerite dyke swarms and extensional fractures indicated that their formation was only completed by the end of the Carboniferous (Rippon et al., 1996; Stephenson et al., 2003; Monaghan and Parrish, 2006). From the Paleogene, the underplating of a magmatic plume associated to the opening of the North Atlantic re-

sulted in an increasing amount of uplift of Scotland (Hillis et al., 1994, White 1988). This uplift might have reactivated the Pentland fault during the early Neogene (Anderson, 1951). It also led to the significant erosion of the Carboniferous and post-Carboniferous strata, especially at basin margins and between the Midlothian–Leven Syncline and Clackmannan Syncline (i.e. at the location of the D’Arcy-Cousland Anticline). Thermal modeling around the Midlothian–Leven Syncline suggested that up to 1.9 km of sediments would have been eroded (Vincent et al., 2010).

The sedimentary succession in the Coalfield is typical of the sequence found within the Midland Valley of Scotland (Fig. 3.3). It consists of 10-m thick cycles of non-metamorphized sandstones, siltstones and mudstones with beds of limestone, coal, fireclay, ironstone and oil-shale, deposited in a basin environment during the Devonian-Carboniferous period (Cameron and Stephenson, 1985), and intersected by andesitic/basaltic lava flows and pyroclastic rocks. Magmatic activity in the MVS extended from the Carboniferous to Permian for a period of about 90 Ma (Upton et al., 2004), and is suggested to have led to an increase in the heat flow during the Carboniferous, especially in the active eastern region.

The sedimentary succession in the MVS is subdivided into the Inverclyde, Strathclyde, Clackmannan and the Scottish Coal Measures groups (Browne et al., 1999). The Clackmannan Group consists of:

- The Upper Limestone Formation (ULGS), characterized by cyclical sequences of limestone, mudstone, sandstone, siltstone, seatrock and coal. Depositional environments are interpreted to range from shallow seas to deltaic and alluvial plains (Hall et al., 1998).
- The Limestone Coal Formation (LSC), which comprises cycles of coal, mudstone, siltstone, sandstone, seatearth and coal with some thicker mudstone intervals, ironstone and limestone. Compared to the Lower and Upper Limestone formations, the Limestone Coal Formation characterizes a return to relatively non-marine conditions in which large quantities of coal have accumulated.
- The Lower Limestone Formation (LLGS), dominated by repeated upward-coarsening cycles of limestone, bedded mudstone, siltstone and sandstone with minor seatrock and thin coal and ironstone deposited in a quiet marine and non-marine backwater (Hall et al., 1998).

The Upper Limestone Coal Formation is separated from the overlying Coal Measures Group by the Passage Formation (PGP). This formation is dominated by relatively coarse-grained sandstone with mudstone, seatclay and fireclay, deposited in a dominantly fluvial system (Browne et al., 1999). The Scottish Coal Measures Group is the youngest observable set of sedimentary rocks in the eastern part of the basin, and are mostly preserved in the centre of the synclines. It is subdivided into the Lower (LCMS), Middle (MCMS) and Upper Coal Measures formations (UCMS), which consist of fluvio-deltaic sedimentary rocks deposited in cyclical sequences of mudstone, siltstone, seatearth, sandstone and coal, in a costal deltaic plain with frequent occurrence of coal swamp conditions. The figure below (Fig. 3.3) shows the typical geological log for the Midlothian Coalfield area.

Most of the coal produced in the Midlothian coalfield originates from the LSC and the MCMS. The thickness of coal seams typically ranges between 1 m and 3 m, depending on the thickness of the sedimentary cycle, with some exceptional seams reaching 15 m (Rippon, 2002 in Trewin, 2002).

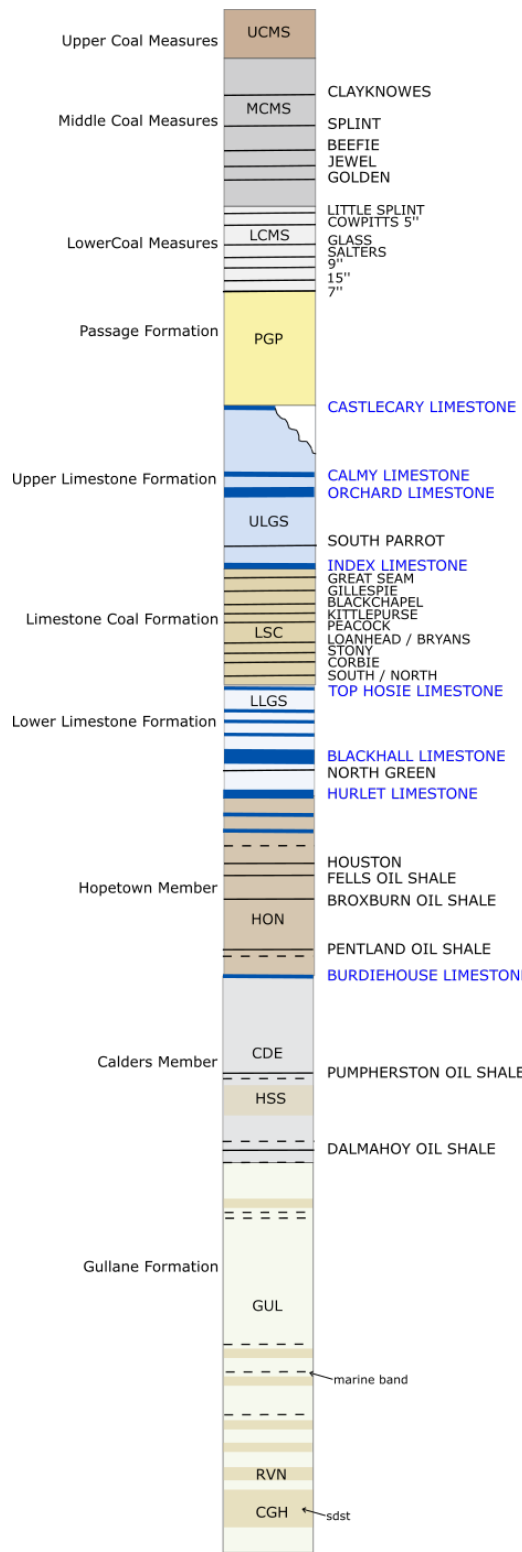


Figure 3.3: Geological log of the Midlothian coalfield area. In the Dalkeith area, the Coal Measures reach about 460 m. The maximum thickness for the UCMS, MCMS, LCMS is 1200, 350, 240 m, respectively, and averages 600, 550 and 240 m for the ULGS, LSC and LLGS, respectively (Monaghan, 2014).

### 3.1.1 Mining history

In the early stage of mining, shallow mines (i.e. the Polton, Whitehill) extracted coal from the Coal Measures located in the central part of the Midlothian syncline, using the pillar-and-stall method. Coal from the Limestone Coal Formation have been mined both from shallow workings on the edge of the syncline, where the formation outcrops (i.e. Roslin, Ramsay, Burghlee on the western limb and Lingerwood, Bryans, Newbattle, Arniston on the eastern limb), and later on by deep longwall mines located in the centre of the syncline (i.e. Bilston Glen, Lady Victoria, Easthouses). Some of the shallow early mines were also laterly reworked using the longwall extraction method. Consultancy reports ordered by the Coal Authority have suggested that no hydraulic connections exist between the mines from the Coal Measures and the mines accessing the Limestone Coal Formation. While water has already filled the shallow workings, it is currently still rebounding in the deepest mines (i.e. WYG Engineering, URS and JMC reports). Shallow mines located in the Limestone Coal Formation on the western side of the coalfield (i.e. Ramsay, Roslin, Burghlee) are interconnected, but no clear connections have been identified with the deep mines accessing the same coal beds (i.e. Bilston Glen). Old panels from the Burghlee mines are located about 40 m above Bilston Glen workings in the Great seam and are separated by 330 m in the Craigie seam. However, it has been suggested that the Roslin Colliery might drain into the Bilston Glen mine. Fig.3.4 shows a preliminary 2D conceptual model developed for the Midlothian Coalfield, based on a NW-SE cross-section through the syncline structure (Fig. 3.2).

Similar rises in water level (i.e. 20 m/yr) have been measured in the Bilston Glen and Easthouses shafts (Figs 3.5 and 3.6). Those mines, situated on both side of the Midlothian syncline, are connected by roadways and through the Great Seam at -502 m depth (Owens, 2015). On the eastern side of the syncline, the Easthouses, lady Victoria and Lingerwood mines, accessed by the Easthouses pumping pit, Bryan's pit and Easthouses inclines, are interconnected at different levels, mostly within the Great and Parrot/Splint seams. This includes roadway connection between Lingerwood Dicken's shaft and Lady Victoria shaft, incline connection between Easthouses Great Seam and Lady Victoria Splint Seam, goaf connection between Lady Victoria and Lingerwood Parrot Seam. In addition, the Eastwood pumping shaft connects the Parrot seam to the great seam from Easthouses, and the Eastwood Great seam connects to both the Lady Victoria Splint and Parrot seams by two steep drifts.

During mining activities, most of the workings located in the Limestone Coal Group were dewatered via shallow drainage adits (Bamforth, 2014). While shallow mine workings in the Coal Measures now drains from the Eldin Adit at Elginhaugh (i.e. Eldin Day Level at 48 m) to the river South Esk (WYG, 2005), discharge levels from deeper mines include the Old Fordel/Junckies Day Level portal (35-37 m AOD), Bryan's adit (50 m AOD) and the Burghlee Day Level (110 mAOD). First, the decant location for the Junckies Level is at about 44 m AOD in the Easthouses incline C, which access the interconnected Lingerwood, Lady Victoria, Easthouses and Bilston Glen mines via the deep Great seam. Recent reports suggested that the Junckies adit actually only drains the northern area and/or shallow workings of Easthouses-Lingerwood-Lady Victoria the in the Limestone Groups, and potentially of the Lower Coal Measures. Chemical analysis of the water discharged at Junckies indeed supported a shallow source and low residential time for this water. This might either be explained by rainwater infiltration into shallow workings of deeper Coal Measures or the drainage of water from workings separated from the Easthouses-Lingerwood-Lady Victoria workings located in the same Limestone Measures, at greater depth or to the South (Bamforth, 2014).

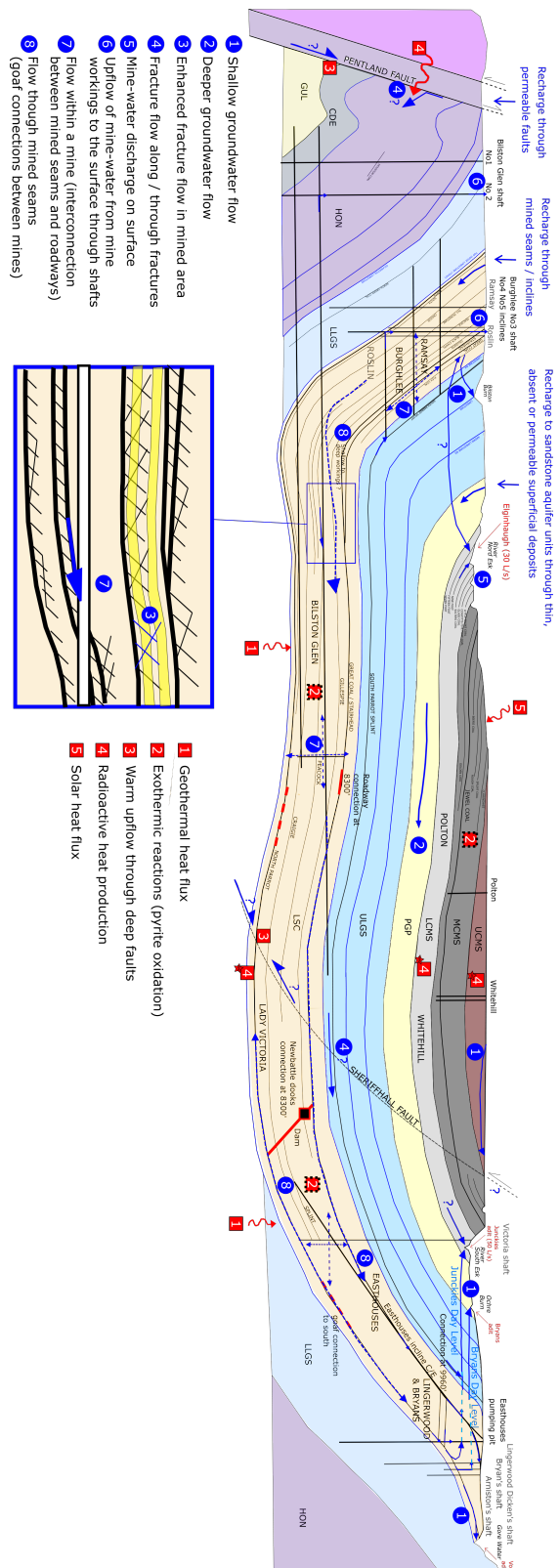


Figure 3.4: Conceptual model for the Midlothian Coalfield

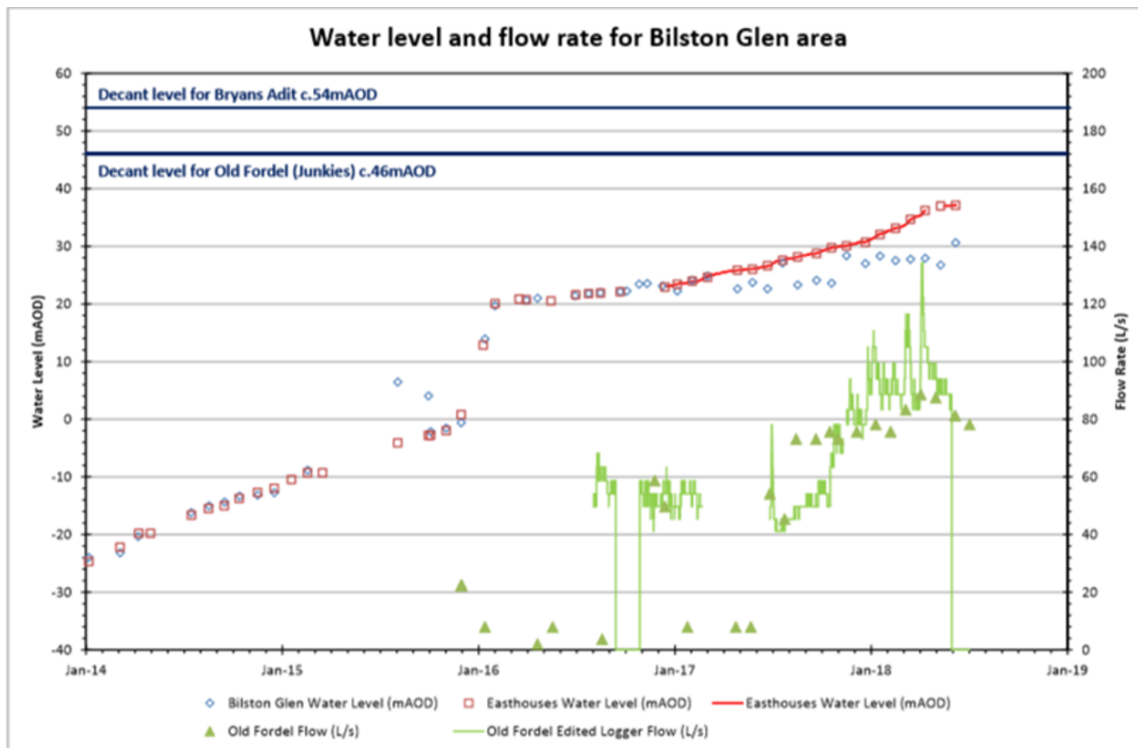


Figure 3.5: Change in water level measured in Bilston Glen shaft

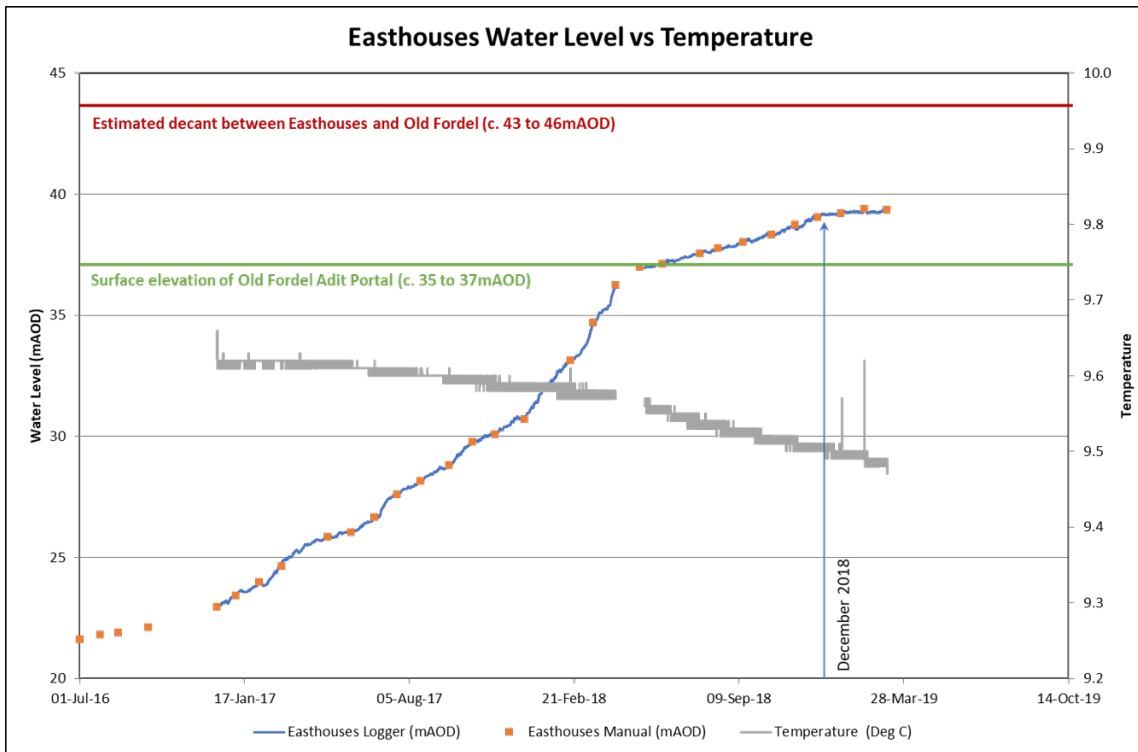


Figure 3.6: Change in water level measured in the Easthouses shaft

On the other side of the syncline, waters from the deep Coal Measures and Limestone Coal workings are drained by the Bilston Glen shaft to Elginhaugh. The increased CaCO<sub>3</sub> alkalinity (but low Mg/Ca content) at Elginhaugh compared to water at Junckies indicates a longer residential time in the deep limestone formations. The high sodium chloride content of the water at Bilston Glen was moreover suggested to characterise saline connate groundwater originating from the limestone deposition period. The Bryan's adit was finally designed to drain deep mining units of the Lady Victoria and Lingerwood via gravity draining of the shallow workings above, to the Ochre Burn. The decant level for the Bryans discharge is located in the Bryan's shaft (54.28 mAOD) that connects to Lingerwood Parrot seam and Easthouses Great seam (Bamforth, 2014). No discharge has occurred yet from the Bryan's adit, which is considered as a potential secondary discharge after Junkies's. Both the Burghlee's adit and Roslin's adit drains water from the shallow workings in the Limestone sequence on the west (reported as filled), to the Bilston Burn and Kill Burn watercourses, respectively. Water has been reported as stabilized in the Arniston mine, that connects to the Lingerwood mine through roadway in the Great seam, and discharge at Vogrie (Bamforth, 2014; Owens, 2015).

## 3.2 Dawdon-Horden Mining Block

The Dawdon mining area is located in North East England. There, 7 main seams have been worked using both pillar-and-stall and longwall mining. The coalfield consists of slightly dipping strata (1 - 5 °) extending below the sea toward the south east. The main seams are summarized in table 3.1, together with their thickness.

Seam code	Ref letter	Name	thickness
NE120H	E	HIGH MAIN	1.8
NE140H	F	MAIN	1.2
NE170H	G	YARD	1.7
NE190H	H	MAUDLIN	1.1
NE210H	J	LOW MAIN	1.4 - 2.1
NE260H	L	HUTTON	1.5

Table 3.1: Main seams worked in the Dawdon area

Water pumping started in Dawdon in 2004. Since then, connections between the Dawdon, Easington and Horden mines have been identified despite the presence of a E-W trending volcanic dyke between them and the existence of a dam that might no longer be active. Those coastal mines are also connected with the Hawthorn mine, located further west. Besides, the Dawdon shaft is interconnected with the Easington Colliery (roadways in seams J and F), Vane (connection in seam J) and Seaham (roadway in seam E) and with the general body of mine workings via the Murton Colliery. From the analysis of mine plans, we also suggest that a roadway might explain the interconnection between Horden, Easington and with the Blackhall Colliery. Potential roadway and goaf connection in Main seam and High Main might have been identified between Murton and Seaham, as well as a roadway connection between Shotton and Murton in Hutton seam. Finally, a roadway might link Easington and Murton in Main seam.

## 4 Conceptual models of mines

Geological systems are inherently complex and simplifications are therefore required to fully evaluate and understand the mechanisms that occur with them (Kruse and Younger, 2009). In addition, mining activities are indeed likely to have caused perturbations of natural thermal regime of the mine systems (i.e. change in ground-water flow) and participated to the development of specific processes responsible for anomalous temperature distribution (Jessop, 1995). In that view, constructing a comprehensive conceptual model of mine workings is the first step toward a good understanding on the heat sources and transfer processes in mines, and thus of the heat recharge potential of mine reservoirs. The present chapter aims at reviewing the current knowledge about mine reservoir systems in terms of geological and hydrological aspects.

### 4.1 Hydrology of mine aquifers

Mine aquifers are characterized by a triple-porosity composed of the primary rock porosity (i.e. unaffected rock), the mining voids (i.e. galleries, shafts, roads...) and mining-induced fractures (Wolkersdorfer, 2008). In mined strata, difficulties in predicting groundwater flow generally results from the complex geometry of interconnected open voids inherited from the mining history, not always well documented (Henton, 1974). Those tend to form high-permeability pathways in the mine, altering the natural groundwater flow within original aquifers. In the Midlothian Coalfield, the Carboniferous sedimentary sequence is composed of low permeability layers (mudstone) interbedded with higher permeability strata (sandstone, limestone) that tend to form complex multi-layered and moderately productive aquifers, with borehole yields in the range 5-15 l/s (Robins, 1990; MacDonald et al., 2005; O Dochartaigh et al., 2015). The natural layering tends to create complex flow path, dominated by horizontal inter-granular flow and fracture flow. Lateral compartmentalization can also result from the intrusion of igneous rock (dykes, sills, plugs) or faults that can act either as permeable pathways or barriers to groundwater flow.

Despite the presence of coal seams adding more low-permeability layers between the sandstone aquifer units, the Carboniferous strata mined for coal generally have slightly higher productivity than the aquifers not mined for coal (O Dochartaigh et al., 2015). Mining activities indeed resulted in an increase in permeability of the Carboniferous strata both by increasing the void space in zones where seams were mined out and through fracturing of competent horizons above the mined seams. The residual volume and geometry of mining voids will however depend both on the extraction method (i.e. pillar-and-stall, longwall mining), on the extent of induced fracturing, and on the amount of backfilling and subsidence. Despite many shafts, roadways or drifts might remain opened after the closure of a mine (Younger, 2001), some galleries might indeed be filled with collapsed roof material (i.e. the "goaf") while mining shafts might be backfilled before being capped (Younger et al., 2002). With time, ground subsidence also tends to reduce both the initially high volume of void created by mining, but also the transmissivity and storage capacity of mined strata (Saaltink et al., 2002).

Only a few aquifer properties data from pumping test are available for boreholes intercepting former mines.

However, dewatering rates used to maintain low levels during mining activities (see Tab. 4.1) is assumed to balance water inflow in mines and can therefore be used as a reference for natural recharge rate.

Formation	Colliery	Flow rate
LCF	Prestongrange Colliery	40-75 l/s over 140 h/week at 165-225 m depth
	Kilsyth Colliery	150 l/s at 206 m depth
	Twechar Colliery	13 l/s for 12h/day ay 317m depth
	Monktonhall Colliery, Midlothian	35 l/s
MCMS	Bothwell Colliery	230 l/s at 396 m depth
LCMS	Polkemmet Colliery, West Lothian	75 l/s
	Frances Colliery, Fife	120 l/s
LCF / CM	Falkirk District	30-55 l/s
	Blindwells Colliery, East Lothian	315 l/s

*Historical mine pumping rates (Gillespie et al., 2013). MCMS: Scottish Middle Coal Measures Formation; LCMS: Scottish Lower Coal Measures Formation; LCF: Limestone Coal formation; CM: Coal Measures*

## 4.2 Thermal system

### 4.2.1 Geothermal heat flux

The geothermal gradient represents the rate of increase in the subsurface temperature with depth. It is determined by the geothermal heat flux and the thermal conductivity of the rocks (Busby et al., 2011). In theory, the average temperature gradient can be calculated from the mean annual ground surface temperature and an undisturbed, topography corrected temperature measured at a known depth (Rybäck et al., 2000). In practice, measured temperatures will often differ from theoretical temperatures calculated from purely conductive geothermal gradients (Busby et al., 2011). Those anomalies can be explained by several reasons, such as the effects of groundwater circulation (i.e. convective flux), local internal heat production (i.e. decay of radioactive elements), inefficient heat transfer through low conductivity rocks (i.e. trapped heat), heat refraction processes (i.e. due to tilted layers) or the presence of anthropogenic heat sources, superimposing onto the conductive heat flow (Beltrami et al., 2015).

Heat flow and temperature measurements from onshore boreholes and mines in the UK have been collected in the BGS Catalogue of Geothermal Data for the UK (Burley et al., 1984; Rollin, 1987) or are available as Hard Copy temperature logs in BGS archives. Additional values were published by Downing and Gray, 1986, Lee et al., 1987 and (Barker et al., 2000), but no new data has been acquired since the 1980s (Gillespie et al., 2013). In 2013, Gillespie et al., 2013 used a compilation of 35 heat flow data reported from Burley et al., 1984 and Brereton et al., 1988 to map the heat flow in Scotland (Fig. 4.1). Most of the values were measured at depth < 400 m in onshore boreholes, 13 of which are located in the MVS. Results indicated an average heat flow of 56 mW/m<sup>2</sup>, with values ranging from 29 to 82 mW/m<sup>2</sup>. Apparent ‘hot spots’ corresponding to granite intrusions were identified in the central part of the Midland Valley and in the East Grampians region, with heat flows of 60 mW/m<sup>2</sup> and 70 mW/m<sup>2</sup>, respectively (Gillespie et al., 2013).

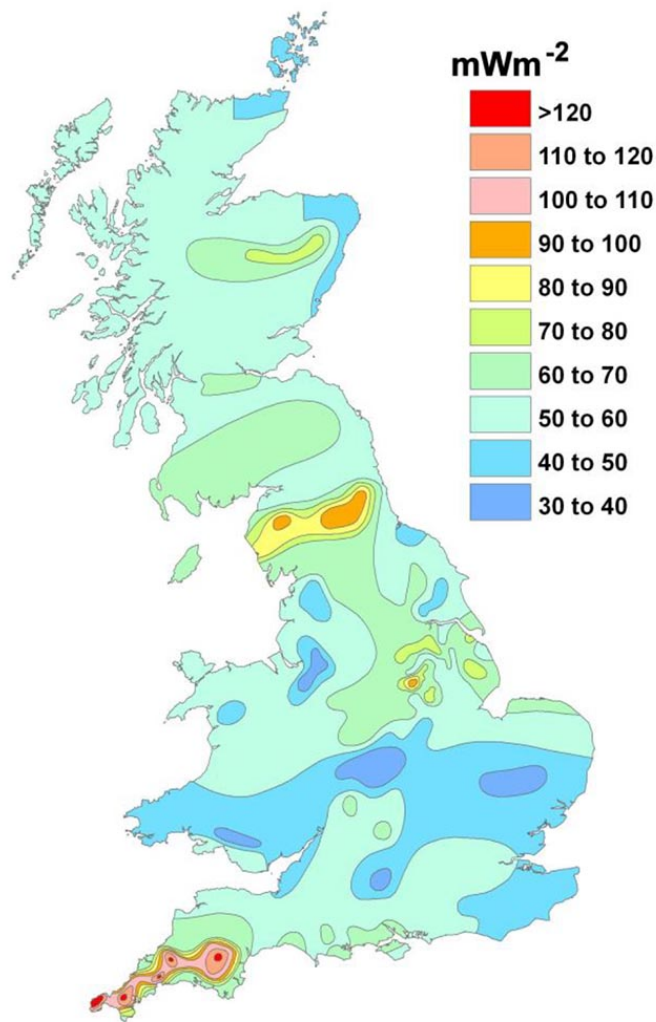


Figure 4.1: Heat flow map for the UK (Busby, 2011).

In borehole where no heat flow has been measured, geothermal gradients have been calculated based on the temperature measurements made at the bottom or near-bottom of 61 boreholes, down to 1300 m depth (Burley et al., 1984). The average temperature gradient for all boreholes ranges from 3.7 to 45 °C/km, with a mean of 22.5 °C/km and a median of 21.5 °C/km. Plotted together, the data indicate an average gradient of 30.5 °C/km which correlates throughout the entire depth range intersected by those boreholes. Using 133 BHT acquired from depth >1.5 km in 72 offshore wells in the North West Margin area (Gatliff et al., 1996 in Gillespie et al., 2013) however noted the increase in the deep geothermal gradient from about 35.8 °C/km at 1 - 3.5 km to 46.7 °C/km at 3.5 - 5 km, relatively consistent across Scotland, and independent of the location (i.e. onshore or offshore) and the type of rock (i.e. sedimentary, crystalline basement) in which measurement were taken. Plotted together, onshore and offshore temperature measurements indicated an average geothermal gradient of 31.9 °C/km.

Despite temperature measured below 1.5 km depth are assumed to be only little affected by surface perturbations, (Westaway and Younger, 2013) suggested that near-surface temperatures in Scotland might have been disturbed by climate warming since the last prolonged glaciation (i.e Ice Age), accounting for the lower

geothermal gradient near the surface. When extrapolated to the surface, the best-fit shallow geothermal gradient estimated from boreholes < 400 m depth indeed indicates a surface temperature of 4.0 °C, which is lower than the current yearly average surface temperature in Scotland of about 9°C (Gillespie et al., 2013). Several studies already mentioned the importance of considering the effects of past climatic variations on the shallow geothermal gradient, especially at high latitudes (i.e. Carslaw and Jaeger, 1959; Majorowicz et al., 2012; Raymond, 2018; Beltrami et al., 2017; Gosnold et al., 2011). Paleo-climate signals have been described as a series of mean surface temperature change before present day, that propagates downward by conduction and tends to superimpose to the quasi-steady state thermal field associated to the Earth's internal heat (Beltrami et al., 2017). While the extent of the perturbations mainly depends on the magnitude and time scale of the past variations, the amplitude of the temperature change due to surface disturbances will tend to decrease exponentially with depth depending on the thermal conductivity of the ground, and with a time lag since the onset of the perturbation at the surface (Westaway and Younger, 2013; Beamish and Busby, 2016; Busby et al., 2015). In the UK, Wheildon and Rollin, 1986 suggested that boreholes < 100 m depth are sensitive to surface temperature variations over the past 500 years, while Beltrami et al., 2017 showed that past climatic signals > 1000 years B.P are still contributing to the thermal state of the subsurface down to 500 m depth. Using individual temperature measurements from shallow depth (< 400m) would therefore tend to underestimate the true "steady-state" background geothermal gradient and thus the extent of the geothermal resource at depth. New interests in re-evaluating the heat flow including paleo-climate corrections have recently grown in the UK. Westaway and Younger, 2013 suggested that heat fluxes measured in shallow boreholes in Scotland would need to be increased by 18 mW/m<sup>2</sup> to account for the effects of palaeo-climate. The correction would be reduced to 8.8-13.5 mW/m<sup>2</sup> for 1 km deep boreholes and 0.2-9.1 mW/m<sup>2</sup> for 1.5 km deep boreholes.

#### 4.2.2 Radiogenic heat production

The Earth's natural heat flow is generally attributed to a primordial heat (i.e. inherited from the formation of Earth) and to up to 45% to a contribution from the natural decay of radioactive isotopes of uranium (<sup>238</sup>U, <sup>235</sup>U), Thorium (<sup>232</sup>Th) and potassium (<sup>40</sup>K) (Pollack and Chapman, 1977). Radiogenic heat production from rocks A (uW/m<sup>3</sup>) can be calculated as the sum of the contribution from those four elements using the following relationship (Beck and Balling, 1988; Vilà et al., 2010; O'Neill, 2016; Rybach et al., 1988):

$$A = 10^{-5} \rho \times (9.52[U] + 2.56[Th] + 3.48[K]) \quad (4.1)$$

with  $\rho$  the average rock density (kg/m<sup>3</sup>) and [U], [Th] and [K] the concentrations of Uranium (ppm), Thorium (ppm) and Potassium (wt%), respectively. Due to geochemical differentiation, partial melting and magma crystallization processes, the upper crust is enriched in heat producing elements (HPEs) compared to lower levels (Beamish and Busby, 2016), and U, Th and K can be found in minerals in most crustal lithologies. Measurements of RHP in continental rocks has shown that acidic rocks have the highest heat production rate (i.e granites), followed by basic and ultrabasic rocks (Rybäck, 1986; Cermak, 1990; Brown and Mussett, 1995).

Scotland is located on a geologically stable part of Earth's crust, where only granite intrusions would contain sufficient concentration of K, T and U element to generate radiogenic heat at significant levels and thus represent an additional source of in-situ heat (Gillespie et al., 2013). In Scotland, the largest and greatest concentration

of intrusions is located in the block of crystalline rocks bounded by the Highland Boundary Fault and the Great Glen Fault (Fig. 4.2). Some granite intrusions can be found south of Inverness and near Aberdeen, but only have small heat producing (HP) values (0.6–2.2 uW/m<sup>3</sup>), in the Grampian Highlands and in the Northern Highlands (HP of 2.2 to 7.3 uW/m<sup>3</sup>). Two large intrusions (Fleet and Crieff), with HP values of 3 and 2.2 uW/m<sup>3</sup> were emplaced in Southern Scotland, at the end of the Caledonian Orogeny (410–390 Ma). Only one intrusion of significant size, the Distinkhorn intrusion, can be found in the MVS and consists of diorite and granodiorite with relatively low HP capacity (2.0 uW/m<sup>3</sup>).

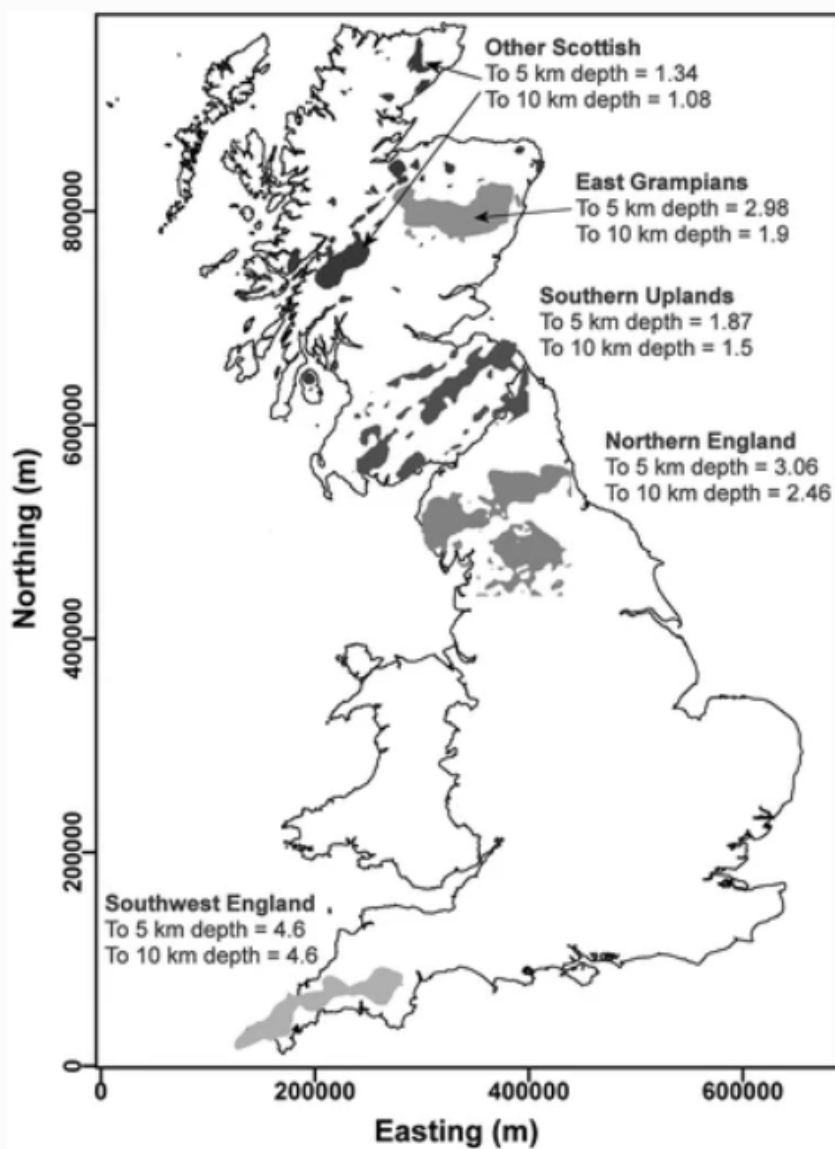


Figure 4.2: Locations in Great Britain with significant quantities of heat producing granites within the upper crust. Quantitative figures of average heat production in, uW/m<sup>3</sup> (Busby, 2017)

Table 4.1 summarizes representative RHP values for the main lithological groups that compose the lithosphere.

lithology	density	mean	std	25th	Median	75th
granite	2650	2.827	2.176	1.741	2.429	3.233
granodiorite*	2718	1.838	2.401	0.938	1.501	2.214
basalt	2750	0.358	0.394	0.077	0.214	0.533
alkalic basalt*	2957	0.69	0.355	0.342	0.543	0.801
Andesite*	2811	1.059	1.203	0.452	0.817	1.246
rhyolite*	2674	3.084	5.975	1.72	2.546	3.732
mudrock	2400	1.392	0.702	0.968	1.442	1.657
wacke	2400	0.984	0.535	0.548	0.993	1.212
sandstone	2400	0.896	0.468	0.536	0.819	1.206
carbonate	2400	0.477	0.356	0.216	0.416	0.618
limestone*	2789	2.066	24.568	0.387	0.777	1.632

Table 4.1: RHP values for different lithological groups in uW/m3 (Vilà et al., 2010, \*Hasterok et al., 2018). Mudrocks include fine-grained consolidated or unconsolidated sedimentary rocks such as mud/mudstone, silt/siltstone, clay/shale, argillite, lutite.

According to Vilà et al., 2010, density plays a important role for radioactive heat production (RHP) in sedimentary rocks due to compaction effects. Their RHP appears to be relatively low (<1.5 uW/m3), except for organic, K-rich sediments and K-rich evaporites that have values exceeding 3 uW/m3. While U and Th are negligible in major minerals, K indeed contributes the most to radioactive heat generation and occurs in major silicates (i.e. feldspar, micas) (Webb et al., 1987).

RHP is moreover highly correlated to grain size in detritic rocks, with the higher the grain size and the lower the RHP. In the sandstone group, arkoses have the highest values (about 1.25 uW/m3). Hasterok et al., 2018 suggested that aluminous shales are generally high heat producing (HP = 2.9 uW/m3) while iron shales are low heat producing (HP = 1.7 uW/m3). The weathering of (K-rich) feldspars and mica, that can be found in higher concentration in felsic rocks (i.e SiO<sub>2</sub> rich) tends to form K-rich clays such as illite that are therefore good heat producers (Hasterok et al., 2018). Evaporites (except KCl-rich rocks) and non-detritic siliceous and Fe-MN-rich rocks have values <0.5 uW/m3 (Hasterok et al., 2018). Carbonate-rich rocks and pure quartzite generally have lower HPE than detritic sedimentary rocks, with values ranging between 0.2 and 1 uW/m3. Rybach, 1986 proposed values of 0.57 and 0.34 uW/m3 for limestone and dolostone, respectively. In crystalline rocks, andesite and tholeiitic basalts have mean RHP of 0.82 and 0.05 uW/m3, respectively (Hasterok et al., 2018). RHP from granite is very variable and generally depends on their petrogenesis. Finally, Hasterok et al., 2018 showed that metamorphic rocks tend to have similar heat producing capacities as their protoliths.

The distribution of radiogenic HPEs therefore provides an important control on the temperature distribution within the earth lithosphere (Sandiford, McLaren, et al., 2006). Where the heat flow is not disturbed by heat convection, it can therefore be used together with a determination in the radiogenic heat production (RHP) to constrain the thermal field within the crust (Jaupart and Mareschal, 2005).

### 4.2.3 Mine-water temperature

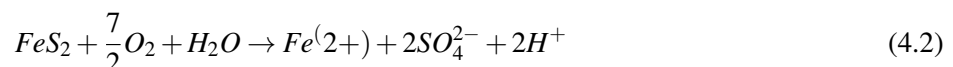
While rock temperature in deep mines is expected to be controlled by the geothermal gradient (Anderson and De Souza, 2017), Burnside et al., 2016 suggested that the heat flow in flooded workings is dominated by advection. Analysis of temperature in mines in the UK showed that there are significant variations in the temperature of mine waters measured down to about 1500 m depth in shafts (Gillespie et al., 2013). In the Midland Valley of Scotland, temperatures measured from nine boreholes range from 12 to 21 °C, with a mean and median of 17 °C (Burley et al., 1984). Mine-water temperature is typically higher than the typical natural groundwater temperature from Carboniferous aquifers in the MVS. However, no clear correlation has here been found between the measured temperature from mines and the depth of the measurements. This suggested that other factors might contribute to the definition of the mine-water temperature. However, predict the temperature of water pumped from former mine shaft can be difficult, as water of different temperature might enter the borehole at different depths (Gillespie et al., 2013).

Additional data collected as part of the Scotland Baseline Project in 2008, indicate temperatures of 19.2 °C for mine-water pumped from the Polkemmet mine shaft, and temperature of 9.8 °C for gravity-driven discharged mine-water. Farr et al., 2016 suggested that measured temperatures are highly dependent on the location of the logger relative to the surface features and influences by 1) cold recharge entering the drainage system (i.e. shallow logger in gravity driven adit, highly correlated with air temperature), 2) localized recharge events such as period of intense rainfall (i.e. adits with transfer pumps with more stable yearly temperature) or 3) the absence of connection with surface recharge (i.e. deep warm water with constant temperature throughout the year).

The subsections below aim at getting an overview of the different processes that might be responsible for anomalous temperatures in mines.

#### Exothermic reactions

Mine waters generally contain a high concentration of iron that result from the oxidation of sulphide minerals (i.e. pyrite, marcasite, sphalerite, galena) contained within the coal deposits. As most of the geochemical reactions occurring in mines, oxidation reactions are exothermic and therefore contribute to the overall temperature in mines. The oxidation of crystalline pyrite to ferrous iron can be expressed as (Banks et al., 1997; Farr et al., 2016):



Banks, 2008 estimated that 1400-1500 kJ/mol of heat energy can be released through pyrite oxidation, which generally occurs when water is lowered by pumping and enter in contact with oxygen. Using discharge value at Ynysarwed with a total iron concentration of 0.001377 mol/L, Farr et al., 2016 moreover estimated that pyrite oxidation is able to generate a temperature increase of 0.5 K/L of water.

#### Heat convection

Anomalous temperatures i.e. where the water temperature is greater than the rock temperature, have been observed in abandoned mines. Those were partly explained by the existence of free 'natural' convection of water

flowing from different mined levels into open vertical shafts (Krige, 1939) and by recharge from greater depth through faults. Large mining voids (i.e. shafts, roadways) indeed create highly transmissive flow pathway across large areas and depths by connecting both laterally and vertically formerly separated groundwater flow systems. Those tend to promote convective heat transport within aquifers of poor natural transmissivity, adding more complexity to the groundwater flow. Faults can also have substantial impact on subsurface temperatures due to their influence on rock permeability. They can either act as a barrier or as a highly conductive flow pathways, allowing water recharge from surface and/or depth or from the coast, such as i.e. Highland Boundary Fault (O Dochartaigh et al., 2015).

In large mining voids, water bodies tend to form density-related stratification resulting from the mixing of cold meteoric water and warmer saline water originating from depth (Nuttall and Younger, 2004). Hamm and Bazargan Sabet, 2010 showed using numerical models that efficient intra-well mixing induced by water density differences (i.e. free convection) tends to fix the temperature along the shaft close to the average of the temperatures at the top and bottom, when no pumping is performed. The presence of several galleries intersecting the shaft at different levels induces local water mixing and allows the establishment of higher temperatures at the bottom of the shaft. Pumping water from mine generally encourage turbulent water mixing, which can destroy density-related stratification in wells and reduce the water quality (Hamm and Bazargan Sabet, 2010; Burnside et al., 2016).

Turbulent flow is particularly prominent in large open voids such as roadways, which favor high velocities. This contrasts with low velocities and laminar flow observed in the less permeable porous rock mass and in the backfilled part of goaf materials, drivings and caverns, that represent the highest volume of void in mines (Renz et al., 2009).

### **Blanketing effects**

In mines in the Carboniferous succession of the MVS, the presence of many low-conductivity horizontal rock layers such as mudstone or coal are finally likely to form “cap” rocks, creating situations where the inflow of geothermal heat from below might be trapped, forming positive heat anomalies. Such blanketing effects has been described by (Busby et al., 2011) for the NE England, where low conductivity Carboniferous rocks are present above the Weardale granite, which has a high heat production (Downing and Gray, 1986).

# 5 Chapter 1 : Heat extraction Model

## 5.1 Background

With the growing interest in geothermal energy for domestic heating and cooling, borehole heat exchanger (BHEs) coupled ground source heat pump (GSHP) systems have been increasingly used worldwide (Chen et al., 2019). Analytical and numerical approaches have been developed to assess the system performances and the sustainability of heat extraction through the study of its thermal response over time (i.e. Rybach and Eugster, 2010; Signorelli et al., 2005; Lyu et al., 2017; Zhang et al., 2016; Stylianou et al., 2017; Zanchini et al., 2010; Lazzari et al., 2010). Studies showed that the energy performance of GSHPs strongly depends on the heat transfer process between the BHEs and the ground. In a purely diffusive medium, it mainly depends in the long term on the thermal conductivity of the ground (i.e. Stylianou et al., 2017; Chen et al., 2019; Choi and Ooka, 2015). The presence of groundwater was suggested to improve the long-term performance of BHE both by increasing the heat exchange rate during production (Zanchini et al., 2010; Stylianou et al., 2017; Wang et al., 2013) and by favoring heat recovery (Hein et al., 2016; Erol et al., 2015). In medium with groundwater circulation, analysis showed that soil heat capacity and thermal conductivity only have minor impact on the sustainability of a GSHP system and that dispersion tends to increase the area of impact of heat extraction.

### 5.1.1 Analytical solutions

Analytical solutions are necessary to benchmark (quasi-) linear problems and are required to verify numerical methods that will be used to solve for problems with greater geometrical complexity. Solutions of the partial differential equation for heat transport in porous media have been developed for scenarios with different boundary conditions. A general solution for the calculation of the residual heat dissipated by conduction after an instantaneous heat pulse of energy  $q$  in an infinite homogeneous and isotropic medium, derived by Carslaw and Jaeger, 1959, is given in Bauer et al., 2015:

$$\Delta T(r,t) = \frac{q}{\rho c(4\pi\alpha t)^{\frac{n+1}{2}}} \exp\left(-\frac{r^2}{4\alpha t}\right) \quad (5.1)$$

where  $\Delta T$  is the temperature difference between the measured temperature and the background temperature at the time  $t$  elapsed since the heat pulse and at a radial distance  $r$  from the source (i.e.  $r^2 = x^2 + y^2$ ), and  $n$  is a factor accounting for the geometry of the heat source ( $n_{1D}=0$  for a plan,  $n_{2D}=1$  for a cylinder and  $n_{3D}=2$  for a point source).  $\alpha = \lambda / \rho c$  is the thermal diffusivity of the subsurface ( $m^2/s$ ), with  $\lambda$  the bulk ground thermal conductivity ( $W/m.^{\circ}C$ ) and  $\rho c = \phi \rho_w c_w + (1 - \phi) \rho_s c_s$  the volumetric heat capacity of the saturated porous media ( $J/m^3.^{\circ}C$ ), calculated from the weighted arithmetic mean of the solid matrix  $\rho_s c_s$  and water  $\rho_w c_w$ .

The problem of heat diffusion in a porous media due to heat extraction/injection from BHE has first been described using the Infinite Line Source (ILS) model (Carslaw and Jaeger, 1959). For a constant heat injection

$q$  (W/m) along the vertical axis of a line source, the temperature distribution around a BHE can be solved using the following solution (Monzo, 2011; He et al., 2018):

$$\Delta T_{ILS}(r,t) = \frac{q}{4\pi\lambda} E_1 \frac{r^2}{4\alpha t} \quad (5.2)$$

where  $E_1$  is the exponential integral function. This function can be approximated by  $\ln(\frac{4\alpha t}{r^2}) - \gamma$  for large values of  $\frac{\alpha t}{r^2}$ , with  $\gamma$  the Euler's constant = 0.5772. In BHE models, a thermal resistance factor  $R_b$  is generally added in order to faithfully characterise the heat transfers between the borehole walls the circulating fluid (i.e. Monzo, 2011). To account for axial effect, Zeng et al., 2002 derived a solution for the response of a constant line-source with finite length H in a porous media by applying the method of images (Eq. 5.3).

$$\Delta T_{FLS}(x,y,z,t) = \frac{q}{\rho c(4\pi\alpha)} \left[ \int_0^H erfc\left(\frac{r}{\sqrt{4\alpha t}}\right) \frac{dz'}{r} - \int_{-H}^0 erfc\left(\frac{r}{\sqrt{4\alpha t}}\right) \frac{dz'}{r} \right] \quad (5.3)$$

Heat dissipation in a porous aquifer can however be described as a coupled process of heat conduction through the solid matrix and the water together with heat advection within advancing groundwater (Su et al., 2004). Recent studies therefore attempted to include the effects of groundwater flow to evaluate the impact of heat convection on the performances of BHE system, based on the Moving Infinite Line Source theory (Diao et al., 2004; Sutton et al., 2003). For the application of an instantaneous heat source in an isotropic medium with groundwater flow in the x direction, the following solution has been proposed by Marshall, 1958 (Vandegehuchte and Steppe, 2012; Erol et al., 2015):

$$\Delta T(x,y,t) = \frac{q}{\rho c(4\pi\alpha t)} \exp\left(-\frac{(x-v_T t)^2 + y^2}{4\alpha t}\right) \quad (5.4)$$

Considering a constant line source of energy  $q$  (W/m) with infinite length along the z-direction, the Moving Infinite Line source solution can be written as followed (i.e. Molina-Giraldo, 2011):

$$\Delta T_{MILS}(x,y,t) = \frac{q}{\rho c(4\pi\alpha)} \exp\left(\frac{v_T x}{2\alpha}\right) \int_0^{\frac{v_T^2 t}{4\alpha}} \exp\left(-\frac{v_T^2(x^2 + y^2)}{16\alpha^2 u} - u\right) \frac{du}{u} \quad (5.5)$$

Here,  $v_T$  the heat pulse velocity or thermal velocity of the water (m/s), defined as  $v_T = u_x \frac{(\rho c)_f}{\rho c} = \frac{u_x}{R_T}$ , with  $u_x$  the Darcy velocity,  $R_T$  is a retardation factor that expresses the delay of the heat front with regards to the true pore waterfront. It is explained by the energy required to heat up or cool down the matrix (Barends et al., 2010).

One of the main limitation of this MILS model is the that water temperature is not impacted by temperature at the boundary conduction (Rivera et al., 2015). Advection transport instantaneously the heat fluxes induced by the BHE over the porous fluid and solid matrix and thus, advancing thermal plume delineates the domain where reservoir exhaustion takes place (Rivera et al., 2015). In real systems, temperature drawdown in the matrix is expected to stimulate net heat influx from advection  $q_w$  ( $\rho_w c_w \frac{dT}{dx}$ ).

To account for the relative contribution from reservoir exhaustion or groundwater advection in the overall power balance, Rivera et al., 2015 therefore developed a new analytical approach that quantify both vertical and horizontal transient heat flux regime stimulated by BHE, including uniform horizontal groundwater flow and heat exchange with the atmosphere. Study the relative contribution of conductive and convective heat transfers processes in porous systems requires the use of dimensionless parameters such as the Peclet number  $Pe = \frac{v_T h}{\alpha}$  and

the Fourier number  $Fo = \frac{\alpha t}{h^2}$  or specific variables such as the characteristic length  $L = \frac{k}{\alpha \rho_w c_w}$  or characteristic time  $T = \frac{k \rho c}{(\alpha \rho_w c_w)^2}$  (Diao et al., 2004; Molina-Giraldo, 2011; Rivera et al., 2015; Biglarian et al., 2017; Tye-Gingras and Gosselin, 2014; Gordon et al., 2017). Those allow eliminating the dependency of the results on i.e. the borehole length  $h$ , operation length  $t$ , temperature, on the medium thermal diffusivity  $\alpha$  or the convective heat transport velocity  $v_T$  (Molina-Giraldo, 2011).

### 5.1.2 Sustainability issue

Most of the studies aiming to assess the performances of BHE focused on the temperature evolution within the system throughout the production time. However, sustainable heat production from BHE can be achieved if the heat load extracted is balanced by the rate of heat recovery in the subsurface. According to Banks, 2008, heat extraction from the ground in the early stage of production is expected to create a zone of depressed temperature around the borehole, leading to radial conduction of the heat stored in surrounding rocks toward the BHE. The cooling of the area might then induce an increasing heat flow of solar energy from the surface that will eventually balance the heat abstracted. In Chen et al., 2019, the authors showed that using a specific heat extraction rate of 100 W/m, quasi steady-state outflow temperature could be reached after 20 years of production from a BHE in China, considering a geothermal gradient of 0.03 °C/m. Some studies showed that other ways to achieve sustainable heat extraction were to perform cyclic production or artificial heat recharge (i.e. Cruickshank and Baldwin, 2016). Being able to discriminate between the energy sources through a detailed understanding of the heat fluxes induced during heat extraction (both axial and radial) is therefore essential to get a better insight on the sustainability of heat extraction (i.e. Rivera et al., 2015).

Extensions of the standard Moving Infinite Line Source model have therefore been made to better study the fluxes induced by heat extraction/injection whilst accounting for axial effects, based on the Finite Line Source approach (Molina-Giraldo, 2011) and for seasonal/cyclical effects (i.e. Rivera et al., 2015; Erol et al., 2015; Biglarian et al., 2017; Saadi and Gomri, 2017). In a system without groundwater flow, Zhao et al., 2020 showed that radial heat conduction tends to dominate during operation, while vertical heat flux dominates during recovery. Sufficient thermal recovery period after each heat extraction cycle allows the elimination of coldness accumulation near the borehole and a quasi-total heat recovery of the ground (Zhao et al., 2020). In a system with groundwater, Rivera et al., 2015 showed that horizontal advective transport tends to enhance vertical conductive heat fluxes, but the relative power source from groundwater and storage varies over time. In the early stage of production, energy is mainly extracted from storage. Local depletion then enhances the vertical fluxes. While the relative contribution from the bottom reaching a limit of 24% of the total power demand, the contribution from the surface becoming dominant for  $Fo > 0.13$ . Study of heat recovery after a production period showed that in terms of power, quasi-steady state might be reached within a much longer time period compared to results from recovery based on temperature analysis (i.e. Rybach and Eugster, 2010; Signorelli et al., 2005). Further analysis showed that axial heat fluxes tend to accelerate recovery and that the ground surface provides up to 2/3 of the power over the full life-cycle of the system, meaning that for shallow BHE (less than 100 m depth), heat from the earth's interior is not the main source of heat.

### 5.1.3 Surface boundary condition

The majority of studies of heat transfers around BHE implied isothermal boundary conditions (i.e. Zhao et al., 2020). The importance of considering heat flux boundaries has however been underlined by Saadi and Gomri, 2017. During production, the temperature distribution around BHE is not equal to the undisturbed ground temperature from the surface to the bottom, and axial effects become important at both ends of the borehole (Erol et al., 2015). Using a Neumann boundary condition rather than an imposed temperature at the surface therefore appears to be more appropriate to avoid overestimating available recharge. Furthermore, using heat flux boundaries makes possible the simulation of temperature change at the surface, when extraction of heat is made at shallow depth and for long periods. In Saadi and Gomri, 2017, surface heat flux also permitted to treat seasonal effects as a physical balance between convective heat transfer between the ambient air temperature and the soil surface, and the solar radiations. Heat conduction through the ground surface is indeed the results of the combination of convective heat transfer between the atmosphere and the ground surface, which depends on the solar radiations absorbed by the ground surface (SR), longwave thermal radiations emitted from the ground (LR), latent heat related to evapo-transpiration process (ET) and convective heat flux due to wind velocity (CE):

$$q = SR - LR - ET - CE \quad (5.6)$$

Based on this relationship, Singh and Sharma, 2017 moreover expressed the variations in the effective ground surface temperature as a time-variant first type boundary condition calculated from a general convective heat transfer coefficient, depending on the ambient air temperature and solar radiation. This allowed to realistically assess the contributions of the surface boundary on the energy recharge to the ground, considering seasonal variations. Studies on the effect of seasonal temperature change on the ground thermal state showed that annual variations only propagated down to about 20 m depth. At that depth, the ground temperature equals the mean annual air temperature and below, it tends to follow the local geothermal gradient. While daily soil temperature variations are relatively difficult to model (Ozgener et al., 2013), they only reach about 20 cm depth and wont be of interest in this study.

## 5.2 Research Gaps

Despite the performances and sustainability aspects of BHE have been well studied using both analytical and 1D to 3D numerical studies, a few of them assessed the area of the ground impacted by heat extraction to provide the necessary energy to consumers. Some studies gave an insight of the direction of the conductive flux induced during production and recovery, allowing to express the thermal impacts in terms of energy balance rather than absolute temperature. However, there is still a lack of investigation regarding the relative extent of the heat recharge provided by solar input, geothermal flux, groundwater flow or from rock storage, for deep systems (e.g. mine reservoirs). From Rivera et al., 2015, in which the model considered uniform temperature distribution along the BHE, we suggest that further analysis would be require to evaluate the relative contribution from the deep geothermal gradient and geothermal heat flux for deeper borehole. The current state of knowledge for advective-diffusive heat transfers induced by BHE-GSHP systems will moreover here be used to study the heat exchange processes in porous layers to get an insight of what might happen in mines coal seams.

### 5.3 Aims and methods

The aim of this chapter is therefore to get a better understanding of the heat fluxes and heat transfer mechanisms in the subsurface, through energy balances. We will need to describe 1) the relative contribution of surface/bottom recharge during heat extraction and recharge, using 1D model, 2) lateral recharge using 3D diffusion model, 3) the relative contribution from heat convection and conduction through the porous medium, using 2D advection-diffusion models (i.e. with groundwater flow). Analytical solutions will be developed to assess what is the proportion of heat absorbed/released by the porous media from/to the circulating fluid.

We also want to evaluate the extent of heat depletion caused by a constant heat load extraction from simple mine systems and evaluate the key parameters to reach a steady state production temperature. To achieve this, energy balance calculations will be made based on the estimations of how much heat is produced and diffused from surrounding rocks. We will attempt to estimate the footprint area of heat extraction for a single house in the UK, and compare it to the available recharge to assess the sustainability of BHE-GSHP systems from the heat resource perspective.

### 5.4 Research questions

What are the key heat recharge mechanisms and heat sources controlling the water temperature in flooded coal mines?

- What are the main heat sources in coal mines?
- Can thermal steady state (energy balance between heat extracted and heat recharge) be reached, and what is the footprint area of the heat extracted for a typical single house energy consumption?
- What is the nature of the heat fluxes and the relative contribution from heat diffusion and advection during production (i.e. heat/water extraction) and heat recovery/flooding ?

### 5.5 Hypothesis

- H0 – Heat sources in deep mine systems include radiogenic heat production, pyrite oxidation, the geothermal heat flux and advective warm water from depth. Pyrite oxidation only slightly contribute to heat renewal in mines.
- H1 – During production, heat is mainly sourced from advective mine-water in tunnels and horizontal conduction in goaf, with limited depletion from surrounding rock (i.e. vertical conductive heat flux).
- H2 – During recharge, vertical heat flux are dominant, but solar recharge is negligible relative to the geothermal heat flux. Groundwater advection and deep warm water upflow enhance heat recovery rate.
- H3 – Thermal balance can be reached for low extraction rate, and the footprint area is mainly dependent on the thermal conductivity of the host rock and/or on the hydraulic gradient.

## 5.6 Preliminary results

### 5.6.1 Heat generation in mine

#### Conceptual model

Fig. 5.1 shows a conceptual model for a mine of simple geometry composed of 3 seams of coal. The uppermost one is unmined, the middle one is mined according to the longwall method (i.e. collapsed goaf material) and the lower most is mined according to the pillar-and-stall method.

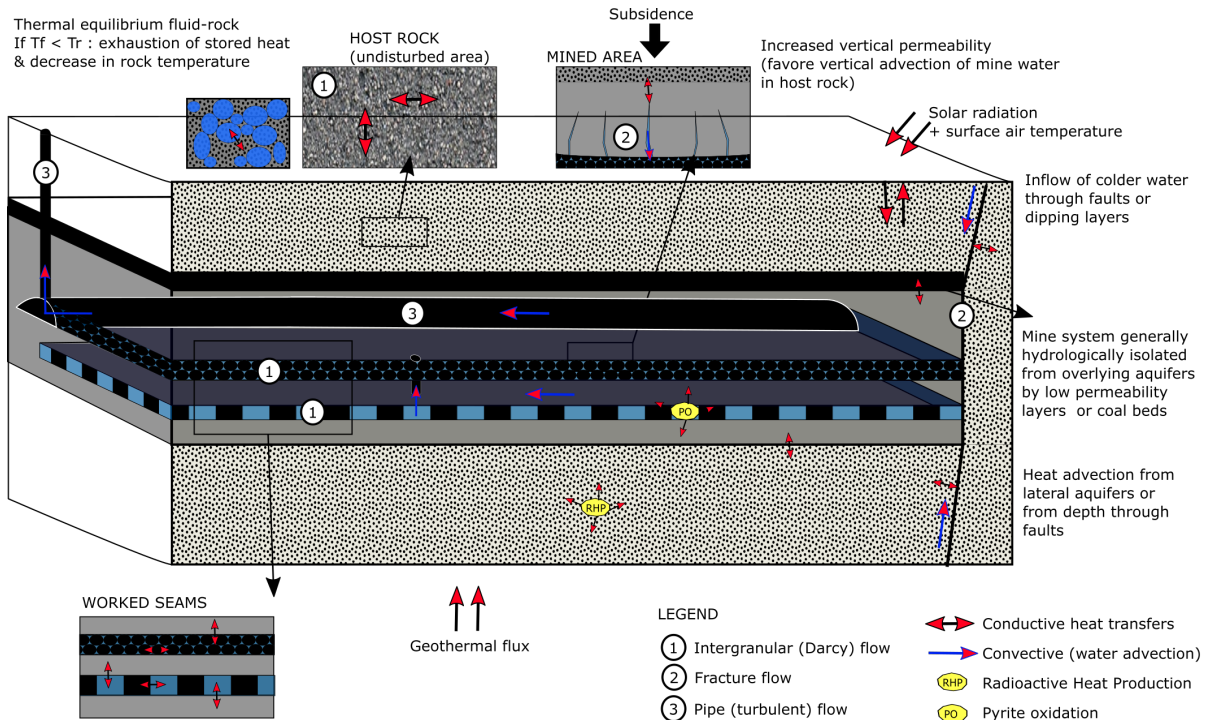


Figure 5.1: Conceptual model of mines showing the potential hydrological, thermal and geometrical aspects in mines. See legend for more details.

#### Radiogenic heat production

We first evaluate the impact of radioactive heat production from different lithologies on the undisturbed geothermal gradient using a fictive vertical column of rocks (Fig 5.2). Initial temperature distribution within the model was first determined from steady state and transient simulations using purely diffusive heat transfers (Fig. 5.3). The model consists of a 1 dimensional finite-element mesh composed of 4000 line elements.

The steady state temperature profile is determined from surface and bottom temperatures of 9 ° and 40° at 1 km depth, respectively (see dotted black line in Fig. 5.3). In the transient simulation, an initial gradient of 40 °C/km is used, allowing visualizing the effects of long term surface warming (i.e. 1000 years) on the shallow temperature gradient (orange line in Fig. 5.3). The significant difference in the profiles obtained from steady state and transient simulation show that for  $\Delta T = 9^\circ\text{C}$  on surface, 1000 years is not sufficient for the gradient

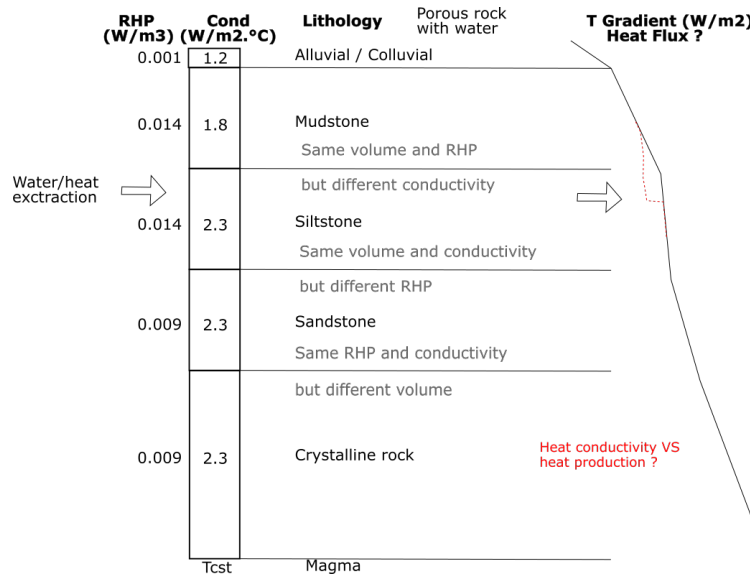


Figure 5.2: Radioactive heat production rate (RHP), thickness and conductivity values for a fictive column composed of different lithologies used to estimate the contribution from radiogenic HPEs on the geothermal gradient

to reach its undisturbed steady state, with perturbations visible down to 180 m depth. Based on the harmonic mean of the thermal conductivity of the different lithologies composing the rock column (2.145 W/°C/m), we then calculate the geothermal heat flux necessary to conserve the average steady-state gradient of 0.031 °C/km. Calculations indicate an average flux of 66.5W/m<sup>2</sup> across the rock column, which is confirmed after running a 1000 years steady-state simulation based on heat-flux boundary conditions (i.e. no change in gradient). RHP source terms are then added to evaluate their contribution on the steady state temperature profile. Results for 100 year long simulations using either constant flux or fixed temperature at the upper and bottom boundaries are shown in Fig. 5.3 (green line and dashed black lines, respectively) and show a consistent increase in temperature along the trend of the geothermal gradient that might indicate that RHP has been overestimated.

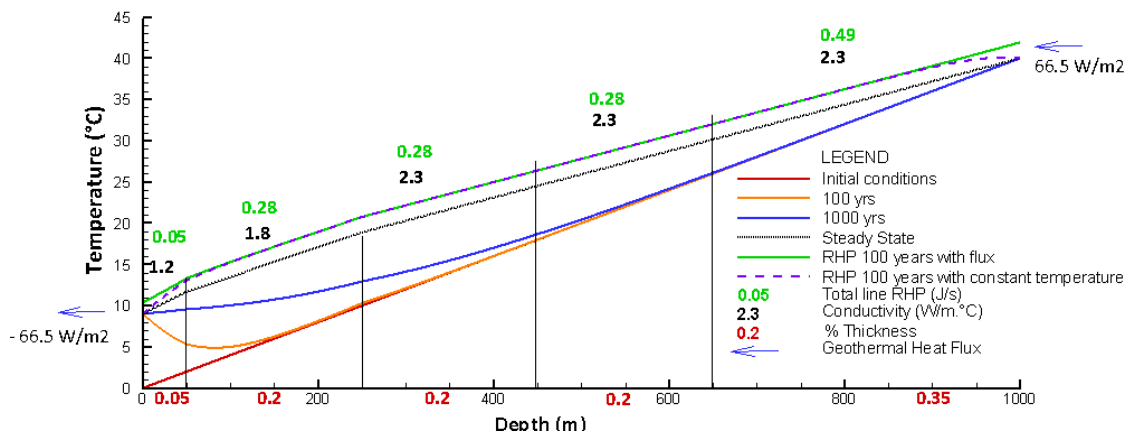


Figure 5.3: Geothermal gradients obtained for steady-state, unsteady-state and RHP with constant heat flux and/or constant temperature boundary conditions.

Finally, we add source terms aiming to simulate heat extraction at a rate of 15 J/s (W) at 140 m (in the mudstone section), 335 m (in the siltstone section) and 550 m depth (in the sandstone section), in three different 30-year long simulations. Temperature profiles after 30 years of extraction are plotted together in Fig. 5.4.

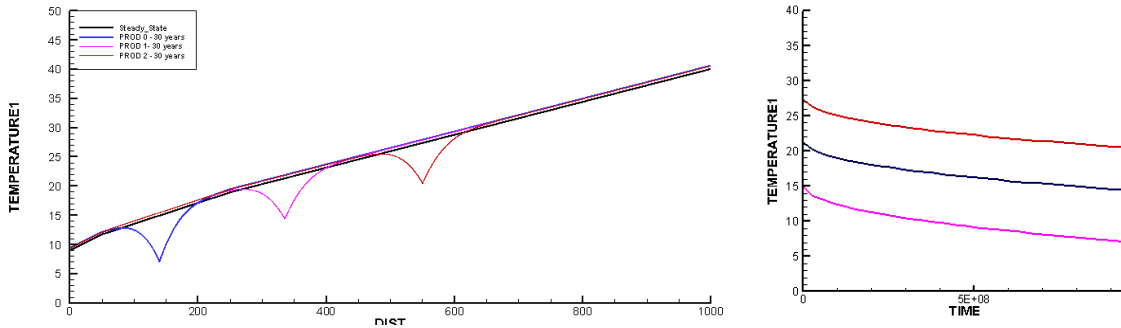


Figure 5.4: Results from RHP simulations

Further work is required to estimate the relative contribution of RHP production versus rock thermal conductivity and of the geothermal heat flux on the undisturbed geothermal gradient in the UK. Data from geological logs of the Carrington-1 well (Monaghan, 2014) have been used as a reference to assess the thickness of each formation in the Carboniferous succession of the Midlothian Coalfield and the proportion of the different lithologies in each formation. Based on data from the literature, we made a rough estimation of the radiogenic heat production and average thermal conductivity for each formation (Fig. A.1).

## 5.6.2 Heat extraction model

### Mathematical approach

The average energy consumption for a single house in the UK is 12 400 kWh per year, with a maximum of 18 000 kWh in winter and 8 000 kWh in summer. To satisfy this yearly demand, a heat pump would need to deliver an average heat load of 1415 W by extracting heat from the underground. This represents a total energy of  $4.47 \times 10^{10} J$  over a year. In reality, the total heat load  $H$  delivered by a heat pump corresponds to the sum of the heat extracted from the ground  $G$  and the electric heat  $E$  required for air compression (Banks, 2008).

$$H = G + E \quad (5.7)$$

The coefficient of performance (COP) of GSHP is used to characterize the efficiency of the system. It can be used to calculate the total heat delivered by the heat pump  $H$  as a function of the electrical power  $E$  provided.

$$COP = \frac{H}{E} \quad (5.8)$$

Using an average COP of 3.4, the average heat that would need to be extracted from the ground to satisfy a heat demand of 1415 W is therefore:

$$G = H(1 - \frac{1}{COP}) = 1000W \quad (5.9)$$

This corresponds to a total energy of  $3.15 \times 10^{10} J$  over a year. Considering a 40 m long borehole heat exchanger, the specific heat absorption from the rock (as defined in Banks, 2008) would here be  $1000/40 = 25 \text{ W/m}$ . GSHP are however generally designed to cover 60 % of the peak heat demand. Assuming that a 3000 W heat pump is used to cover for the peak heat demand of a single 90 m<sup>2</sup> house, which generally averages 5000 W, the actual specific thermal output for a 40 m long borehole would be 75 W/m, and the specific peak heat absorption from the rock, calculated using equation 5.9, with  $H = 75$  and  $\text{COP} = 3.4$ , would instead equals 53 W/m (Banks, 2008).

On the other hand, the total heat content of a rock mass can be estimated using the Equation 5.10.

$$Q = \rho_r V (1 - \phi) c \Delta T \quad (5.10)$$

with  $\rho_r$  the dry rock density,  $V\phi$  the volume of the rock mass,  $c$  the specific heat capacity and  $\Delta T$  the maximum temperature change allowed across the heat exchanger. Assuming  $\rho_r = 2650 \text{ Kg.m}^{-3}$ ,  $c = 950 \text{ J.(kg.K)}^{-1}$ ,  $\phi = 0.1$  and  $\Delta T = 5^\circ\text{C}$ , the volume of rock required to provide a total heat load  $Q = 4.47 \times 10^{10} \text{ J}$  (i.e. energy for one year) is about  $4000 \text{ m}^3$ . Assuming that the heat is extracted radially from a borehole with a length  $h = 40 \text{ m}$  situated in the center of a cylindrical volume, the radius of the cylinder would be 5.6 m, corresponding to a surface area of about  $100 \text{ m}^2$ . For  $Q = 3.15 \times 10^{10} \text{ J}$ , the required volume is reduced to about  $2800 \text{ m}^3$ , which corresponds to an area of about  $70 \text{ m}^2$  (i.e. cylinder radius of 4.7 m). Over a 30 year operation period and if no recharge is considered, the total volume of rock affected would equal  $83\,500 \text{ m}^3$ , which corresponds to an area of about  $2000 \text{ m}^2$ .

Alternatively, we can calculate the surface area that would be required to provide heat recharge to the BHE system. We first assume that the heat is extracted from a vertical 1D BHE and that recharge occurs from above (i.e. heat flux generated from solar energy) and below (i.e. geothermal heat flux). Where ground temperature has not been disturbed by heat production, heat conduction from or toward the surface depends on the effective surface temperature relative to the sub-surface temperature.

The effective surface temperature depends on a complex combination of several factors, such as the amount of solar shortwave radiations, longwave radiations emitted from the ground or wind speed (i.e. convective heat flux from the air to the ground surface), that will impact daily/yearly heat recharge from the surface. In Edinburgh, the average annual rate of insulation is in the order of 94 W/m<sup>2</sup>, with a minimum of 13 W/m<sup>2</sup> in December and 181 W/m<sup>2</sup> in July (Whitlock et al., 200). Due to the low diffusivity of soil (i.e. low thermal conductivity but high specific heat capacity), the refraction of solar radiation and the emission of long-wave radiation by the ground, the net incoming shortwave radiation into the ground only equals 10s of W/m<sup>2</sup> and solar radiations only heat up the upper meters of the ground. Despite heat transfers to the ground can be affected by precipitation, water infiltration and evapo-transpiration processes, Fig 5.5 shows that shallow subsurface temperature tends to roughly follow the trend of the air temperature on a daily basis. Annual variations of the air temperature generally propagate down to about 20 m depth only. Below that depth, the ground temperature is no longer influenced by the yearly changes in surface temperature and equals the annual average surface temperature, before following the local geothermal gradient at greater depth. In the shallow sub-surface, ground temperature is generally assumed to be equal to the mean annual air temperature. As a result, ground temperature will be higher than the average air temperature in winter and thus, the heat flux is directed from the ground toward the surface. In summer, the ground is colder

than the air temperature and thus the heat flux is reversed, recharging the ground with heat.

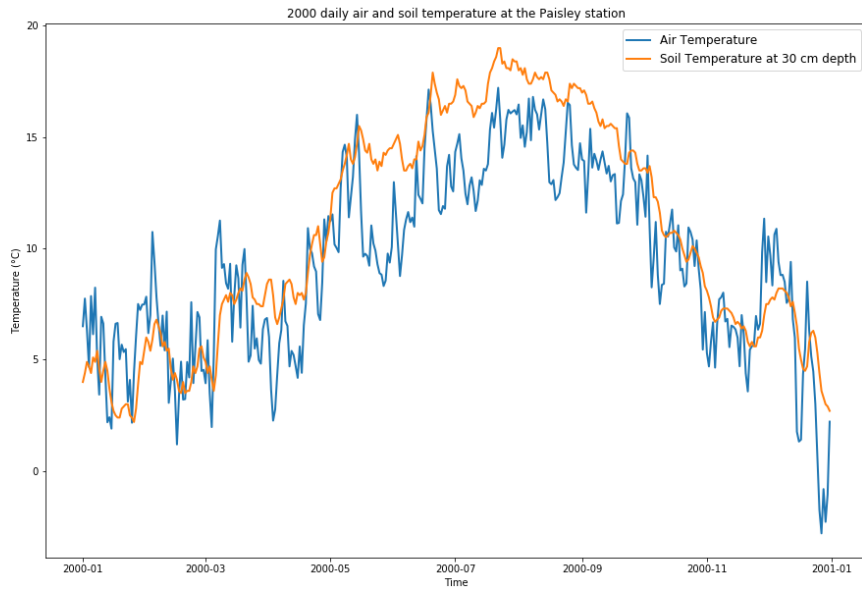


Figure 5.5: Daily air temperature and soil temperature measured at 30 cm depth at the Paisley station, Glasgow area, in 2000

If we assume a yearly average solar heat recharge of about  $0.01 \text{ W.m}^2$  and a geothermal heat flux of  $0.06 \text{ W.m}^2$ , the area required to provide the necessary recharge to the BHE (for  $G = 1000 \text{ W}$ ) is in the order of  $14\ 300 \text{ m}^2$  (see Eq. 5.11).

$$\text{Area} = \frac{1000W}{0.06 + 0.01} = 14300m^2 \quad (5.11)$$

We then assume that heat extraction from BHE induces lateral heat flow from surrounding rock (i.e. Heat mining). Based on the estimated  $70 \text{ m}^2$  footprint area required for heat consumption for one year, the geothermal heat flux and solar heat flux would contribute up to  $0.06 \times 70 = 4.2 \text{ W}$  and  $0.01 \times 70 = 0.7 \text{ W}$  to the total heat recharge, respectively. That means that about  $994 \text{ W}$  will be mined from surrounding rocks. Assuming a borehole length of  $40 \text{ m}$  and a perimeter of  $30 \text{ m}$  ( $2\pi r$  with  $r = 4.7 \text{ m}$ ), the lateral heat flux would be in the order of  $994/40 \times 1/30 = 0.84 \text{ W.m}^{-2}$  (Fig. 5.6).

### Numerical results for heat extraction with diffusion only

We use the OpenGeosys finite element modelling software to simulate the change in temperature within a volume under heat extraction and evaluate the impact of the recharge rate/parameters and available surface area on the temperature decline (i.e. Kolditz et al., 2012; Chen et al., 2019). We consider the borehole heat exchanger as a 1D finite-element model consisting of a vertical line source composed of 4000 elements of  $0.1 \text{ m}$  in length. The BHE is treated as a homogeneous porous medium with a specific heat capacity of  $950 \text{ J/Kg.K}$ , thermal conductivity

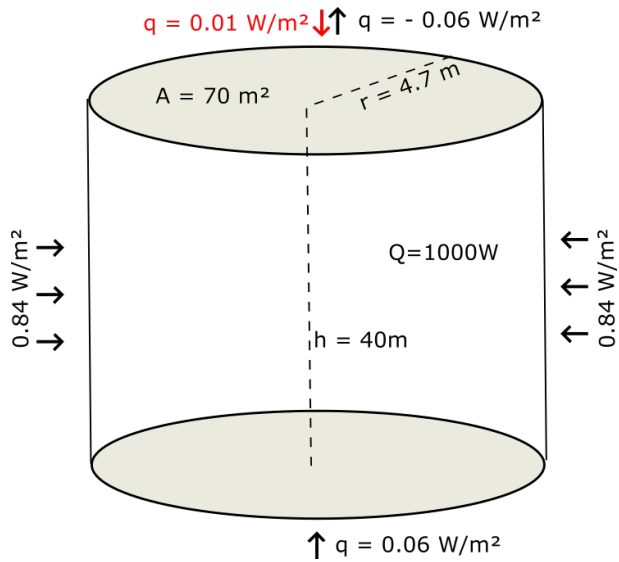


Figure 5.6: Conceptual model for the BHE with induced heat flux

of  $3.0 \text{ W/m.K}$  and thermal expansion of  $1 \times 10^{-5} \text{ }^{\circ}\text{C}^{-1}$ . The initial temperature distribution through the vertical line is defined by a geothermal gradient of  $0.02 \text{ }^{\circ}\text{C/m}$ , corresponding to a surface temperature  $T_0 = 7 \text{ }^{\circ}\text{C}$  and a bottom temperature  $T_z = 15 \text{ }^{\circ}\text{C}$  at  $z = 400 \text{ m}$  depth. Natural steady state conditions are calculated using constant top and bottom heat flux boundaries of  $-0.06$  and  $0.06 \text{ W/m}^2$ , respectively. Those are assumed to represent the geothermal heat flux entering the model from below, flowing through the BHE and coming out at the surface. They were defined accordingly to the geothermal gradient and the thermal conductivity, using Eq. 5.12.

$$q = K \frac{dT}{dx} \quad (5.12)$$

In the long term, it is assumed that the flux coming in is equal to the flux coming out of the system through purely conductive heat transfers. A first simulation was run to ensure that the geothermal gradient within the model remains stable over a total duration of 30 years, using the constant heat flux boundaries.

We then use a series of transient simulations to determine the amplitude of the variations in the surface heat flux required to reproduce the change in surface temperature observed in Scotland. The average yearly temperatures in east Scotland is calculated from the data available on the UK Meteorological Office website. The mean annual temperature over the 1910-2019 period is  $7 \text{ }^{\circ}\text{C}$ , with a mean winter temperature of  $2 \text{ }^{\circ}\text{C}$  and a mean summer temperatures of  $12 \text{ }^{\circ}\text{C}$ . Simulations are run using a series of different heat flux variations at the upper boundary. The yearly fluctuations in the surface heat flux are approximated using equation (Eq. 5.13):

$$Q = -A \sin(2\pi * \frac{\Delta t}{t}) - q \quad (5.13)$$

with  $A$  the amplitude of the variations,  $\Delta t$  the time increment (days),  $t$  the total duration (365 days x 30 years) and  $q = 0.06 \text{ W/m}^2$  the geothermal flux from below.

Using amplitudes of  $A$  ranging from  $0.01$  to  $10 \text{ W/m}^2$ , we find that the expected yearly surface temperature changes can be simulated for  $A = 6 \text{ W/m}^2$  (see black curve in Fig. 5.7). The change in the subsurface temperature under the effect of the fluctuating heat flux is simulated for a period of 20 years. Following a slight increase in

the yearly average surface temperature, a fluctuating steady-state temperature is reached at the surface after a period of about 9 years (see red profile in Fig. 5.7). The last output temperature profile of the simulation ( $t = 30$  years), assumed to no longer be affected by the initial conditions, was therefore used as initial conditions for the subsequent simulations using fluctuating surface heat flux. Fig 5.7 (right) shows that the impact of fluctuating surface heat flux at  $t = 30$  years does not extend further down to 27 m deep, where the average temperature is  $7.4^{\circ}\text{C}$  all year long.

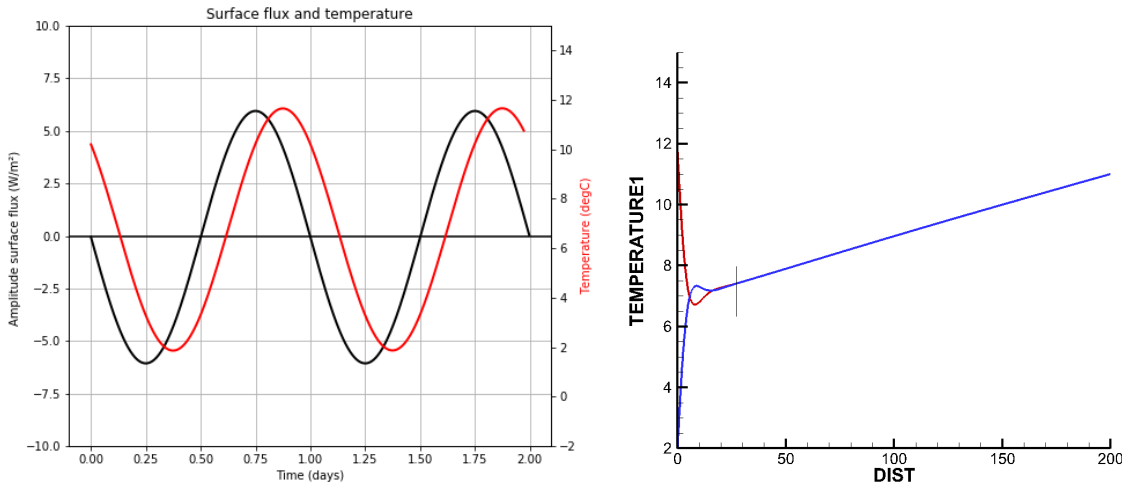


Figure 5.7: left) Surface heat flux input and resulting surface temperature change. The negative flux indicate flux from the ground to the surface (winter) and positive flux from the surface to the ground (summer); right) a. Winter (blue) and summer (red) temperature profiles

We then simulate the change in temperature in the rock mass over time due to heat extraction, using purely diffusive heat transfers within a porous media (i.e. dry porous rock with a conductivity of  $3 \text{ W}^{\circ}\text{.m}$ ). At first, we use the steady state geothermal gradient as initial condition, with constant heat fluxes at the surface and bottom of a 630 m<sup>2</sup> line source (note: following a calculation error, this analysis needs to be corrected to match the mathematical model). Heat is extracted from a BHE situated between 80 and 120 m depth. Two heat extraction scenarios that satisfy the thermal load of a single house are compared. The first one assumes constant heat extraction of  $-1000\text{W}$ , while the second considers seasonal heat extraction, with a minimum of  $-1294 \text{ W}$  in winter and a maximum of  $-706 \text{ W}$  in summer, distributed along the 40m long BHE. The fluctuating heat load is calculated using Eq. 5.13, with  $A = 294 \text{ W}$ , the amplitude of the variations and  $q = 1000 \text{ W}$  the average year heat load. After 30 years of production, similar temperature profiles are obtained (Fig. 5.8), indicating that average yearly extraction rate is representative of a fluctuating extraction rate around this average. In parallel, we assess the impact of the length of the BHE on the final temperature and the temperature distribution within the line source. By dividing the borehole size by two (i.e. 80 to 100 m depth), the specific specific heat absorption of the BHE is doubled (i.e. from  $25$  to  $50 \text{ W/m}$ ). Simulations for a constant and seasonal extraction rates done for a constant surface heat flux are displayed in Fig. 5.8. Results show that reducing the BHE length tends to increase the temperature decrease of the rock mass while maintaining the same thickness of rock affected after 30 years.

We then evaluate the impact of the available stored energy on the temperature decrease in the system, using line source areas of 200, 350 and 600 m<sup>2</sup> and yearly fluctuating surface heat flux. For each case, the solar and

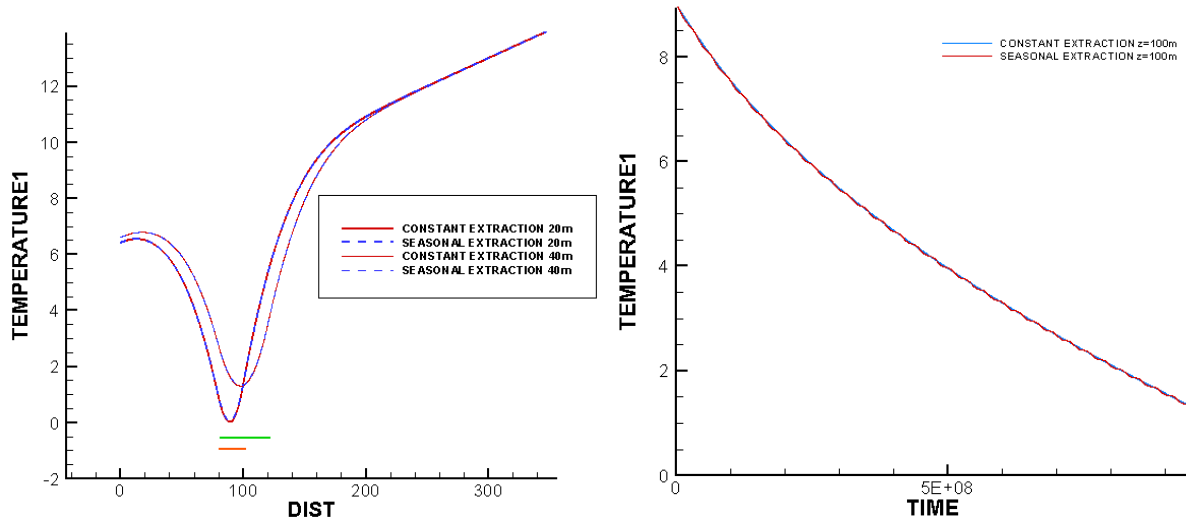


Figure 5.8: Left) Temperature profile for a constant and seasonal extraction rate from a 630 m<sup>2</sup> and 20m (orange) and 40m (green) long BHE after 30 years of production. Right) Temperature changes at 100 m depth under constant and seasonal extraction from a 630 m<sup>2</sup> line source for 30 years

geothermal heat flux are scaled up appropriately and simulations are performed for constant extraction (Fig. 5.9).

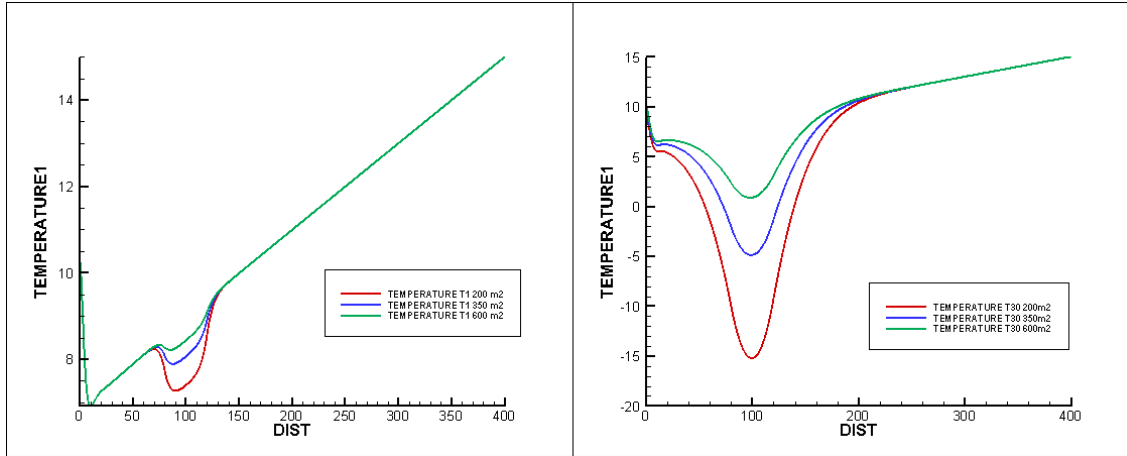


Figure 5.9: Temperature profiles after a) 1 year and b) 30 years, for a constant extraction rate of -1000 W

In those vertical 1D models, recharge is assumed to occur from the surface only half of the year, when the extraction rate is the lowest, while geothermal recharge occurs all year long. Additional simulations are therefore made in order to assess the impact of different boundary conditions on the final temperature profile, comparing results using constant surface and bottom temperature of 7 and 15 °C, respectively, constant flux of -0.06 W/m<sup>2</sup> and/or seasonally fluctuating surface heat flux. Fig. 5.10 shows the temperature profiles for each scenario using a line source area of 630 m<sup>2</sup>, after a production period of 30 years, together with the temperature change over time at 0 and 100 m depth.

As the BHE is located below the depth of influence of yearly solar variations, the temperature change at 100 m is not impacted by the surface boundary conditions. However, in the simulations based on heat flux boundary

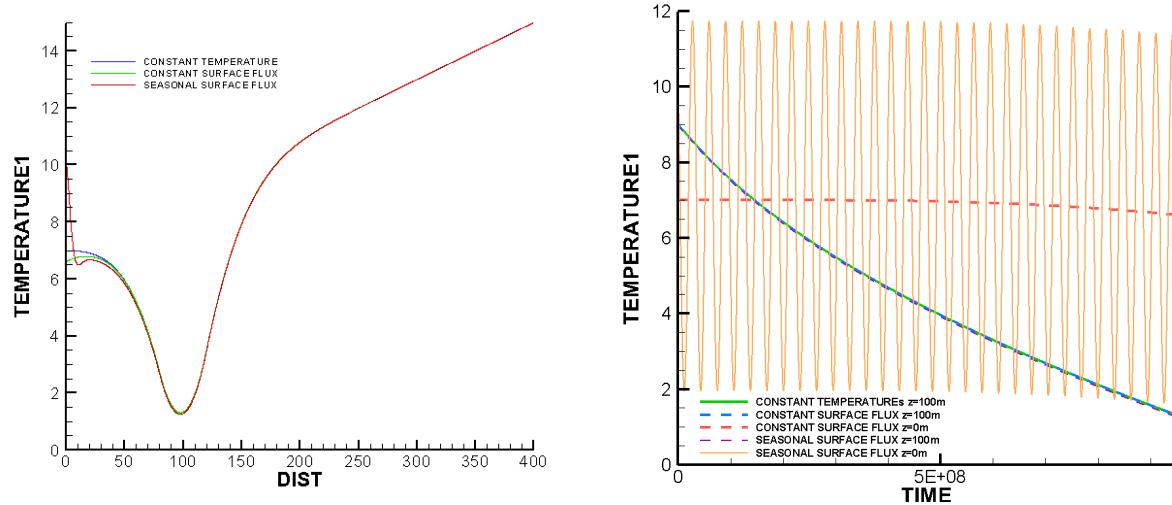


Figure 5.10: a. Temperature profiles and b. Temperature change at 0 and 100m depth due to constant heat extraction using different boundary conditions.

conditions, the ground surface temperature starts to decrease after about 15 years due to the extension of the thickness of the layer of rock that is depleted in heat. However, as no lateral heat flux is allowed in 1D models, no recharge occurs from neighboring areas. Thus, 1D models tend to overestimate the temperature decline and represent a most pessimist case. Next step would therefore to compare results from a 3D model able to represent the transient heat transfers laterally and vertically.

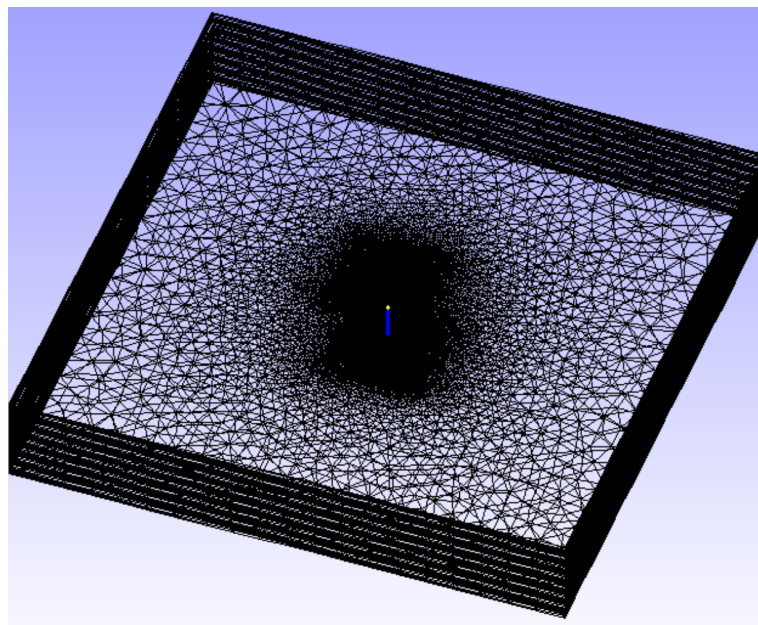


Figure 5.11: 3D FEM mesh for BHE

## Heat flux and time scale analysis

A preliminary analysis on the effect of climate warming since the last Ice Age has been made to evaluate the impact of the temperature profile on the sub-surface heat flux. To achieve this, we used the steady and unsteady geothermal gradients generated from the virtual rock column (Fig. 5.3) and calculated the vertical fluxes at selected time step  $t$  along the profile (see Fig. 5.12 and script available here). For each scenario, we used the heat flux calculated at the surface and at the bottom at  $t = 1000$  yr as boundary conditions for subsequent simulations. Our analysis indicates a surface heat loss of  $-0.066495$  W/m<sup>2</sup> for the steady state gradient while the unsteady gradient allows a surface recharge at a rate of  $+0.01207$  W/m<sup>2</sup>.

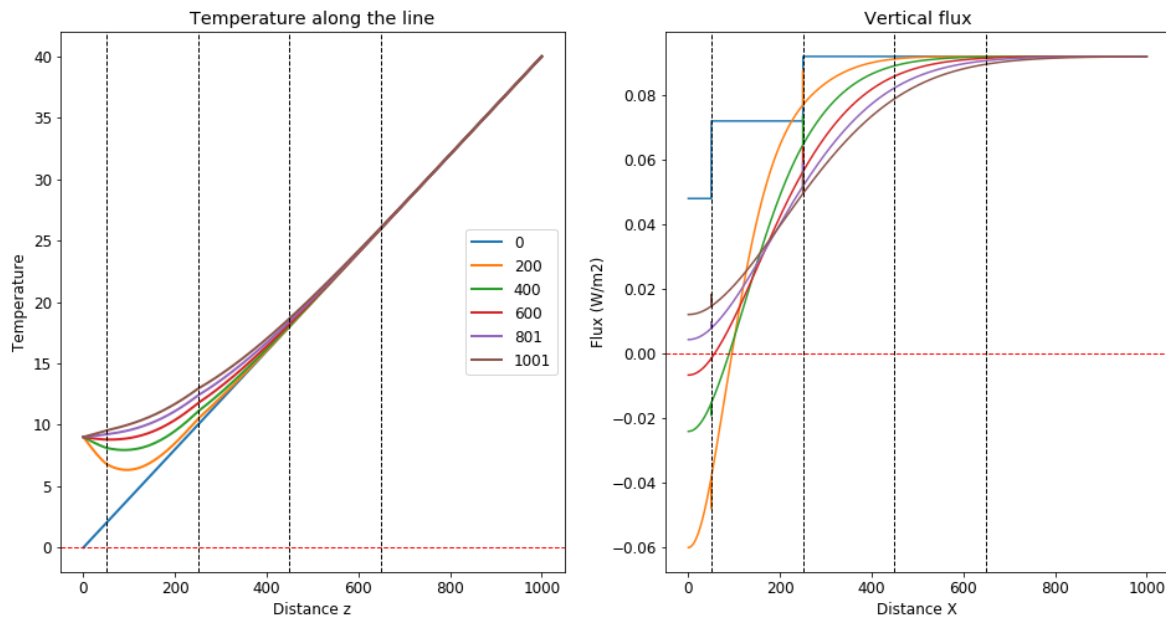


Figure 5.12: Change in temperature profile and heat flux due to climate warming for 1000 years

A first 50-year long simulation was performed to verify that those heat flux boundary conditions can maintain the initial temperature gradients. Results showed that while the surface heat flux for the steady state scenarios tends to be slightly overestimated (cooling of the surface temperature by  $0.15^\circ\text{C}$  in 50 years), the heat flux used for the unsteady situation led to a slight temperature increase at the surface (about  $0.5^\circ\text{C}$ ). A varying heat flux of about  $\pm 6$  W/m<sup>2</sup> was then added at the surface, based on Eq. 5.13. In both cases, surface temperature reach a fluctuating steady state, after about 7 and 20 years for the unsteady and steady state scenarios, respectively.

Production was finally added at a rate of 1 W, distributed along a polyline located in the mudstone layer at 50-90 m depth. The low heat flow has been chosen to account for the small geometrical area (1 m<sup>2</sup>) of the polyline used here. Resulting fluxes induced in the unsteady temperature gradient case are displayed in Fig. 5.13. While temperature at the surface tends to decrease by  $2^\circ\text{C}$  in this scenario (Fig. 5.14), a decline of  $3^\circ\text{C}$  was observed in the steady state scenario. Considering unsteady geothermal gradient would therefore enhance heat fluxes from the surface (i.e. increase solar recharge), reducing the impact of heat extraction in the subsurface on the ground surface temperature.

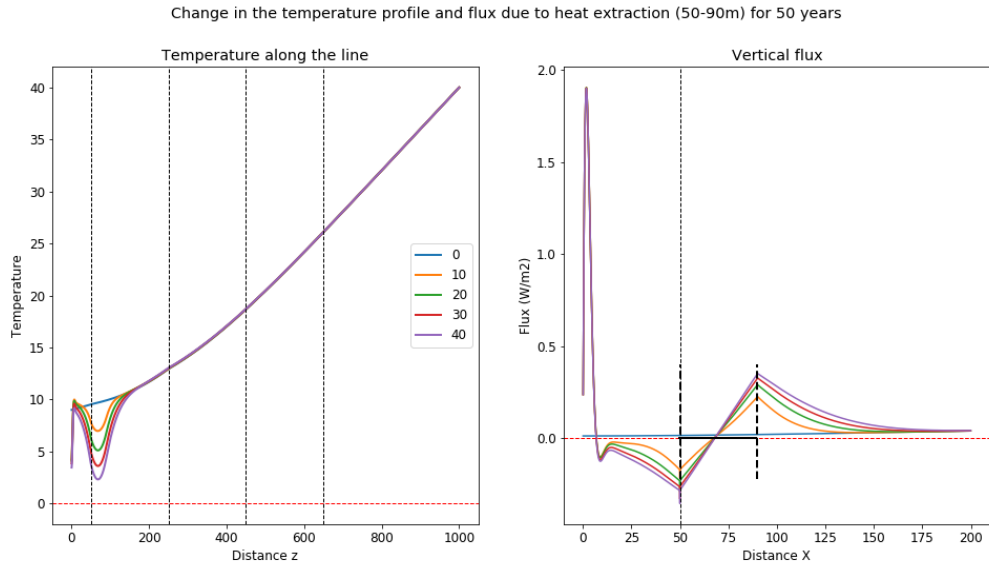


Figure 5.13: Change in temperature profile and heat fluxes due to heat extraction from a borehole, using an unsteady temperature gradient

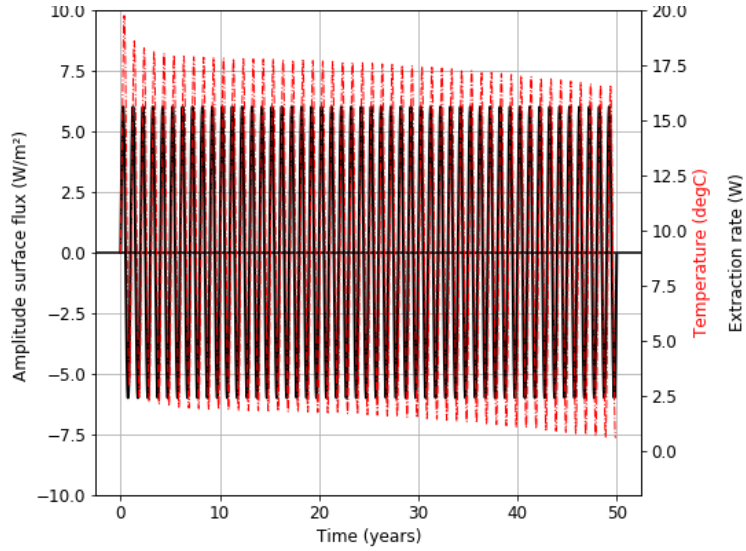


Figure 5.14: Surface flux and resulting surface temperature due to a 1 W extraction rate from a borehole, with unsteady temperature gradient

### 5.6.3 2D heat diffusion-advection

#### Benchmarking

Modelling of diffusive and advective heat transfers with OpenGeosys are assessed through the analysis of the propagation of a heat pulse within 1D and 2D homogeneous incompressible media. The porous media have a density of  $2500 \text{ kg/m}^3$ , a thermal expansion of  $1 \times 10^{-5}$ , a thermal capacity of  $1280 \text{ J/kg}^\circ\text{C}$ , and a conductivity of  $2.78 \text{ W}/^\circ\text{C.m}$ . Considering a permeability of  $k = 2.184 \times 10^{-13} \text{ m}^2$  and fluid viscosity  $\mu = 1.8 \times 10^{-5} \text{ Pa.s}$ ,

a head gradient  $\Delta P = 20000 \text{ Pa}$  along a distance  $\Delta x = 0.96 \text{ m}$  allows groundwater to flow eastward at a Darcy velocity of  $u_x = 2.5 \times 10^{-3} \text{ m/s}$ , according to the following equation:

$$u_x = k \frac{\Delta P}{\Delta x} \frac{1}{u} \quad (5.14)$$

The circulating fluid has a specific heat capacity of  $4068 \text{ J/kg } ^\circ\text{C}$  and a heat conductivity of  $0.63 \text{ W}/^\circ\text{C.m}$ . The propagation of constant heat or heat pulse injected for 1 sec at  $t = 0$  within the model of initial temperature  $T_0 = 0$   $^\circ\text{C}$  are first solved numerically for a 1D line model. The heat source corresponds to a fixed temperature  $T_1 = 100$   $^\circ\text{C}$  situated on the left boundary of the model. For each model, we evaluate the impact of the mesh size (1 and 8 mm line elements) and of the material porosity (0.1 and 0.5) on the final temperature distribution (at  $t = 1000 \text{ s}$ ). Results are then compared for a 2D domain composed of 480 quadratic elements for the 8mm mesh and of 34560 elements for the 1 mm mesh, and for different dispersivity values (0 or  $0.1 \text{ m}^2$ ). Figs A.5 and A.6 show the results for the benchmark analysis together with final temperature distribution in the 2D domains, temperature profiles and time-series for both pulse and continuous injections. In addition, we attempt to validate numerical results against the corresponding analytical solutions, using Python. This approach is essential to verify the validity of the numerical solutions and be able to better discriminate between the heat transfers mechanisms taking place throughout space and time, when groundwater circulation is involved. Results are displayed in appendix A.4.

### **Assessment of the potential geometrical simplifications for mine system modeling**

We explore the possibility of creating a stack of highly permeable layers (i.e. mined coal seams) versus host rock to evaluate the impact of reservoir geometry on overall temperature change and timing of heat depletion in terms of thermal energy content. To do this, we first extended the initial 2D benchmark model to evaluate the effect of various rock properties and the contribution from thin layers ( $h = 0.1 \text{ m}$  or  $0.2 \text{ m}$ ) situated above and below the original  $0.36 \text{ m}$  thick model, on the final heat distribution. Results are shown in appendix A.5 (Figs A.7 to A.9).

Then a complex model is created, composed of 3 porous coal seams ( $0.02 \text{ m}$  thick) in between 4 host rock layers ( $0.05 \text{ m}$  thick). The whole model is embedded within two  $0.01 \text{ m}$  thick impermeable layers, resulting in a total model thickness of  $0.28 \text{ m}$ . In the "sandwich model" (term used by Le Brun et al., 2011 for modelling of the Dogger Aquifer, France), the stacked permeable coal beds ( $0.06 \text{ m}$  thick) are embedded between two  $0.1 \text{ m}$  thick host rock layers. In a first set of simulations (V1), rock properties similar to those used in the benchmark analysis are attributed to the different layers (see Fig. 5.15). In a second set of simulations, rock properties are defined accordingly to those likely to be found in mine systems. Four different classes of materials have been used in the literature to describe the mine. It includes the unaltered rock (i.e. quasi-impermeable, homogeneous, isotropic and unconfined porous medium, with  $0.1\%$  porosity,  $K = 1 \times 10^{-7} \text{ m/s}$ , i.e. Fandos et al., 2004), the mined volume (i.e. altered material in the zone between galleries, with various porosity range  $2-22\%$  and  $K = 2 \times 10^{-4}$ , i.e. Andres et al., 2017), the open voids (i.e. galleries with rectangular cross sections and circular shafts, with  $\phi = 100\%$   $K = 1$  to  $5 \text{ m/s}$ , i.e. Renz et al., 2009) and the overlying strata ( $K = 1 \times 10^{-4}$ , i.e. Zhai et al., 2019). The permeability is calculated from the hydraulic conductivity  $K$ , the fluid viscosity  $u$  and the fluid density as followed:

$$k = \frac{Ku}{\rho g} \quad (5.15)$$

V1	Impermeable boundary	Coal	Host rock:
	n = 0.01	n = 0.25	n = 0.1
	k = 2.184e-17 m <sup>2</sup>	k = 2.184e-7 m <sup>2</sup>	k = 2.184e-13 m <sup>2</sup>
	K <sub>th</sub> = 1.3 W/C.m	K <sub>th</sub> = 0.40 W/C.m	K <sub>th</sub> = 2.2 W/C.m
	c = 950 J/kg.C	c = 1300 J/kg.C	c = 950 J/kg.C
	rho = 2500 kg/m <sup>3</sup>	rho = 2500 kg/m <sup>3</sup>	rho = 2500 kg/m <sup>3</sup>
V2	Impermeable boundary	Coal	Host rock:
	n = 0.05	n = 0.25	n = 0.1
	k = 1e-17 m <sup>2</sup>	k = 2e-11 m <sup>2</sup>	k = 1e-14 m <sup>2</sup>
	K <sub>th</sub> = 1.3 W/C.m	K <sub>th</sub> = 0.40 W/C.m	K <sub>th</sub> = 2.2 W/C.m
	c = 950 J/kg.C	c = 1300 J/kg.C	c = 950 J/kg.C
	rho = 2500 kg/m <sup>3</sup>	rho = 2500 kg/m <sup>3</sup>	rho = 2500 kg/m <sup>3</sup>

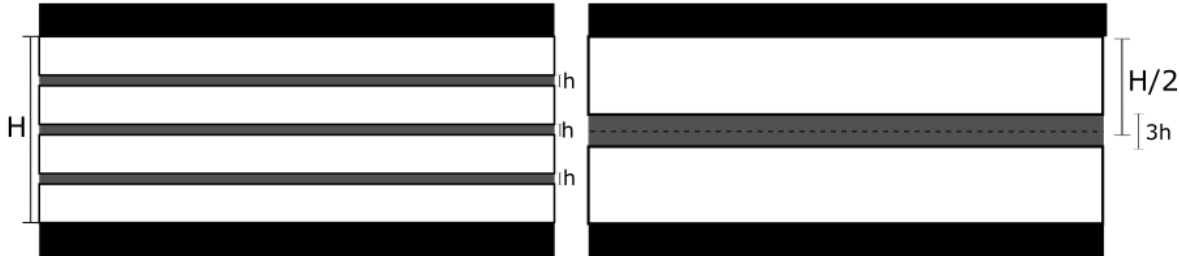


Figure 5.15: Rock properties for model complex and simplified "sandwich" model

The resulting temperature distribution, vertical/horizontal temperature profiles and temperature time series are displayed in figures A.10, A.11 and A.12, respectively. In addition, we integrated the element temperature within the models for each time steps in order to get an insight on the overall change in energy stored in the system, depending on the modeling approach (Fig. A.12). Results suggest that the sandwich model tends to highly underestimate the overall temperature change within the model. Finally, a code (available here: part 1 and part 2), is being developed in order to visualize the net horizontal and vertical heat fluxes within the 2D model (A.13), but more work is necessary to determine the relative contribution from convective/diffusive flux.

## 5.7 Conclusion and research outputs

We aim at publishing a first paper in the near future based on the purely-conductive heat extraction model. The objective of the paper will be to demonstrate that long-term energy balance requires external energy input to the ground in order to ensure sustainable heat extraction. Then, the effect of advective groundwater will be added to the analysis, in order to evaluate its contribution on heat recovery. Sensitivity analysis will be required to better understand how the permeability contrasts between different layers, their porosity, thermal conductivity and geometrical arrangement impact the heat fluxes during production and contribute to the overall temperature change over time. We will also study the results through steady-state simulations and determine the time necessary for the systems to reach equilibrium, based on the modeling approach. From this, energy balance calculations will be made and the area of influence of heat extraction determined.

# **6 Chapter 2: Thermal state of the mine**

## **6.1 Background**

Until the 1990's, most of mine modeling studies aimed at predicting water rebound in mines after the cessation of the mining activities and the stop of dewatering. In those studies (i.e. Younger and Adams, 1999), the authors developed strategies to create realistic but simplified representation of mine workings and of the hydraulic problem. More recently, the growing interest in evaluating the geothermal potential of flooded coal mines worldwide increased the complexity of mine modelling through the addition of the heat transfer problem.

In mine modeling, initial temperature distribution and surface/bottom boundary conditions are generally set up accordingly to the local geothermal gradient, with the mine water temperature being in thermal equilibrium with the rock mass. Constant heat flux and constant or variable temperature conditions (i.e Andrés et al., 2017) are commonly attributed to the bottom and surface boundaries, respectively.

In the UK, Gillespie et al., 2013 however pointed out the lack of correlation between the temperature of the mine-water measured in mine shafts and the depth of measurements. It was therefore suggested that other parameters are controlling the mine water temperature in addition to the geothermal gradient or that temperature gradients in mines may therefore not represent purely conductive heat flows (Beamish and Busby, 2016). Another possibility is that the geothermal gradient in mines does not follow the regional gradient. During mining activities, water is indeed pumped to allow access to deep part of the mine and air-ventilation is installed to guarantee the removal of gas and dust in the underground mine, minimize the stresses on the equipment and ensure safe conditions for the miners (Anderson and De Souza, 2017; Małolepszy, 2003). The inflow of cold air in the pumped sections of the mine is therefore expected to decrease temperature in the galleries. On the other hands the remains of highly conductive mining voids after the flooding of the mine tends to create large-scale interconnections between different parts of the mines or between aquifers previously isolated. Such hydraulic perturbations might favor advection of heat and explain the perturbations of the geothermal gradient in mines.

Despite it is well known that extensive periods of mining activities would have disturbed temperatures in mines and affected virgin rock temperatures (Tammemagi and Wheildon, 1974), only a few studies considered the effect of early mining activities on the thermal state of flooded mines before the start of geothermal production. Małolepszy, 2003 estimated the rate of cooling of the rock mass resulting from ventilation in the Nowa Ruda mine in Poland, using measurements of rock temperatures taken during periods of mining. In the vertical 2D model representing a geological cross-section preserving the dips and thickness of the rock beds, the authors calculated the natural-state conditions in the mine by simulating the conditions under mining activity (assuming a cooling of 8 °C) and the temperature recovery in the working after the stop of the mining activities. After a period of mining of over 200 years and a subsequent flooding period of 5 years, the authors showed that about 10 years would be required for the rock of the to heat up back to its initial temperature of 23 °C at 890 m depth.

## 6.2 Research Gaps

Despite many mine modeling studies have been performed to estimate the geothermal potential of worldwide mines as well as the sustainability of heat production, only one considered to our knowledge the effects of past mining activities and flooding on initial temperature distribution within the mines. Knowing the time for the mine to return to its undisturbed thermal state (i.e. equilibrium with regional gradient) and the temperature distribution before geothermal production is however essential to assess the initial heat capacity of the mine and understand the heat fluxes that might participate to heat recharge.

## 6.3 Aims and methods

The study aims at understanding the temperature distribution in deep coal mines before production start, and the effect of the duration of the mining and flooding periods. We will attempt to quantify the cooling induced by air and cold water infiltration during mining and the time required for heat recovery during water rebound, to understand the perturbations of the geothermal gradient induced by mining activities. Available mining and post-mining data (i.e. water level, temperature time series and profiles, timing and location of mining activities, volume of residual voids) will be used to verify our analysis and evaluate the potential impact of mining activities on the current hydraulic and thermal state of the mines, depending on their current state (i.e. flooded, in current recovery...) and geological context.

We will moreover assess the influence of the hydraulic lateral and bottom boundary conditions on temperature distribution within the mines using simple 2D numerical model. In the literature, hydraulic boundaries to model are generally set as no flow boundaries, and away from the mine system to limit their influence on the results (i.e. Raymond and Therrien, 2008; Ghoreishi-Madiseh et al., 2012). This assumes that mines are hydraulically isolated from other systems.

## 6.4 Research questions

What is the impact of past mining activities on the thermal state and temperature distribution in mines?

- Does the temperature gradient in mines re-equilibrate with the undisturbed regional gradient after a period of mining with ventilation/dewatering and a subsequent period of flooding?
- How does water advection in large voids impact the temperature distribution in mines?
  - Are the mine waters at equilibrium with the host rock temperature?
  - What is the rate of heat exchange between the recharge mine-water and the surrounding host rock in mined areas and in tunnels, depending on the origin/temperature of recharge water, on its flow rate, on the flow path length and on the properties of the host rock.
- Can we reproduce temperature profiles in shafts during flooding, heat/water recovery and during production, using numerical modelling?

## 6.5 Hypothesis

- H0 - The geothermal gradient in the flooded mine reaches a state of "partial equilibrium" within 20 years after flooding is completed.
- H1 – The temperature gradient in mines follow the regional trend, with a dominant conductive heat profile in the host rock and isothermal conditions in tunnels/shafts.
- H2 - The temperature of mine water is in equilibrium with the rock temperature in goaf materials, but mainly depends on the source/depth of water recharge and on the residence time of water in tunnels.
- H3 – It is possible to simulate both recovery rate and temperature profiles in shaft during flooding, heat recovery and production to fit existing data when appropriate boundary conditions are set.

## 6.6 Preliminary results

### 6.6.1 Model set up

The two-dimensional vertical model consists of three horizontal coal seams embedded in an homogeneous host rock. A stapple shaft is connecting the seams on the western side of the model and a deep shaft is connecting the seams from the surface on the eastern side. The seams are 3 m thick and the main and staple shafts are 6 and 3 m in diameter, respectively. Each element (i.e. host rock, seams, shaft) are assumed to be porous materials with different solid, hydraulic and thermal properties.

### 6.6.2 Initial and boundary conditions

We simulate change in head and temperature over time, during mining, after mining (i.e. water rebound), and during pumping for geothermal utilization purpose, using different boundary conditions. Initial steady state conditions are first calculated during an initial run, depending on the different scenarios. Those are summarized below and include:

- Thermal boundary conditions: geothermal gradient of 0.027 °C
  - Constant temperatures of 9.5 °C and 18.2 °C at the top and bottom, respectively.
  - Constant vertical flux of 0.06 W/m<sup>2</sup> in and out of the model.
- Hydraulic boundary conditions
  - Fixed head boundary conditions of 0 m on both west and east boundaries, with a constant head of 0 m across the model.
  - Fixed head boundary conditions of 0 and -100 m on the west and east BC, respectively, with a head gradient from west to east.
  - Horizontal flux of 4e-6 m<sup>3</sup>/s from west to east (corresponding to the 100 m head difference).

- Inflow of 4e-6 m<sup>3</sup>/s from west (initial head of 100 m) with constant head of 0 m on the east.
- Outflow of -2e-6 m<sup>3</sup>/s on the east (initial head of -100 m) with constant head of -50 m on the west (unsaturated system with initial head difference of 50 m).

For each scenarios, initial conditions were calculated from Dirichlet-type boundary conditions in a steady-state simulation without extraction of mine water or precipitation (i.e. undisturbed situation. In scenarios where hydraulic and thermal fluxes are used, undisturbed conditions are then simulated using the corresponding Neumann-type boundary conditions to ensure stable initial conditions before simulating flows under mining conditions. The equivalences between Dirichlet boundary conditions (i.e. constant head or constant temperature) and Neumann boundary conditions (i.e. thermal / hydraulic fluxes) are calculated according to Eq. 6.1.

$$q = K \frac{dh}{dx} \quad (6.1)$$

We assume that the model is saturated with water with a density of 1000 kg/m<sup>3</sup>, a viscosity of 1e-3 Pa.s, a specific heat capacity of 4680 J/Kg.K and heat conductivity of 0.6 W/m.K.

### 6.6.3 Material properties

The initial undisturbed temperature and head distributions are determined for a uniform porous aquifer interbedded with three coal seams. During simulations under mining and flooding conditions, different hydraulic property values (i.e. porosity, hydraulic conductivity and storage coefficient values) are assigned to the mined area, shafts and coal beds to account for the changes induced by mining activities. Those were attributed based on existing data for the Carboniferous strata in the UK and on previous hydraulic modelling studies in mines, and are summarized in Table 6.1.

Zone	Host rock		Minced area		Seams		Shaft	
Simulation	1	2	1	2	1	2	1	2
Porosity (%)	0.1	0.1	0.1	0.15	0.05	0.25	0.1	1
Hydraulic Conductivity K (m/s)	1e-7	1e-7	1e-7	1e-5	0.5e-7	1e-2	1e-7	1
Storage Coefficient S	1e-5	1e-5	1e-5	1e-5	1e-5	2e-4	1e-5	1

Table 6.1: Summary of the hydraulic properties for each material/elements used in (1) steady-state and (2) mining/flooding/production simulations. Values of storage for the workings area and host rock are based on Raymond and Therrien, 2008. In their study, the authors suggested values of Hydraulic conductivity of 2.30E-02 and 4.50E-05 m/s and porosities of 0.25 and 0.05 for the workings and host rock, respectively.

Thermal properties for the Carboniferous rocks of the Midland Valley of Scotland are summarized in Table A.1. Average matrix thermal conductivity of 0.31 W/m.K and 1.7 W/m.K have been reported for coal and goaf (i.e. unconsolidated roof material), respectively, in Herrin and Deming, 1996. Due to fracturing and partial filling of the coal with water, its bulk thermal conductivity has however been suggested to raise up to a value of 0.4 W/m.K (Herrin and Deming, 1996). Here, thermal properties are kept constant for all simulations and scenarios. For the host rock, we assume a thermal conductivity k and thermal capacity c of 3.14 W/m.K and 950

J/Kg.K, respectively. The seams have values of  $k = 0.31 \text{ W/m.K}$  and  $c = 1380 \text{ J/Kg.K}$ . All elements are attributed a thermal expansion coefficient of  $1e-5$ . In Guo et al., 2018, different densities are attributed to the mining area to account for the difference between the intact and the fractured rock due to mining. We here assume that the host rock and the seams have densities of  $2650 \text{ kg/m}^3$  and  $1500 \text{ kg/m}^3$ , respectively, for all simulations. We finally assume an isotropic heat dispersion coefficient of  $0.5 \text{ m}$  to account for the size of the mesh in the wells.

#### 6.6.4 Water extraction

For all scenarios, water extraction during mining activities (i.e. dewatering) is simulated for a period of 30 years using an extraction rate of  $-0.01$ ,  $-0.08$  or  $-1e-4 \text{ m}^3/\text{s}$ . We then simulate water recovery for a period of 50 years in order to evaluate the time necessary for the geothermal gradient to re-equilibrate within the mined area. Finally, we simulate pumping for geothermal utilization purpose for a period of 30 years following the flooding of the mine. For each scenario, we moreover compare the evolution of the temperature profile with cases where surface inflow (i.e. precipitation) is added. To evaluate the impact of the pumping depth on the temperature profile in the shaft, we finally perform a series of simulation in mining or production conditions using three different pumping depth: between 50-70 m, between 110-130 m and between 150-170m. For each situation, the chosen flow is divided accordingly between the nodes intersecting the borehole line.

### 6.7 Results and research outputs

Results are displayed in Figs 6.1 to 6.3. Preliminary analysis showed that the use of different material properties in the dewatering simulation relative to those used for the initial undisturbed conditions simulations tend to create instabilities in the beginning of the simulation. The significance of the choice of different boundary conditions will be used to determine the main processes and rate of heat recharge. The objective will be to improve those preliminary models to produce similar temperature profiles than the ones measured in shafts of the study areas. Conductivity profiles could moreover be used as an additional data source for the model calibration, both as hydraulic constraints (i.e. define the origin of water depending on its temperature/salinity) or thermal constraint (i.e. density relative free-convection in open voids). This would imply the addition of a mass transport term in the numerical simulations. Examples of temperature/conductivity logs in the Bilston Glen shafts and Dawdon Victoria shaft are shown in Fig. 6.4 and Fig. 6.5.

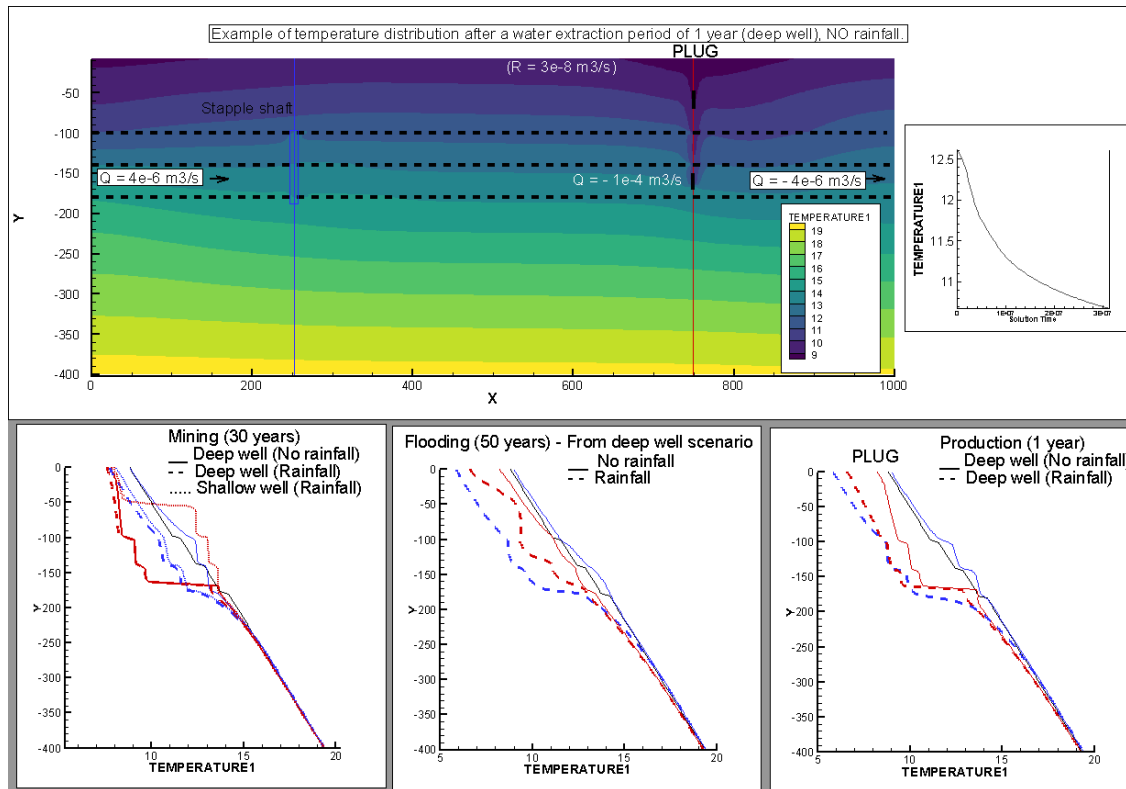


Figure 6.1: Results using hydraulic flux across the model

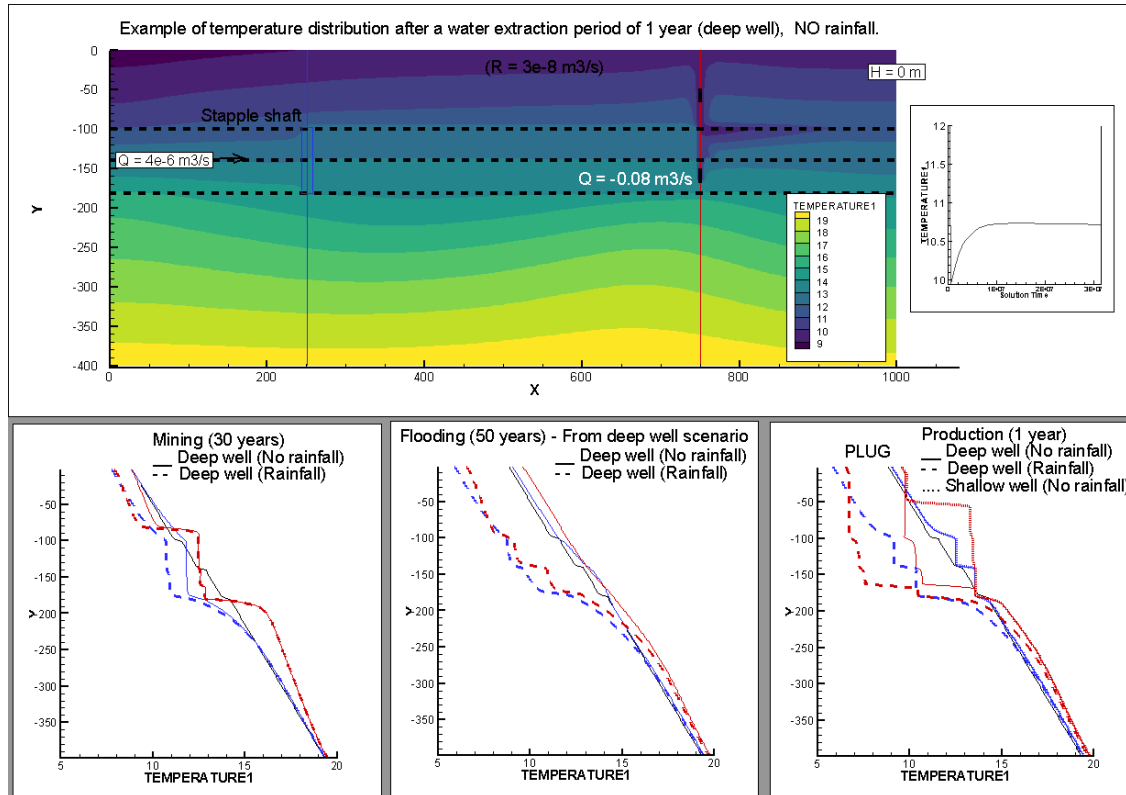


Figure 6.2: Results using entering flux on the west and fixed head on the east

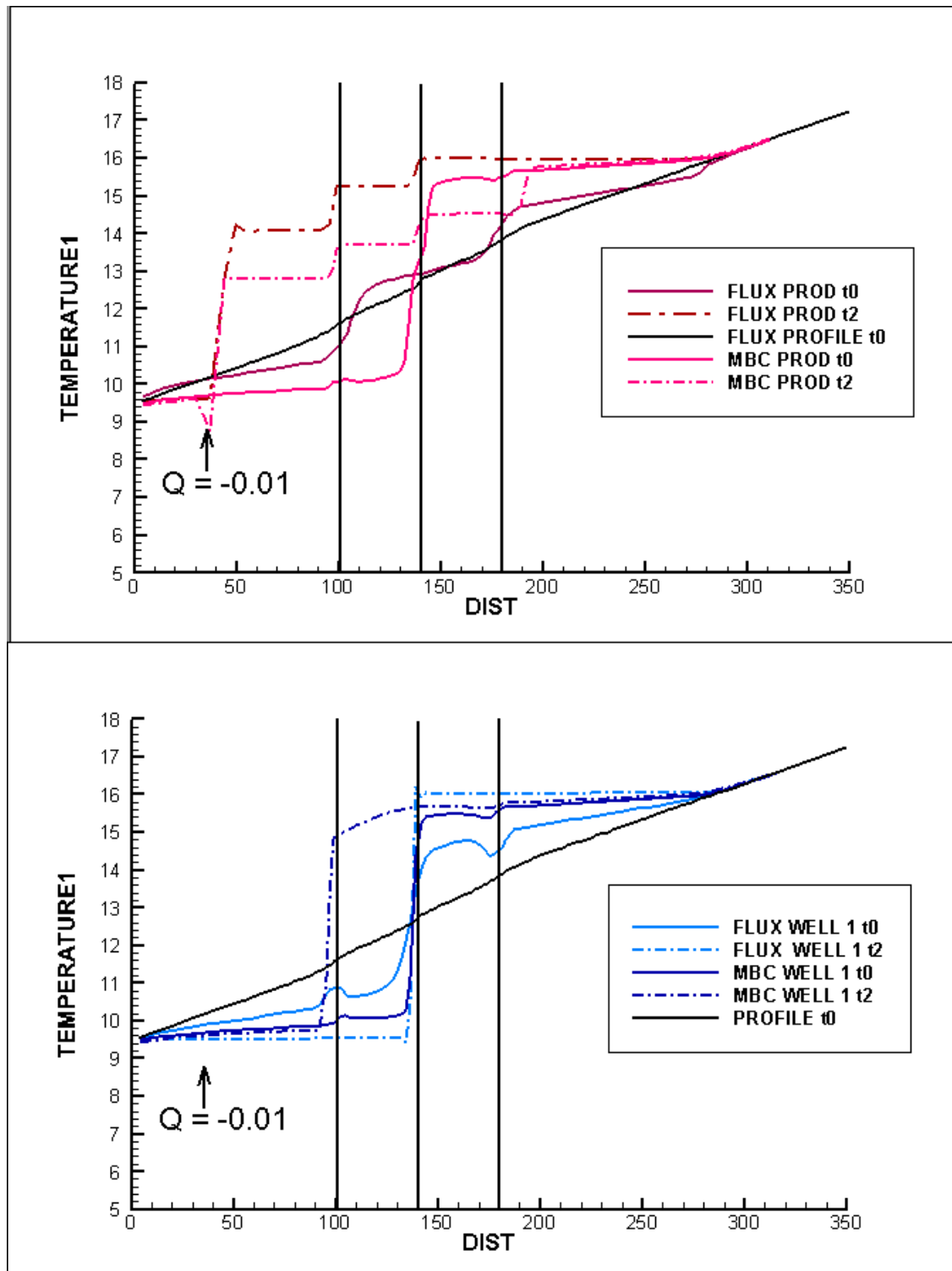


Figure 6.3: Results using closer well distance (shallow water extraction from undisturbed situation)

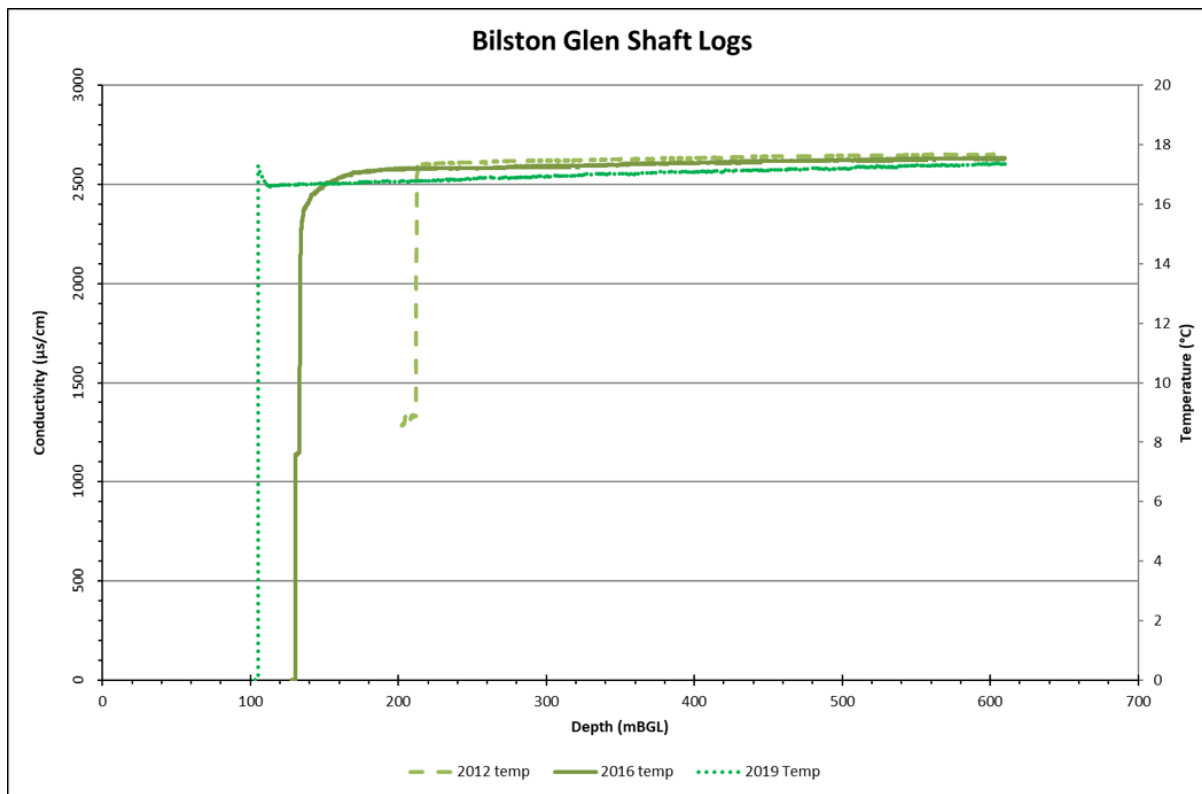


Figure 6.4: Bilston Glen a shaft logs

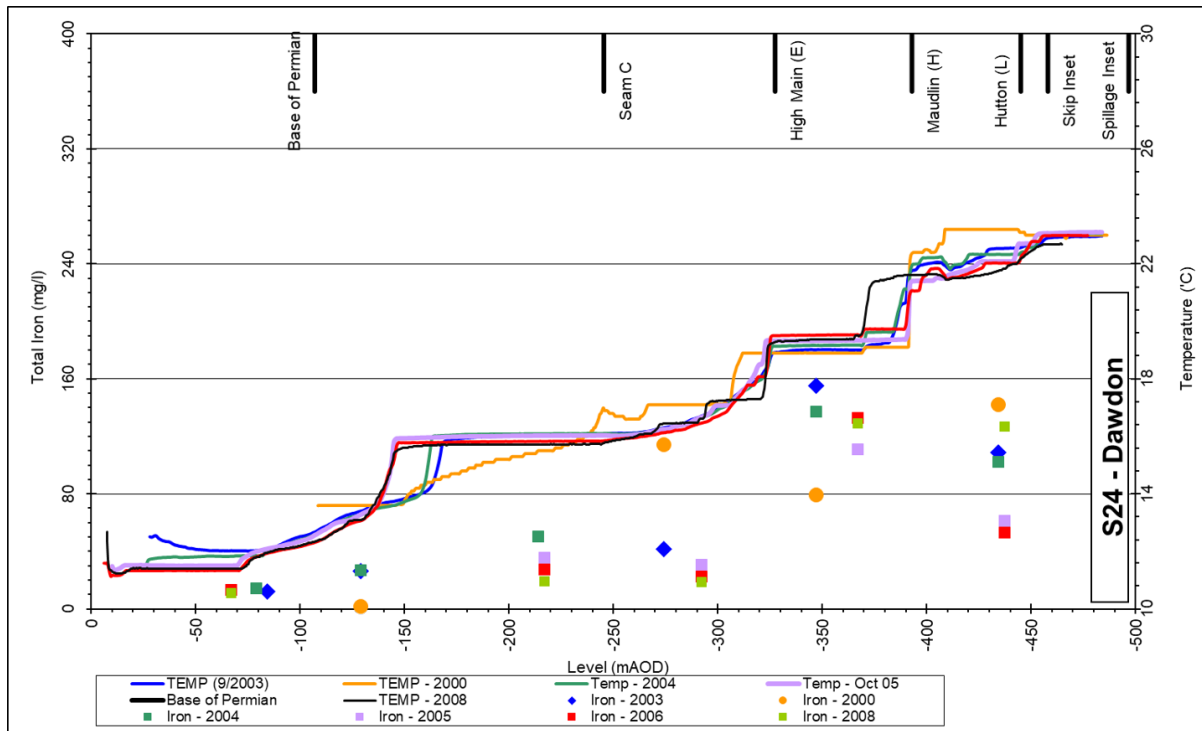


Figure 6.5: Dawdon shaft logs

# **7 Chapter 3: Recharge potential of the Midlothian and Dawdon-Horden coalfields: an investigation of the key features for thermal modeling of flooded coal mines**

## **7.1 Background**

### **7.1.1 Numerical approaches for mine systems**

Past researches involving modeling of abandoned flooded coal mines have been faces to the important difficulties arising from the complex geometry of the mine workings. In most of the studies, abandoned coal mine reservoirs have been described as a dual-porosity medium (i.e. Renz et al., 2009; Guo et al., 2018; Raymond and Therrien, 2008, composed of two main domains:

- The mine open voids, that are assimilated to tunnels of simple geometries. There, the heat transfer problem can be view in a similar way to heat exchanger, allowing to solve for simple 1D heat transfer equations using either semi-empirical method (Rodríguez and Díaz, 2009), analytical (e.g. Lauwerier-Pruess-Bovardsson model, Pruess and Bodvarsson, 1983; Lauwerier, 1955) or numerical model (e.g. Loredo et al., 2016; Renz et al., 2009; Ghoreishi-Madiseh et al., 2012).
- The mined areas, that corresponds to the volume surrounding the open mine voids. It is composed of different type of materials (i.e. "goaf", fractured rock) with secondary porosity that is closely related to the mining method and the roof conditions (e.g. Guo et al., 2018; Esterhuizen and Karacan, 2007).

In mine reservoir modeling, the main difficulty arises from the necessity to solve simultaneously for heat transfer and mass flow within a porous matrix (i.e. undisturbed rock, galleries, "goaf", caverns and drivings), open pipes (i.e. shafts, roadways, tunnels) or fractures (Ferket et al., 2011; Renz et al., 2009). Different approaches have been used in the literature to represent mining voids (Renz et al., 2009) whilst avoiding numerical instabilities caused by the permeability contrasts between the open mining voids (i.e. dominantly turbulent flow) and the porous aquifers (i.e. dominated by laminar flow). This ranges from the combination of 2D/3D porous media approaches with 1-D pipe flow (Adams and Parkin, 2002; Raymond and Therrien, 2008) to the assimilation of the mine as a porous media with different hydraulic conductivities (i.e. host rock and mining voids) dominated by Darcy flows (e.g. Małolepszy, 2003).

For complex real-case mine modeling studies, Raymond and Therrien, 2008 and Andrés et al., 2017 suggested to model the pipe network (i.e. shafts and roadways) as 1D elements embedded within a 3D mesh representing the porous mine aquifer. Despite 1D elements cannot model turbulent flows, interactions between the intact strata of

the mine aquifer and the conduits in mined out areas have been successfully modelled using this approach. Renz et al., 2009 combined the Darcy equation to solve for laminar flow in the porous rock mass (e.g. Diersch, 2005), the Hagen–Poiseuille equations (i.e. slow-moving laminar pipe flow), and the Manning–Strickler equation for 1D pipe/channel turbulent flow (e.g. Diersch, 2005). Similarly, Ferket et al., 2011 used coupled analytical models of heat transfer in mine void and discrete ‘pipe network’ hydraulic models based on semi-empirical approach (Rodríguez and Díaz, 2009) to determine the heat capacity of the Asturias mine in Spain. This model was able to simulate both heat transfers between water and pipe walls and advective flow within a system of complex geometry, using a hybrid node-loop approach.

### 7.1.2 Void volume estimates

Several methods have been deployed to derive estimates of the residual void volume in mines. Those methods imply taking into account the initial amount of void and scale it by a factor accounting for backfilling, subsidence and induced fracturing. Jessop, 1995 suggested that this factor is in the order of 25%, both in longwall and pillar-and-stall mining areas, while Małolepszy, 2003 considered that 5-40% of the initial volume of the mined space remains open depending on the mining method employed. In room and pillar mining method, pillars and open spaces are generally left in place, and only small and local convergence of the roof/floor is expected. Few debris resulting from roof falls are found on the floor and are assumed to be compensated by the creation of voids in the roof. For Younger et al., 2002, 50% of void mines are therefore likely to remain open if no collapse occurs. In contrast, the formation of goaf and the convergence of the workings roof/floor in longwall mining areas generally tend to fill the mined area, reducing the initial void volume in the workings. Gillespie et al., 2013 suggested that about 20% of the mine voids remain after subsidence above longwall panels, while Younger and Adams, 1999 attributed to goaf a porosity of 30% after subsidence and fracturing. Whitworth, 2002 considered that residual void volume in longwall mining area represent 10% of the extracted height in areas of total extraction. The initial void volume can generally be calculated from the volume of coal extracted. As this value is rarely known, Andrés et al., 2017 derived the volume of coal extracted from the mass of coal extracted in the Asturias mine, available from coal production data, and from the mean density of the excavated rock. Other studies suggested to use pumping rate or water recovery data to derive the post-mining void volume.

### 7.1.3 Geothermal potential estimates

Several modeling strategies have been employed to assess the geothermal potential and sustainability of heat production from abandoned flooded mines. In Ghoreishi-Madiseh et al., 2012, the thermal breakthrough issue is addressed by assimilating the mine as a horizontal tunnel, in which cold water is injected at the entrance and produced at the other end after flowing through the tunnel. While conductive heat fluxes are generated along the axe of the tunnel, heat recharge to the water is here mainly attributed to radial conductive heat transfers from the surrounding rock mass, ignoring the effects of natural convection inside the rock mass (i.e. heat advection). On the other hands, Guo et al., 2018 studied the effects of secondary porosity within the fracture zone that generally develops above mined-out area was using a FDM approach. There, the mine was considered as a dual-porosity medium composed of a homogeneous caved zone (i.e. isotropic goaf material) and an overlying fracture zone (i.e. anisotropic medium with regular vertical fractures), surrounded by a large continuous media.

Analytical solutions for heat transport (e.g. Banks, 2009, although necessary to validate numerical models, generally express single processes at the time and does not give an overall understanding of the heat fluxes and recharge potential. Heat transfers in complex system therefore need to be solved through numerical approximations. Numerical models of existing worldwide coal mines includes the Gaspe Mines in Quebec (Raymond and Therrien, 2008), the Nowa Ruda coal mine in Poland (Małolepszy, 2003), the Asturias mine in Spain (Andrés et al., 2017; Renz et al., 2009) or mines in France (Hamm and Bazargan Sabet, 2010). The main conclusions resulting from those studies are summarized below:

- The sustainability of heat production from mines highly depends on the relative contribution of advective/conductive heat transfers, the impact of induced flow circuits, the time required to recover thermal equilibrium between the rock and the water after production.
- The sustainable rate of heat extraction from mine tunnels depends on the thermal conductivity of the surrounding rocks (Ghoreishi-Madiseh et al., 2012). The dimensions of the tunnel tends to impact the total recoverable heat from the mine.
- Backfilled stopes have great potential for sustainable geothermal heat production, with the main heat transfer mechanism being conduction (Ghoreishi-Madiseh et al., 2015).
- The geothermal potential of mines depends on the height of the fracture zone. The permeability of the roof is beneficial to heat transfer, while the fracture permeability in the fractured zone tends to decrease the production temperature (Guo et al., 2018).
- The heat extraction rate is related to the injection temperature (Guo et al., 2018).
- Seasonal heat extraction allow better heat recovery and sustainable heat extraction (Ghoreishi-Madiseh et al., 2012; Hall et al., 2011; Hamm and Bazargan Sabet, 2010).
- For hydraulic conductivity contrasts between the mine void  $K_{mine}$  and the rock  $K_r < 1 \times 10^5 m/s$ , the higher the  $K_{mine}$ , the smaller the decrease in extraction temperature. For higher contrasts, the higher the  $K_{mine}$ , the greater/quicker is the decrease in extraction temperature. From  $K = 1 \times 10^4 m/s$ , mixing of warm and cold water occur as a result of the establishment of free convection within the mine voids, leading to faster transport of cold water toward the extraction well (Renz et al., 2009).

### 7.1.4 2D vs 3D modeling approaches

Hamm and Bazargan Sabet, 2010 suggested that a "equivalent porous media" assumption can be used for mine workings when large-scale modelling is considered. However, this approach could be improved by using a multi-layer models taking into account detailed digital maps of the mine's galleries/shafts, better describing the 3D geometrical and hydraulic connections in the mines. 2D models are suggested to be appropriate for initial sensitivity analysis of rock properties and for model parameter analysis. For some authors, they cannot be used to faithfully represent 3D geometries and the heat capacity of mines and thus, 3D models have generally been directly created or created subsequently to 2D models (i.e. Andrés et al., 2017. To deal with the fact that 2D models cannot realistically represent the high storage capacity of driving and caverns, whose extent is mainly in

the orthogonal direction to 2D models, Renz et al., 2009 however used a "heat capacity equivalent" to represent the real behavior of heat and mass flow in these voids. Their results showed that 2D models cannot properly account for movement due to free convection when density-dependent simulations are performed compared to 3D porous media approach. However, the overall heat storage from large mining voids are better accounted for in the 1D/2D model.

## 7.2 Research Gaps

The geothermal potential of mine has been suggested to be highly dependent on their local hydraulic condition and geometrical structure. Thus, most of the authors developed their own modeling approach, based on the data available and the purpose of modeling, to estimate the geothermal potential of existing mines. Those attempts revealed that wanting to accurately represent the complex geometry of mines can be tedious, and simplifications are generally required (e.g. Raymond and Therrien, 2008; Hamm and Bazargan Sabet, 2010; Małolepszy, 2003; Renz et al., 2009; Andrés et al., 2017). Therefore, no standard mine modeling approaches have emerged yet at this stage and there is no general understanding of the mechanisms occurring in mines (Renz et al., 2009).

However, predictions of groundwater flow in the mines strata are generally limited due to the uncertainties in the boundary conditions, linked to the lack of pre-mining or early-mining data (i.e. thermal and hydraulic properties, cyclic changes of precipitation/evaporation). This adds to uncertainties in the volumetric capacities and the lateral/vertical hydraulic connections within the mines. Indeed, mines plans are sometimes incomplete or nonexistent (i.e. old mine workings), limiting the potential to set up reliable numerical models (Henton, 1974; Sgambat et al., 1980). On the other hands, performing numerical calculations considering a whole complex mine system with detailed geometry would require extreme computing capabilities and amount of time.

## 7.3 Aims and methods

Because of the lack of data and the complexity of the geometry of mining voids, it is therefore essential to understand what elements really matter in modelling thermal processes and in the assessment geothermal potential, at the scale of the mine or interconnected mines. While large open voids in mine (i.e. shafts, tunnels) provide significant potential for heat exchange between the host rock and the mine-water over the whole depth range spanned by the worked coal seams (Banks et al., 2003), goaf and galleries (ie. porous media) tends to represent the greatest proportion of the mine. This chapter therefore aims at assessing the important features to extract from existing mine plans for the estimation of the long-term heat capacity of mines. We want to investigate the validity of using 2D models to avoid constructing complex 3D models, through the definition of "equivalent porosity" and "equivalent heat capacity" factors. To achieve this, we will also develop a methodology and/or a tool able to convert GIS mine features into 2D finite-element mesh, or to use them to calculate input parameters for the models. Our study will be based on available data (i.e. both geometrical data for model construction and monitoring data for model calibration) for the Dawdon-Horden mining field and on the Midlothian Coalfield. The expected outputs from this analysis will be the assessment of the overall heat capacity, sustainable heat extraction rate (i.e. allowing balances heat extraction/recharge) and steady-state footprint area of heat extraction for those two areas, accordingly to knowledge acquired from previous chapters.

## 7.4 Research questions

What are the key mine features allowing to assess the sustainable heat potential of coal mines at the scale of a mine?

- Can 3D processes (i.e. overall heat capacity/change in heat storage) can faithfully be scaled up in 2D?
  - What is the effect of lateral connectivity of roadways on the extent of the heat sink and on the heat exhaustion/recharge rate?
  - How does the density and/or absolute volume of mining void contribute to define the total energy content of the mine?
- Can homogeneous hydraulic and thermal properties accounting for both galleries and induced fractures be attributed to all mined areas?
  - Does the geometry of the voids resulting from different mining approaches (i.e. pillar-and-stall, longwall mining) impact the heat exchange rate between the host rock and the mine-water and the recharge rate at the scale of the mine?
  - How does the relative permeability contrasts between roadway/tunnels, the mined area and unaffected host rock contribute to the rate and overall change in energy content in the system?
- What is the effect of the distribution, density and inter-connectivity of the roadway network and the coal seams on the direction/amplitude of the induced heat fluxes during production/recovery, and on the temperature distribution within the mine?
  - Can we simulate the water recovery rate/temperature measured in shafts in the Midlothian coalfield ?
  - Can the extracted water temperature and the evolution of the temperature profiles within the shafts in Dawdon-Horden be reproduced?

## 7.5 Hypothesis

- H0 - The larger the areal extent of the mine, the greater the recharge rate (i.e. the faster thermal balance is reached).
- H1 - The total residual void volume (i.e. water content) can be used to derived a heat depletion rate factor.
- H2 - The geometry of the voids resulting from different mining approaches (i.e. pillar-and-stall, longwall mining) does not impact the heat exchange rate between the host rock and the mine-water and the recharge rate at the scale of the mine.
- H3 - The relative permeability contrasts between roadway/tunnels, the mined area and unaffected host rock is a key feature to assess the overall change in energy content in the system and the rate of energy transfer.

- H4 - An "equivalent porosity" and "equivalent heat capacity" parameter can be defined to scale up 3D processes in 2D models.
- H5 - The number/geometry of interconnections between tunnels and the model boundary conditions highly affect the temperature distribution and long term production temperature.

## 7.6 Preliminary results

The two figures below are examples of mesh created, here manually, to investigate the impact of the coalfield geometry on the temperature distribution (7.1).

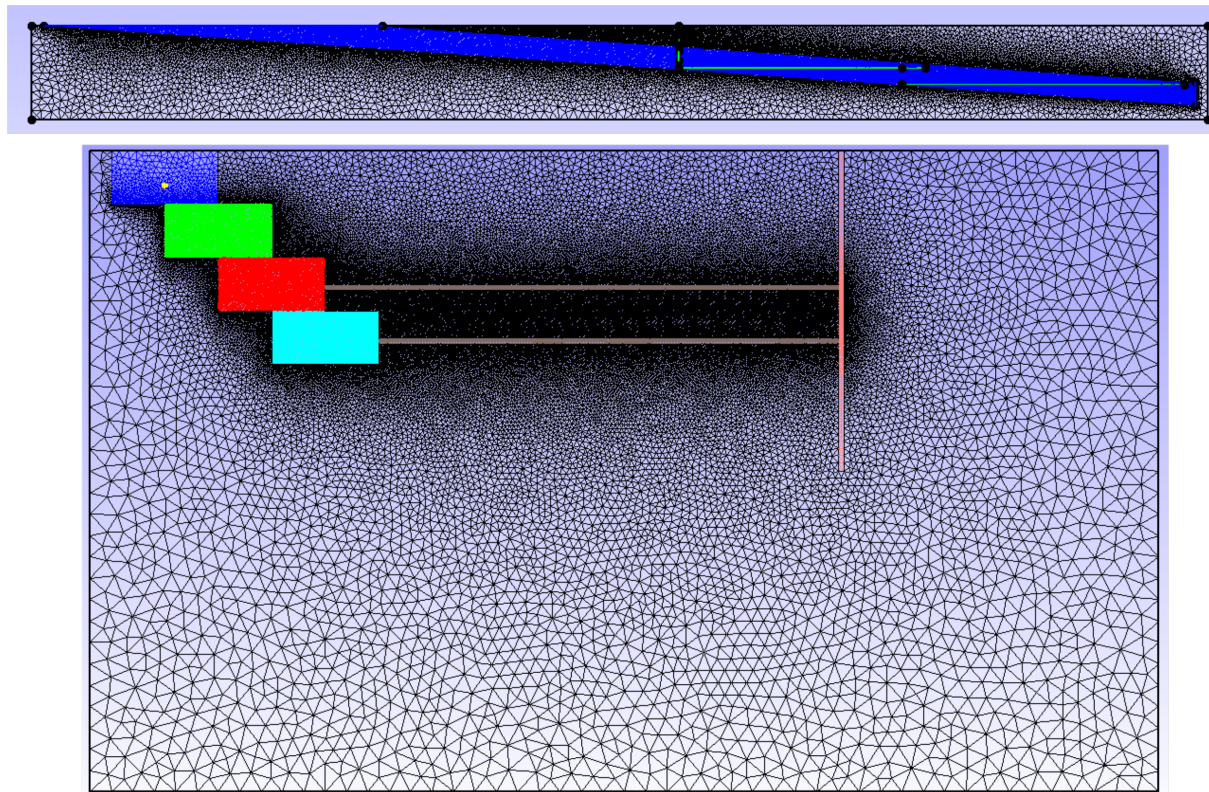


Figure 7.1: Example of mesh for equivalent porosity model for a) the Dawdon-Horden area and b) the Midlothian Coalfield

To attribute the different areas of the model with representative material properties, we first suggest to develop a factor representing the total proportion of void per depth interval, according to the following relation:

$$\Phi = \frac{V_{void}}{V_{minedvolume}}$$

with

$$V_{void} = \sum_{n=1}^n [A_{workedseams} \times h_{workedseams} \times f]$$

with n the number of workings in the considered min volume, A the working area and h the worked seam thickness.

For each "block", specific initial temperature and thermal/hydraulic properties (i.e. thermal conductivity, hydraulic conductivity) will be attributed according to the nature of the geological layer and initial undisturbed state. Appropriate thermal and hydraulic boundary conditions will be set. Each block will moreover be inter-connected through roadways (high conductivity pathway between mine volumes representing connections between different mines and/or mined parts of a same mine) accordingly to the information provided in the mine plans.

## 7.7 Conclusion and research outputs

The main outcome of this study will be to develop a comprehensive methodology for mine modeling, including a description of the important mine features, parameters, rock properties to consider. The analytical or numerical modeling tool will be used to evaluate and assess the sustainability of heat production from the selected case studies. A paper will be written from this analysis, either to demonstrate the "universal" validity of the approach used, or as a "case-study" oriented paper (to be defined).

# 8 Data management plan

## 8.1 Data repositories

File path	Usage	Description
C:	Desktop local space	Modelling and data processing
M:	Personal drive	General/administrative documents
R:	Research data store	GIS Data and projects, long-term storage of modeling results/analysis, bibliography (i.e. scientific papers, reports, books), T&D courses
GitHub	Online university account	Storage repository and version control for reports (i.e. confirmation report, literature review, meeting reports), scripts, figures and overall data storage
One Drive	University drive	Shareable reports/scripts for visualisation
Overleaf	Online university account	Document redaction (i.e. reports, PhD plan)

Table 8.1: Data management

The codes and meshing, modeling and visualization software used (OpenGeosys, gmsh, paraview, Tecplot, QGIS) have been installed on the C: repository. Numerical model simulations are run on the C: repository and numerical output files are then transferred on the R: repository, which has a greater storage capacity.

## 8.2 Version control management plan

Version control for the data, reports and Python scripts is managed through the combined use of GitHub and GitHub Desktop on both personal and university computer. Overleaf is and will be used for report and future manuscript writing, to ensure safe version control, back-up and access from different places. This will also facilitate the exchanges and feedback with the supervisory team. All python scripts written as part of the PhD are currently stored on a personal GitHub repository and run from the Spyder application. Verified codes will be made available through GitHub website in the long-term.

For each modeling study undertaken as part of the PhD project, README files and Excel "Modeling-Data-Management" file has been developed and copied in each corresponding folder. The EXCEL file summarizes the name, input parameters (i.e. medium properties, boundary conditions, initial conditions...) for all models related to the study. It also includes a column for the objective of the model, the observation and the interpretation, that are developed in more details in the README file. Each Excel file also contains an sheet for the calculation of the stability criteria of the models.

## **9 Time plan**

The first year will involve the data collection of available data from the Coal Authority and other sources, the development of conceptual models and the investigation of the key controls on mine water temperature and recharge mechanisms. The second and third year will progress through the development of numerical modelling of temperature profiles and the interpretation of the results particularly with relevance to scoping out the size of the temperature resources available to use (see detailed timeline in Fig. 9.1).

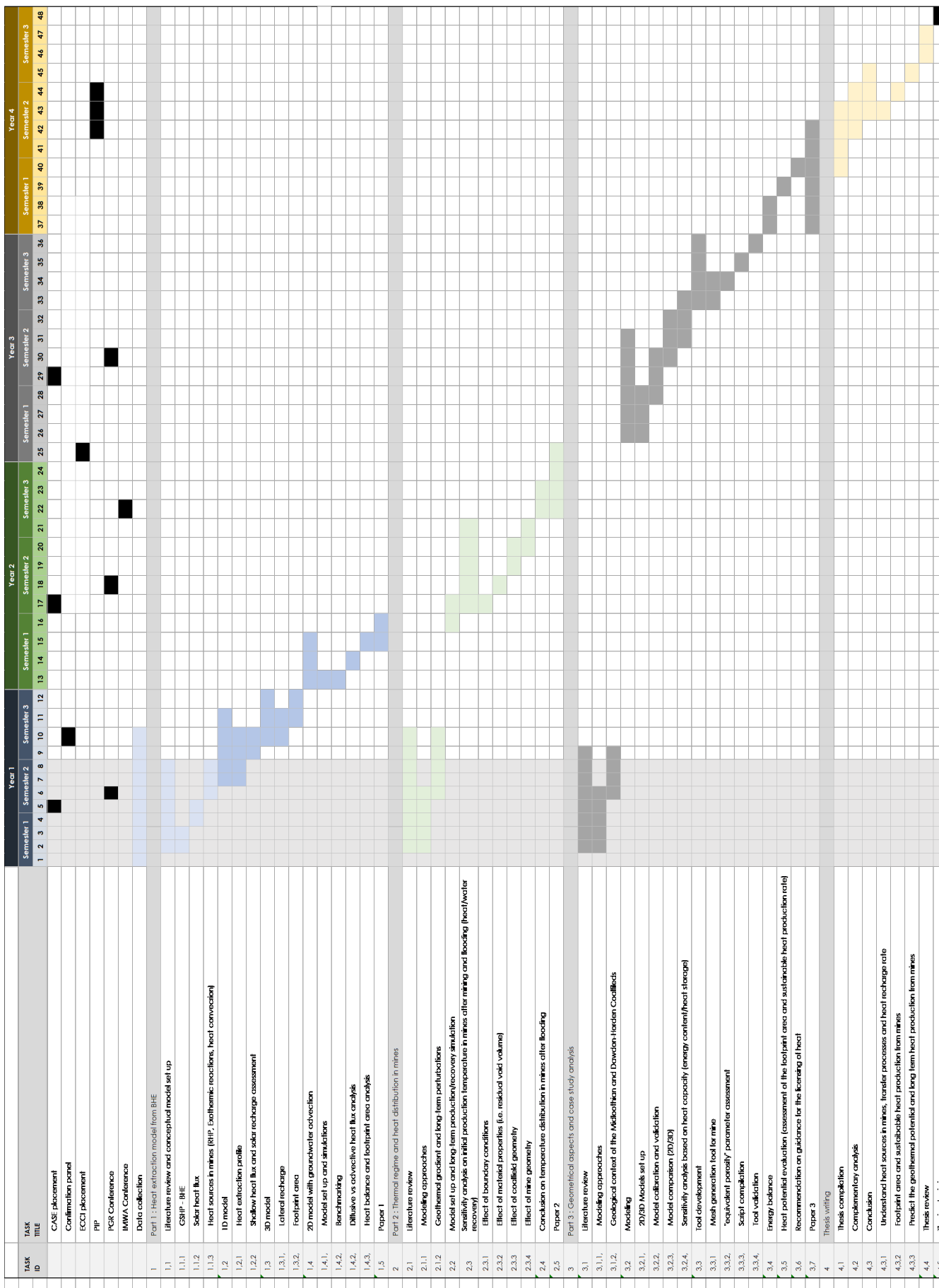


Figure 9.1: GANTT chart

## **10 Supervisory arrangements**

- Principal supervisor : Christopher McDermott (University of Edinburgh) - General guidance
- Co-supervisors (University of Edinburgh):
  - Stuart Gilfillan (geology, geochemistry) - Support for key research questions, guidance for research work and publishing
  - Andrew Fraser-Harris (modeling expert) - Review of OGS models
- Advisor: Wyn Williams (University of Edinburgh)
- External Advisors:
  - Ian Watson (Coal Authority, CASE sponsor)
  - Andrew Gunning (RSK)
- External contacts: David Banks (Holymoor Consultancy Ltd)

# 11 Resources and Training

## 11.1 Training need analysis

Skills / training required	Courses / resources identified
Couples TH modelling (OGS)	Hydrology 2 (self-directed learning)
Hydrodynamics / Geothermics in mines	Journal / books (self-directed learning)
Python coding	NMDM course (E4 DTP training, Datacamp courses)

Table 11.1: Skills and formations required

Other workshop attended are reported below:

The Writing Process: Getting Started (SCE/MVM)	IAD	29-Apr	3 hours
Top tips for writing an abstract	IAD	24-Apr	1 hour
Top Tips for Writing a Literature Review workshop	IAD	17-Apr	1 hour
E4 DTP Online PhD Training: Introduction to Career Pathways		28-Apr	3 hours
An Introduction to Copyright and Publishing workshop	IAD	22-Apr	2 hours
Beating Writers Block (SCE/MVM)		15-Apr	3 hours
Working productively at a distance	IAD	09-Apr	1,5 hours

Table 11.2: Courses attended

## 11.2 Teaching experience

- Hydrology 1 (Tutor, semester 1)
- Hydrology 2 (Tutor, semester 2)
- Earth Dynamics (Field demonstrator, Semester 1)
- Introduction to Geological Records (Demonstrator, Semester 2) and Lake District Field Trip (Field demonstrator, Semester 2, cancelled)

## 11.3 Resources available

Open-source software, including OpenGeoSys, QGIS, Tecplot as well as Python scripts are being used to conduct the PhD project. Modeling results are being visualized and post-processed using Tecplot, for which an extra-license has been provided. A renewal of the license will be required for the following years.

Source name	Total amount (£)	Comment
RTSG	3,450	NERC Research Training Support Grant
CASE funding	3,000	Coal Authority
Travel Grant	500	Estimated (application necessary)
<b>TOTAL</b>	<b>7,000</b>	Estimated

Table 11.3: Sources of income (total for 3 years)

## 11.4 Resources needed

Expenditure source	Amount (£)	Comment
Software license	540	Tecplot
Laptop	??	Need to be investigated
Visit Mining Museum	11.50	Museum + Guided visit
COAL Authority visits	74.40	Reimbursed drom CASE funding
UK 7th Geothermal Synopsium	150.59	TRansport + Conference
Coming conferences:	Estimates:	
WGC	380 + 200	
GeoTHERM	50 + 250	Conference fees +
GradSchool Conference	175 x 2	Transport
IMWA	250 + 100	
EGU	350 + 200	
SUB-TOTAL	3,000	
Open-source publishing licences	1,500	Estimations for 3 publications
Computing capacity/storage	1,500	Reserves
<b>TOTAL</b>	<b>7,000</b>	Include all income sources

Table 11.4: Resources required and potential expenses (NB: The total expenses ignore the expenses types, which might or might not be covered by all income sources. More detailed budget analysis is required to define which expense could be covered by which income source).

To date, no fieldwork has been planned or deemed required. All the data useful to calibrate or validate the model will be provided by the Coal Authority through the PhD lifetime, or acquired during CASE placement (no additional fees). Other external sources/private companies moreover offered to acquire and share additional temperature data that could be used for this study.

## 11.5 Conferences

Conferences attended and planned are summarized in Table 11.5. All the conferences planned between April and August 2020 have been cancelled/postponed due to the Covid-19 Pandemic.

Conference name	Date	Organiser	Location
UK 7th Geothermal Synposium	Nov 2019	Geological Society London	London
Career and Industry Days	4 Dec 2019	Geological Society London	Edinburgh
GradSchool Conference 2020	7-9 Feb 2020	University of Edinburgh	Glasgow
PGR Conference (cancelled)	23-24 April 2020	University of Edinburgh	Edinburgh
WGC (postponed)	24-30 April 2020	International Geothermal Association	Reykjavik, Iceland
GeoTherm 2021	March 2021	European Geothermal Energy Council	Offenburg, Germany
GeoSciences PGR Conference	April 2021	University of Edinburgh	Edinburgh
IMWA Conference 2021	June/July 2021	International Mine Water Association	Cardiff, Wales, UK
EGU 2022	April 2022	European Geosciences Union	Vienna, Austria

Table 11.5: Conferences of interest

## **12 Ethical and Health and safety considerations**

The research conducted through this PhD does not involve any subjects or fieldwork. All research will be exclusively conducted within the UK, either at the University of Edinburgh or at the Coal Authority Mansfield office, under the supervision of Ian Watson. All conditions regarding intellectual property, integrity, publication, authorship, and data confidentiality have been addressed by the “Studentship Agreement” and “Assignment and Confidentiality agreement” signed by all parties: the non-academic CASE partner (The Coal Authority), The University of Edinburgh and the student (Mylene Receveur). Research-related data will be stored and made accessible under the terms set by those agreements.

As part of mandatory placements of at least 3 month throughout the PhD duration, a Coal Authority ICT User Policy and Information Risk Management Policy (IRMP) have moreover been signed. In addition, a DBS security check has been completed and a Basic Disclosure certificate obtained from Disclosure Scotland.

If any new partnership is created to access data from private companies, we will ensure that this is made through written agreement or data license, and we will guarantee to provide feedback on any results and findings obtained from these data.

## **13 Take home message**

Flooded coal mines constitutes potential low carbon heat energy resource. However, the sustainable use of heat from coal mines can only be achieved with an appropriate dimensionning of GSHP systems, which only depends on the good understanding of the heat capacity and recharge mechanisms of the underground. A key outcome of this work will be the development of a predictive tool, model or conceptual approach that enables the scientific estimation of the extent and nature of the heat available over the long term from abandoned flooded coal mines in the UK. This tool could be used to support the design of mine-water based heat extraction schemes, the assessment of sustainable production rate, but also guide the licensing of heat with a scientific approach. In parallel, this approach would participate in determining the external energy input (i.e. injection of heat or heat from other sources) necessary to create a sustainable heat reservoir in flooded coal mines, using energy balances and numerical simulations.

# A Appendix

## A.1 Rock properties

The thermal character of a reservoir rock is mainly dependent on the effective heat capacity  $C_p$  (J/K), thermal conductivity  $\lambda$  (W/m.K) and thermal diffusivity  $\alpha$  (m<sup>2</sup>/s) of the materials that forms it, as well as the amount of saturation. Where conductive processes are dominant, the effective fluid-rock heat capacity and heat conductivity both influence heat transfers. Thermal dispersivity mostly account for heat dispersion in areas where convective heat transfers are dominant (Dethlefsen et al., 2016). However, while the specific heat capacity, conductivity and diffusivity of groundwater are well known, the thermal properties of rocks highly depend on their material composition, texture and structure (Allen et al., 2014; Dethlefsen et al., 2016).

Browne et al. (1985) noted considerable variations both in the proportion of rock types in each formation in the MVS and in the conductivity for each lithology in the Upper Palaeozoic. The average thermal conductivity for the formations of the Carboniferous succession in the MVS is shown in Table A.1 together with values for common rock types reported by Lee et al., 1987; Rollin, 1987; Banks, 2008 and Busby, 2019. Formations thermal conductivity were estimated by Busby, 2019 in the UKGEOS Open Report OR19015 by combining the thermal conductivities of individual lithological units as a harmonic mean, based on the data recently acquired from cores at the Glasgow Geothermal Energy Research Field Site. Due to the absence of thermal conductivity values for the Scottish Coal Measures, the Passage Formation and the Kirkwood Formation, the thermal conductivity for representative sections in those formations were estimated from values measured on similar lithologies in 5 boreholes located in the Pennine Coal Measures of northern England.

## A.2 Radiogenic heat production

Rough estimations of the radiogenic heat production in the Midlothian Coalfield have been made (Fig. A.1) based on the thickness of each Carboniferous formation in the Carrington-1 well (Monaghan, 2014), on the average proportion of lithologies in each group (Table A.2) and on RHP values from the literature (Table 4.1). The area used to calculate the total volumetric RHP consists of the zone covered by the outcrops of the Coal Measures Formation in the Midlothian Coalfield. Similarly, we made an estimation of the average thermal conductivity for each formation (Fig. A.2) based on rock conductivity values estimated from samples from the MVS (Tab. A.1).

## A.3 Heat related equations

The transient heat diffusion equation can be written as follow.

$$\rho c \frac{dT}{dt} = -\rho_w c_w v_w \frac{dT}{dx} + \nabla(\lambda \nabla T)$$

a) Lithology	K (W/m/K)	Reference
Coal	0.31	Lee et al., 1984
Coal Measures Sandstone	3.31, 3.58*	Rollin, 1987; *Busby (2019)
Coal Measures Siltstone	2.22, 2.23	Rollin, 1987; *Busby (2019)
Coal Measures Mudstone	1.49, 1.85*	Rollin, 1987; *Busby (2019)
Coal Measures Ironstone	2.35*	*Busby (2019)
Namurian Millstone Grit Limestone	3.75	Rollin, 1987
Lower Carboniferous limestone	3.14	Rollin, 1987
Upper Old Red Sandstone	3.26	Rollin, 1987
Silurian slates	3.33	Rollin, 1987
Hercynian granites	3.3	Rollin, 1987
Basalt	1.8	Rollin, 1987
Shale	1.3	Busby (2019)**
Fireclay	0.59	Busby (2019)**
b) Formation	K (W/m/K)	Reference
Scottish Coal Measures Formation	$1.91 \pm 0.25$	Browne et al., 1985
Scottish Middle Coal Measures	2.02	Busby (2019)
Scottish Lower Coal Measures Formation	$1.91 \pm 0.25$	Busby (2019)
Passage Formation	$2.91 \pm 0.15$	Browne et al., 1985
Upper Limestone Formation	2.25	Busby (2019)
Limestone Coal Formation	2.24	Busby (2019)
Lower Carboniferous	$2.12 \pm 0.25$	Browne et al., 1985
Lower limestone Formation	1.88	Busby (2019)
Lawmuir formation	4.36	Busby (2019)
Kirkwood Fm	2.1	Busby (2019)
Clyde Plateau Volcanic Formation	2.2	Busby (2019)
Clyde Sandstone Formation	4.19	Busby (2019)
Ballagan Formation	3.14	Busby (2019)
Kinnesswood formation	3.66	Busby (2019)

Table A.1: a) Thermal conductivity for specific lithologies found in the MVS succession, estimated based on laboratory measurements made on water saturated samples extracted from boreholes. \*representative values for the Scottish Middle Coal Measured estimated from 5 boreholes in England. \*\* averages from the Boreland (Anderson, 1940) and Glenrothes (Gebbski et al., 1987) boreholes. b) Average thermal conductivity for the formations of the Carboniferous succession of the MVS (from Busby, 2019), estimated from the Maryhill, Hurlet House, Clachie Bridge, Barnhill, Kipperoch (Oxburgh, 1982), Boreland (Anderson, 1940) and Glenrothes (Gebbski et al., 1987) borehole logs.

lithology	UCMS	MCMS	LCMS	LSC - PGP	BELOW
Sandstone	40	>40	>50	40	30
Mudstone	60	30	30	40	50
Siltstone		24	14		
Coal		6	4		
Ironstone			<1		
Limestone				20	20

Table A.2: Percentage of lithologies for the Carboniferous formations of the Midland Valley of Scotland recorded in existing borehole data. Data for the Lower (LCMS) and Middle (MCMS) Coal Measures are from the BGS Open Report OR19019 (Entwistle, 2019). Data for the Upper Coal Measures (UCMS), Limestone Coal (LSC) to Passage (PGP) Formations and underlying Carboniferous strata (BELOW) were determined from 9 boreholes logs in Vincent et al., 2010.

		1 foot = 0.3048 m 1 mile = 1.60934 km				Groundwater composition			
FORMATION	Volume (m3)	LITHOLOGY	PERCENTAGE	Volume (m3)	RHP $\mu\text{W}/\text{m}^3$	Density (kg/m3)	HPE	H (W/kg)	Concentration
Coal Measures	Dalkeith (full thickness) 457.2	Sandstone*	35%	7.14E+09	0.896	2400	K	3.40E-09	9.19E+00 mg/L
		Siltstone / Mudstone*	60%	1.22E+10	1.392	2400	Th	2.64E-05	9.00E-03 $\mu\text{g}/\text{L}$
		Limestone**	0%	0.00E+00	2.066	2789	U	9.83E-05	2.26E-01 $\mu\text{g}/\text{L}$
		Coal**	5%	1.02E+09	0.5	1200	Al	3.58E-01	1.80E+00 $\mu\text{g}/\text{L}$
	Carrington-1: 250	Ironstone**	1%	2.04E+08	0.7	2650	Fe	3.65E-02	1.22E+03 $\mu\text{g}/\text{L}$
Passage Formation	20396054980	AVERAGE RHP ( $\mu\text{W}/\text{m}^3$ ):	1.181	TOTAL RHP (W):	2.4E+04		A	8.20E+00 $\mu\text{W}/\text{m}^3$	
		Sandstone*	90%	1.54E+10	0.895	2400			
		Siltstone / Mudstone*	10%	1.71E+09	1.392	2400			
		Limestone**	0%	0	2.066	2789			
	Carrington-1: 210	Coal**	0%	0	0.5	1200			
Upper Limestone Fm	in Lonhead (238 m) 165	Ironstone**	0%	0	0.7	2650			
		AVERAGE RHP ( $\mu\text{W}/\text{m}^3$ ):	0.946	TOTAL RHP (W):	1.6E+04		A	2.67E+00 $\mu\text{W}/\text{m}^3$	
		Sandstone*	35%	1.21E+10	0.896	2400	K	3.40E-09	3.08E+00 mg/L
		Siltstone / Mudstone*	40%	1.39E+10	1.392	2400	Th	2.64E-05	2.28E-03 $\mu\text{g}/\text{L}$
	in Lonhead (320 m) 175	Limestone**	20%	6.93E+09	2.066	2789	U	9.83E-05	4.00E-02 $\mu\text{g}/\text{L}$
Limestone Coal	Lower Limestone Fm 85	Coal**	5%	1.73E+09	0.5	1200	Al	3.58E-01	4.00E+00 $\mu\text{g}/\text{L}$
		Ironstone**	0%	0	0.7	2650	Fe	3.65E-02	3.22E+02 $\mu\text{g}/\text{L}$
		AVERAGE RHP ( $\mu\text{W}/\text{m}^3$ ):	1.309	TOTAL RHP (W):	4.5E+04		A	4.85E+01 mg/L	
		Granite*	-	?	2.827	2650			
	873.24	Basalt*	-	?	0.358	2750	GW in aquifers extensively mined for coal		
Carboniferous strata below	71242604204	Sandstone*	30%	?	0.896	2400	K	9.83E-05	7.80E-01 $\mu\text{g}/\text{L}$
		Siltstone / Mudstone*	50%	?	1.392	2400	Th	3.40E-09	1.99E+01 mg/L
		Limestone**	20%	?	2.066	2789	U	3.65E-02	3.28E+03 $\mu\text{g}/\text{L}$
		Coal**	0%	0%	0.5	1200	Al	3.58E-01	1.30E+01 $\mu\text{g}/\text{L}$
		Ironstone**	0%	0%	0.7	2650	Fe	4.56E-02	4.56E+02 mg/L
		AVERAGE RHP ( $\mu\text{W}/\text{m}^3$ ):	1.378	TOTAL RHP (W):			A	3.76E+00 $\mu\text{W}/\text{m}^3$	
*Vila et al. (2010); ** OSIMOBI et al., 2018		TOTAL HEAT PRODUCTION:						85658 W	

HPE values are from Ruedas (2017)

Figure A.1: Estimates of total radiogenic heat produced in the Midlothian Coalfield based on the thickness of each formation in the Carrington 1 well, and on the average concentration of Th, U, K, Al, SO4 and Fe in sampled groundwaters from the Coal Measures, Clackmannan and "Mine" aquifers of the MVS (O Dochartaigh et al., 2011). Heat production rate values for  $^{26}\text{Al}$ , K,  $^{60}\text{Fe}$ ,  $^{232}\text{Th}$  and U were estimated by Ruedas, 2017.

The first term on the right side represents the advective term, with the mass flow being characterized by the product of the water density  $\rho_w$  ( $\text{kg}/\text{m}^3$ ) and velocity  $v$ , and the second term is the conductive heat transfer. The medium heat conductivity  $\lambda_m$  ( $\text{W}/(\text{m} \cdot ^\circ\text{C})$ ) and heat capacity of the wet rock  $\rho c$  can be defined as the product of the porous rock and water properties, as followed:

$$\lambda_m = \phi \lambda_w + (1 - \phi) \lambda_r$$

	Sandstone CM	Sandstone PGP	Siltstone CM	Mudstone CM	Limestone	Ironstone	Coal	Average Fm conductivity	Average RHP	Heat flow (mW/m²)	Gradient (°C/km)
Conductivity	3.58	2.91	2.23	1.85	3.14	2.35	0.31	Calculated harmonic mean	Busby (2019)	Calculated harmonic mean (W/m³)	53
RHP	0.896	0.896	1.392	1.392	2.066	0.7	0.5				30
<b>CARRINGTON 1</b>											
Thickness	35	30	30	5	1	5		2.516	1.91	1.18E-03	?
LOWER COAL MEASURES GROUP	250	90	90	5				2.823	2.91	9.46E-04	?
PASSAGE FM	210			20	20	20	1	2.8433	2.25	1.32E-03	?
UPPER LIMESTONE FM	165	39		20	20	20	5	2.7125	2.24	1.31E-03	?
LIMESTONE COAL	175	35		20	20	20		2.8433	1.88	1.32E-03	?
LOWER LIMESTONE FM	85	39		20	20	20	1	2.722	2.1*	1.38E-03	?
WEST LOTHIAN OIL SHALE	492	30		25	25	20			4.19**	1.40E-03	?
GULLANE	593+								2.2	?	?
CLYDE PLATEAU VOLCANIC FM	70									?	?

Carrington-1 (Monaghan and Brown, 2014)

\*Kirkwood Fm conductivity  
\*\*Clyde Sandstone Fm Conductivity

Figure A.2: Summary of the RHP and thermal conductivity for each lithological group in the Midlothian Coalfield

$$\rho c = \phi \rho_w c_w + (1 - \phi) \rho_r c_r$$

with  $c_r$  and  $c_w$  the specific heat capacity of the rock and water, respectively (J/kg.°C). In a porous rock, the total energy extractable from cooling rocks can be calculated as follow:

$$E = m_r \Delta T c_r = \Delta T V \phi < \rho_r c_r >$$

with E the total energy (J) extracted from cooling rocks of volume V,  $\Delta T$  the change in rock temperature,  $m_r = V\phi\rho_r$  the mass of rock with  $\Phi$  the rock porosity. Raymond and Therrien, 2008 estimated that the total geothermal energy content of rock in mines can be estimated from the sum of the energy associated with each flooded underground section, as:

$$E_r = Vz\alpha\rho c$$

with V the volume of water in a mine section, z its average depth,  $\alpha$  the measured geothermal gradient and  $E_r$  the energy of a given section. The rate  $E_{hp}$  at which geothermal energy can be extracted using heat pumps was calculated as followed:

$$E_{hp} = Q(T_p - T_r)\rho_w c_w$$

with Q the average flow rate,  $T_p$  the pumped water temperature and  $T_r$  the exchanger return temperature. Assuming that the energy is extracted from water flowing at a rate  $Q_w(m^3/s)$ , recharging the system at a temperature  $T_i$  and extracted at a temperature  $T_{out}$ , the rate of cooling of the reservoir  $\Delta T_r(^\circ C/s)$  can be expressed as follow:

$$\Delta T_r = \frac{Q_w \rho_w c_w}{V\phi\rho c} \Delta T_w$$

with  $\Delta T_w = T_{out} - T_i$ . The heat fluxes induced by water advection  $q(W/m^2)$  can be expressed through the coefficient of heat transfer  $h(W/m^2.K)$  as  $q = h \times (T_r - T_w)$ . The power exchange of water in a system with colder fluid reinjection can thus be written as followed:

$$P = \frac{C\phi\rho c}{t} (T_{in} - T_{system})$$

### A.3.1 Periodic heating

The analytical solution for temperature change in a semi-infinite half space under periodic heating/seasonal change in temperature  $T_s = T_0 + \Delta T \cos(\omega t)$  given by Turcotte and Schubert, 2002 is:

$$T = T_0 + \Delta T + \exp(-y\sqrt{\frac{\omega}{2\alpha}}) \cos(\omega t - y\sqrt{\frac{\omega}{2\alpha}})$$

where  $\omega = \frac{2\pi}{\tau}$ , with  $\tau$  the period of the oscillations. A sinusoidal temperature model representing the variations in heat transferred to the soil at the surface was derived by Hillel (1982) using a sinusoidal forcing function (Ozgener et al., 2013), describing the soil temperature at time  $t$  and depth  $z$  as:

$$T(z, t) = T_m + A_z \sin\left(\frac{2\pi}{\tau}(t - t_0) - \gamma z - \frac{\pi}{2}\right)$$

Here,  $\gamma = \sqrt{\frac{\pi}{\alpha\tau}}$  is the inverse damping depth, with  $\alpha$  the thermal diffusivity ( $m^2/s$ ), defined as  $\alpha = \frac{\lambda_m}{\rho_c}$ .  $T_m$  is the mean surface temperature,  $t_0$  the time lag needed for the surface soil temperature to reach  $T_m$ , and  $A_z = A_0 \exp(-\gamma t)$  the amplitude of temperature wave at depth  $z$ , time  $t$ , which decay exponentially with depth. The undisturbed temperature at depth  $z$  and time  $t$  taking into account daily and annual temperature variations was expressed in Radioti et al., 2017 as followed:

$$T(z, t) = T_m - A \exp\left(-z\sqrt{\frac{\pi}{365\alpha}}\right) \cos\left(\frac{2\pi}{365}(t - t_{T_{min}} - \frac{D}{2}\sqrt{\frac{365}{\pi\alpha}})\right) + T_g(z)$$

where  $A$  is the amplitude of air temperature oscillations,  $t_{T_{min}}$  the day number corresponding to the minimum temperature,  $\alpha$  the equivalent ground daily thermal diffusivity and  $T_g$  the product of the geothermal gradient by the testing depth.

### A.3.2 Seasonal production

Angelotti et al., 2018 modelled in 3D the temperature distribution (i.e. thermal plume) in porous aquifer under seasonal production from BHE, considering different groundwater velocity. The temperature response of the medium is here expressed as follow:

$$T(x, y, t) = T_g 0 + \frac{q}{4\pi\lambda} \exp\left(\frac{u_x}{2\alpha}\right) \int_0^{r^2/(4\alpha t)} \frac{1}{\psi} \exp\left(-\frac{1}{\psi} - \frac{u^2 r^2 \psi}{16\alpha^2}\right) d\psi$$

with  $u = v_x \frac{\rho_w c_w}{\rho_c}$  the effective water velocity. A steady state temperature might be reached for high simulation time and can be defined as follow:

$$T(x, y, t) = T_g 0 + \frac{q}{2\pi\lambda} \exp\left(\frac{u_x}{2\alpha}\right) K_0\left(\frac{u\sqrt{x^2 + y^2}}{2\alpha t}\right)$$

## A.4 Analytical solutions

### A.4.1 Advection-diffusion

An analytical solution for continuous heat injection in porous medium is given in Barends et al., 2010. This solution is based on the Lauwerier concept (1955) and was developed to explore the complete heat storage and

transfer processes, including convection by pore fluid flow, conduction, dispersion and thermal bleeding in a homogeneous reservoir with plane uniform steady groundwater flow. In this model, water of temperature  $T_1$  is injected at a rate  $Q(\text{m}^3/\text{s})$  at  $x=0$  and  $t=0$ . No hydraulic and no thermal flows are set to the lower boundary and the upper boundary is defined as impermeable but can conduct heat through thermal bleeding in an overlying rock strata. Result from their analysis showed that despite the effected zone in the overburden is rather limited, thermal bleeding has a large effect on the temperature pattern in a reservoir. The solution used here for the temperature distribution along the line for continuous injection is based on the solution derived for  $z=0$  (no heat diffusion in the overburden) and represents the temperature distribution in the reservoir when there is no heat diffusion in the overburden (Ogata and Banks, 1961):

$$\Delta T = \frac{T_1 - T_0}{2} \left( \operatorname{erfc}\left(\frac{(x - v_T t)^2}{4\alpha t}\right) + \exp\left(\frac{xv_T}{\alpha}\right) \operatorname{erfc}\left(\frac{(x + v_T t)^2}{4\alpha t}\right) \right) \quad (\text{A.1})$$

with  $\alpha = \frac{\lambda_m}{\rho_c c_r}$ ,  $v_T = u_x \frac{\rho_w c_w}{\rho_c c_r}$ , where  $\rho_c = \rho_r c_r (1 - \Phi) + (\rho_w c_w) \Phi$  and  $u_x$  the Darcy velocity. In the script available [here](#), this analytical solution, written as in Eq. A.2 was used to validate the numerical results for constant heat injection in a 1D medium with groundwater advection in the x direction.

$$T = \operatorname{erfc}\left(\frac{x - v_T t}{\sqrt{4\alpha t}}\right) + \exp\left(\frac{xv_T}{\alpha}\right) \times \operatorname{erfc}\left(\frac{x + v_T t}{\sqrt{4\alpha t}}\right) \times \frac{T_0}{2} \quad (\text{A.2})$$

The analytical solution for a heat pulse with groundwater flow is given below:

$$T = \frac{T_0}{\sqrt{8\lambda_r \pi t}} \exp\left(-\frac{(x - v_T t)^2}{4\alpha t}\right) \quad (\text{A.3})$$

Both solutions resulted in a good fit with the corresponding numerical results (see Fig. A.3).

#### A.4.2 Diffusion only

For a instantaneous cooling/heating of a semi-infinite half-space, where a constant temperature  $T_0$  is applied on the top boundary condition of a domain of initial temperature  $T_1$ , the temperature profile can be calculated at a time  $t$  or distance  $z$  from the boundary using the following equation (Heat conduction - Dirichlet BC, with  $q = 0$  on the other boundary):

$$T = T_1 + (T_0 - T_1) \operatorname{erfc}\left(\frac{x}{\sqrt{4\alpha t}}\right) \quad (\text{A.4})$$

with  $\alpha = \frac{\lambda_r}{\rho_r c_r}$  or  $\alpha = \frac{\lambda_m}{\rho_c c_r}$ , for diffusion in a dry solid matrix or in a saturated porous medium, respectively. While this solution fits well the numerical time-dependent results, it has been slightly modified to fit the temperature profile at  $t = 10\,000$  s, as followed:

$$T = T_0 \operatorname{erfc}\left(\frac{x}{\sqrt{16\pi\alpha t}}\right) \quad (\text{A.5})$$

The analytical solution for an instantaneous heat pulse (pulse length = 1 sec) given below () has been tested, but do not fit properly the numerical results (see Fig. A.4):

$$T = \frac{q}{\rho c (4\pi\alpha t)^{\frac{3}{2}}} \exp\left(\frac{-x^2}{\sqrt{4\alpha t}}\right) \quad (\text{A.6})$$

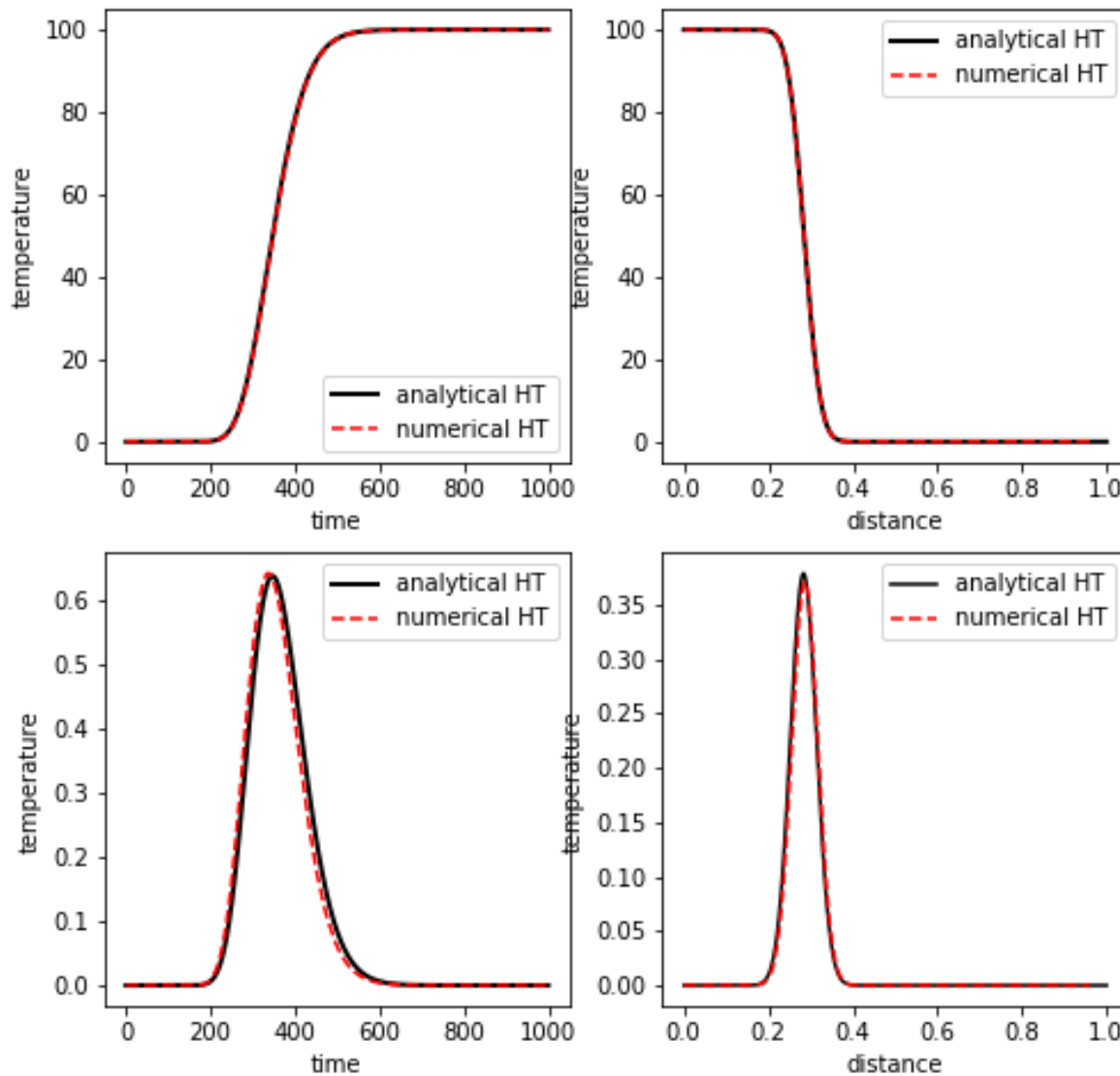


Figure A.3: Comparison of the analytical and numerical solutions for continuous heat and heat pulse injections with groundwater flow

## A.5 Figures Benchmarks Chapter 1

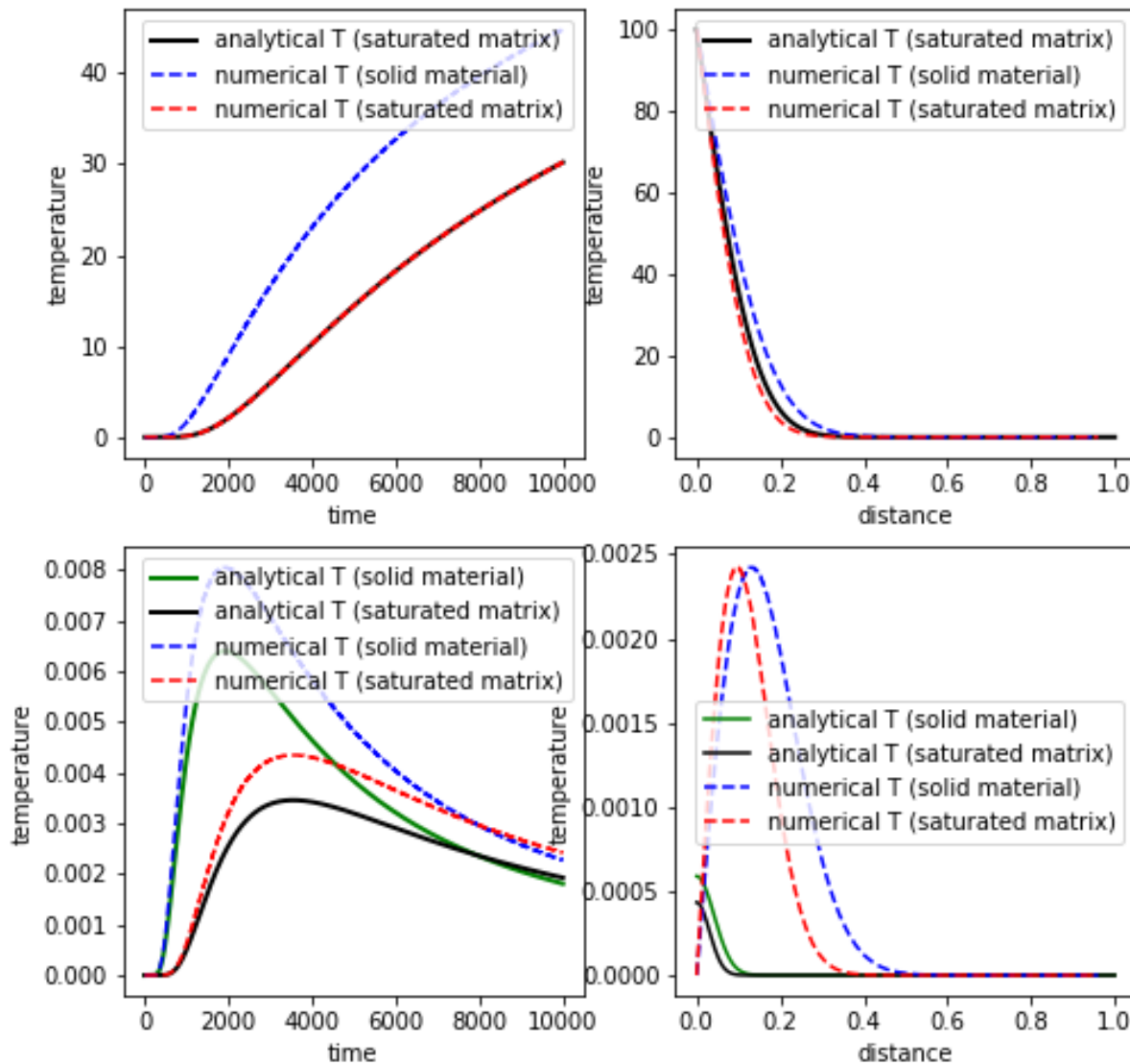


Figure A.4: Comparison of the analytical and numerical solutions for continuous heat and heat pulse injections without groundwater flow

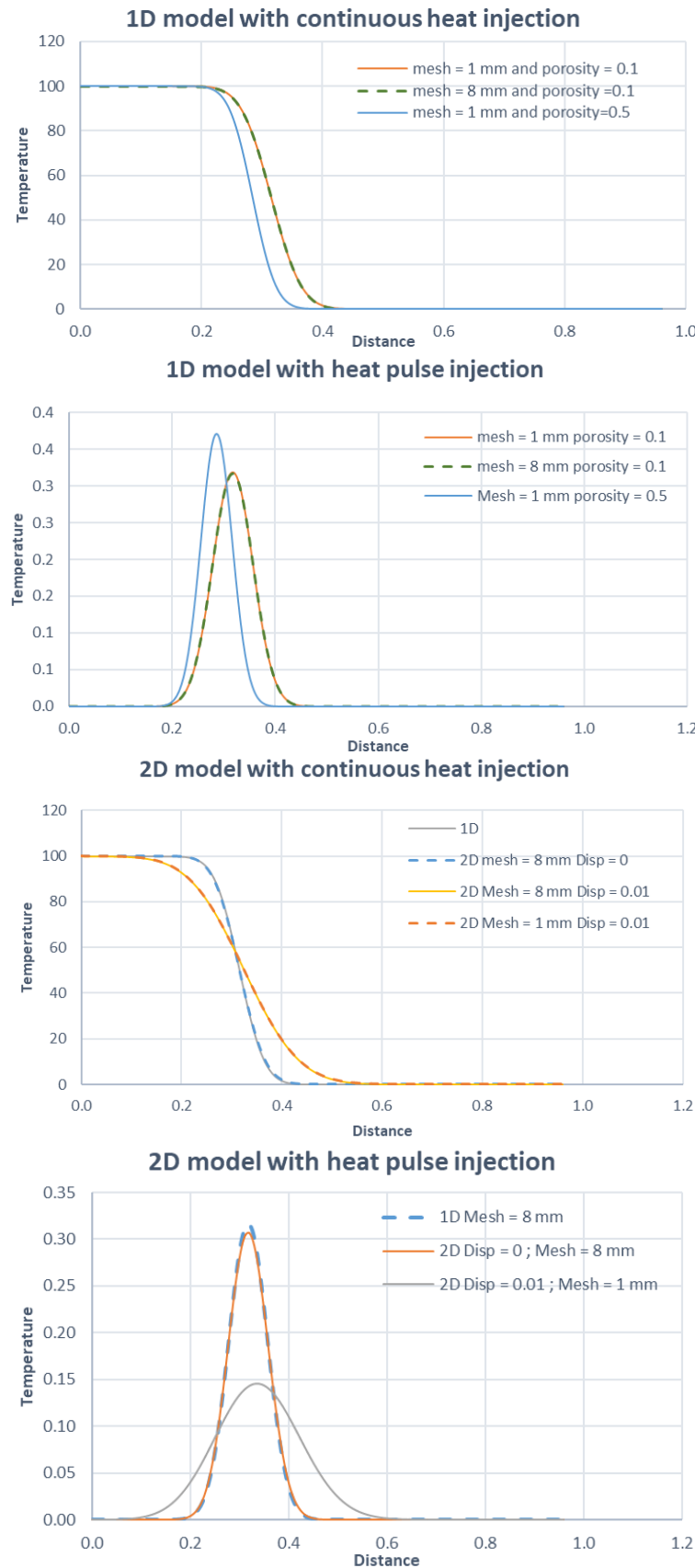
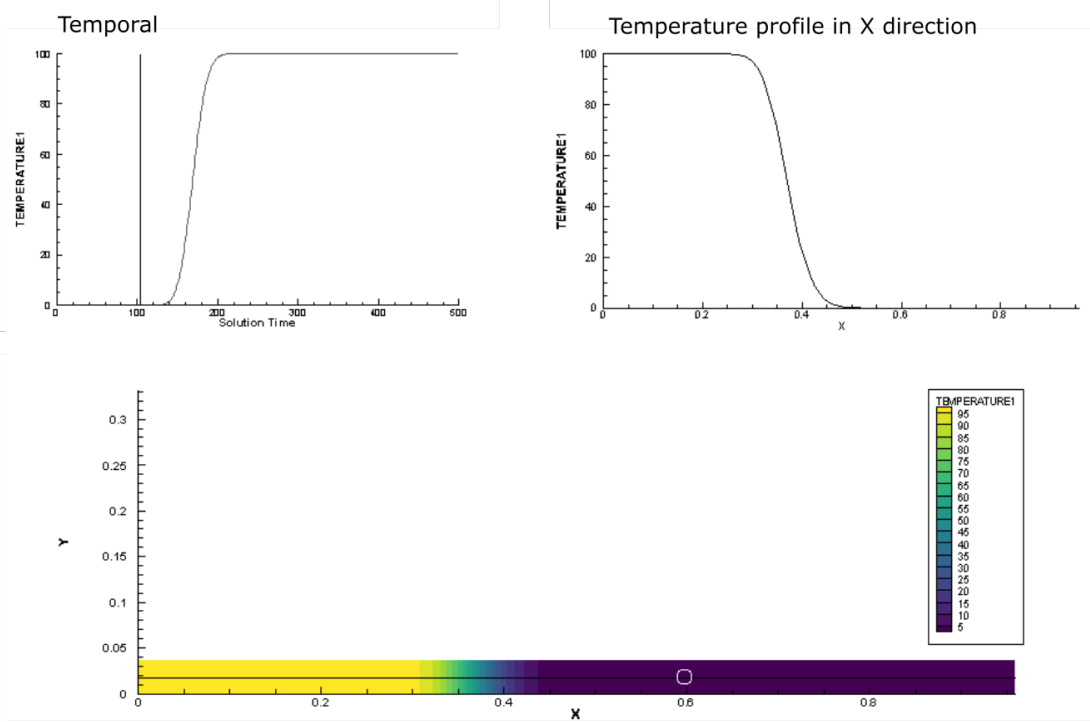


Figure A.5: Sensitivity analysis for porosity and mesh size for a 2D model with quadratic elements for the benchmarking of continuous and heat pulse injection

### Continuous Injection



### Heat pulse Injection

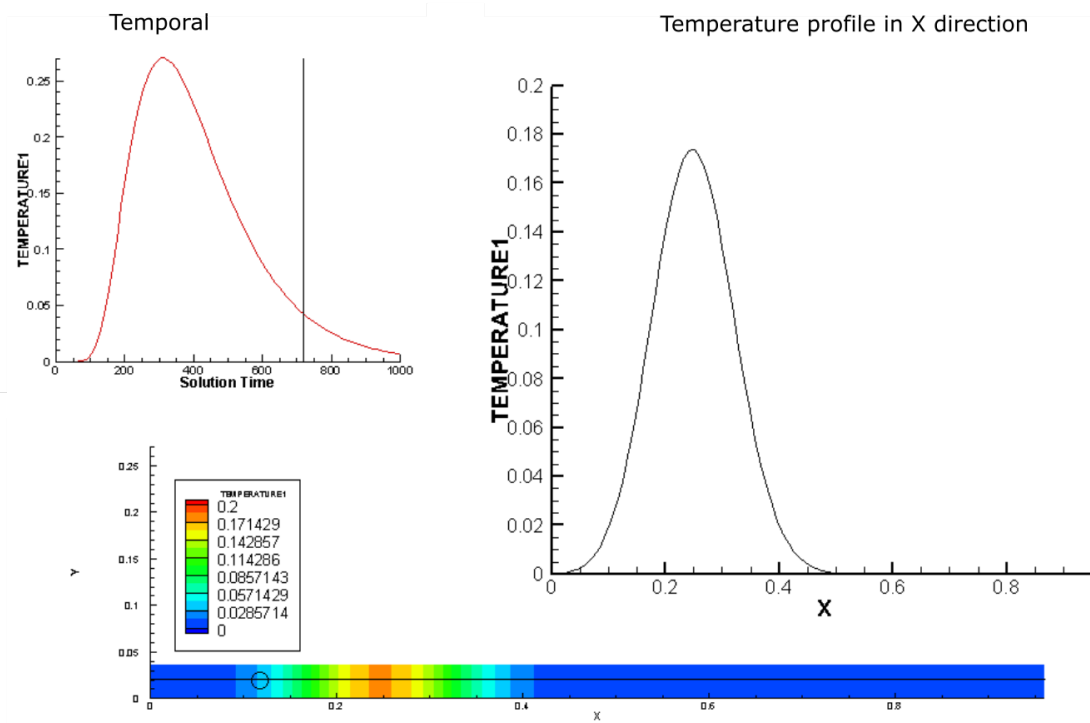


Figure A.6: Example of temperature distribution at  $t=1000s$  from numerical simulation for a) continuous heat injection in 2D domain, and b) heat pulse injection in 2D domain

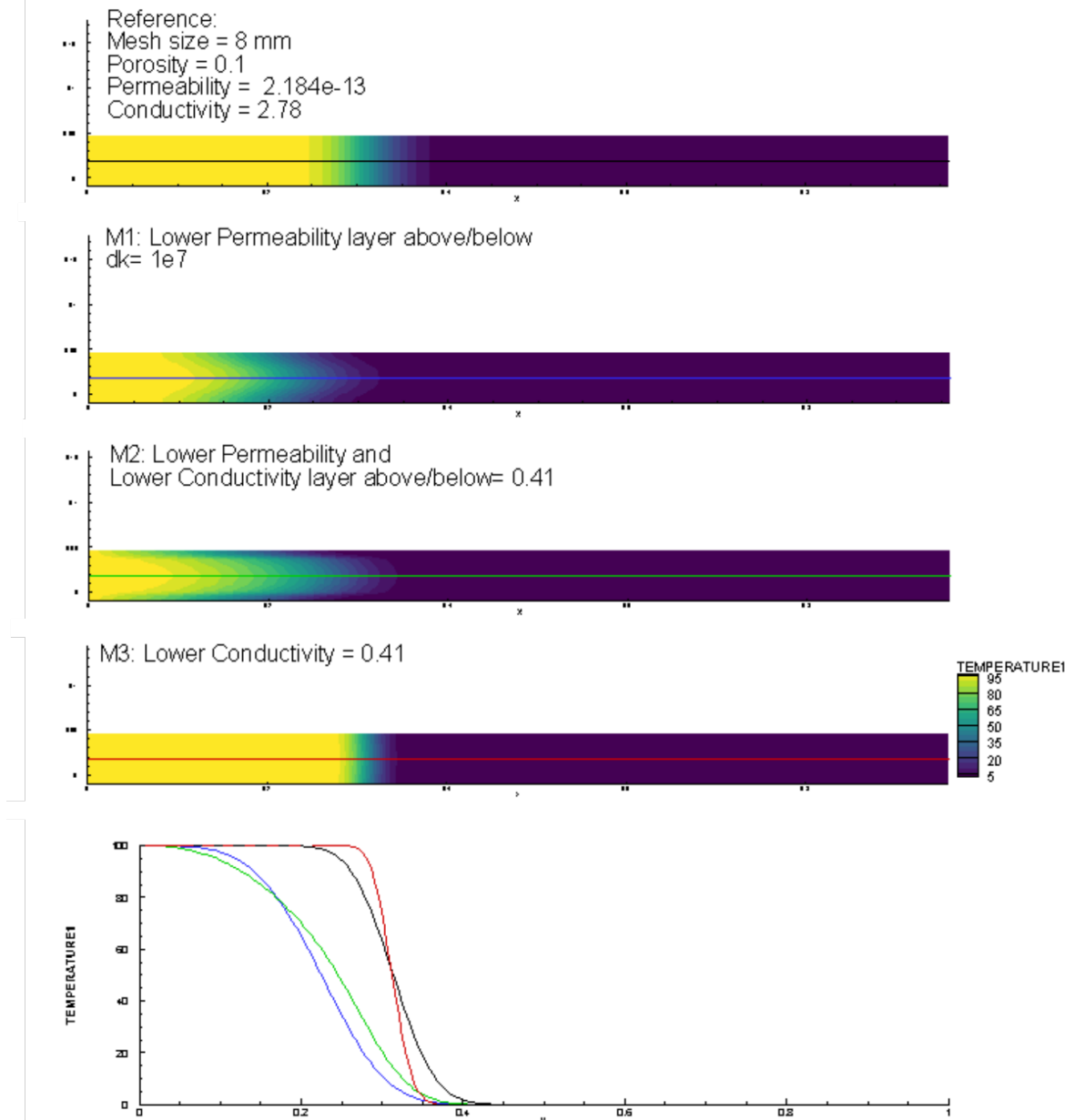


Figure A.7: Analysis of the effect of thin layers situated above/below the reservoir on the final temperature distribution, using different rock properties: a) Reference case with  $k = 2e-13$ ,  $K= 2.78$  and groundwater flow =  $2e-4m/s$  b) with layers of 0.1 m above below with lower permeability, c) with lower permeability and thermal conductivity, and d) for a low conductivity reservoir

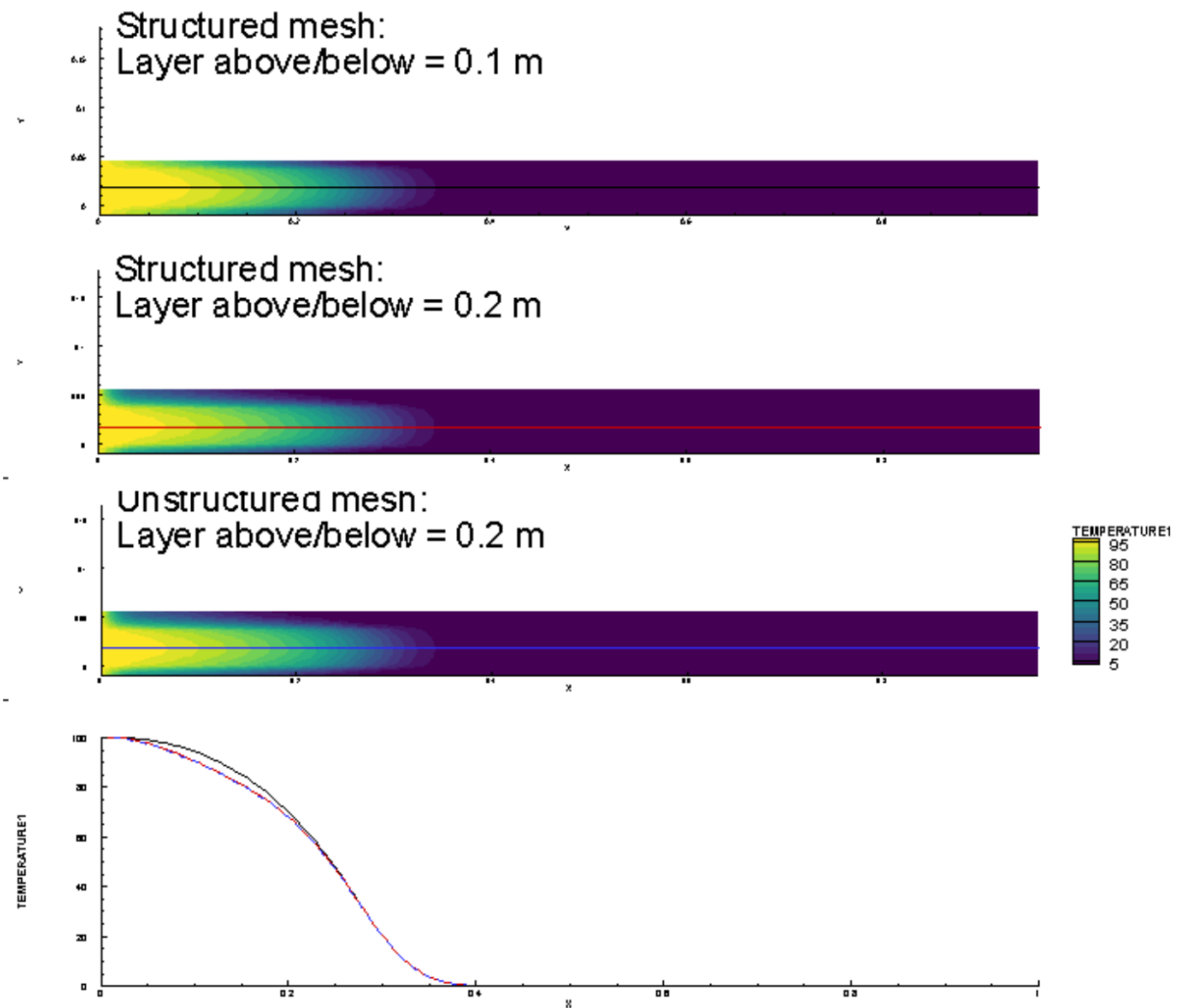


Figure A.8: Comparison of models for structure and unstructured mesh and different impermeable layer thicknesses

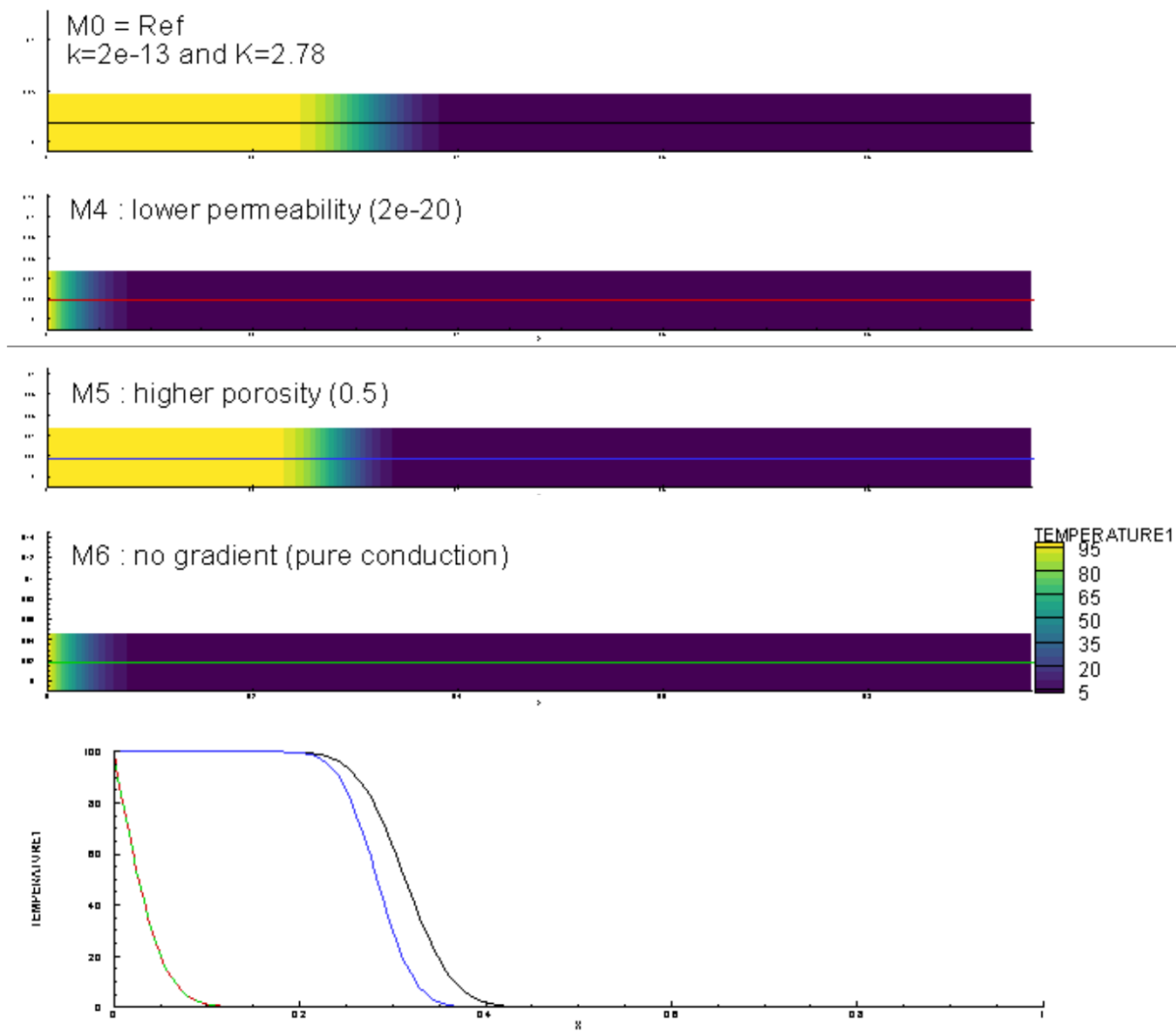


Figure A.9: Analysis of the effect of different rock properties on the final temperature distribution within the porous layer: a) Reference case with  $k = 2e-13$ ,  $K= 2.78$  and groundwater flow =  $2e-4\text{m/s}$  b) with lower permeability, c) with higher porosity (0.5) and d) with conduction only (no advecting groundwater)

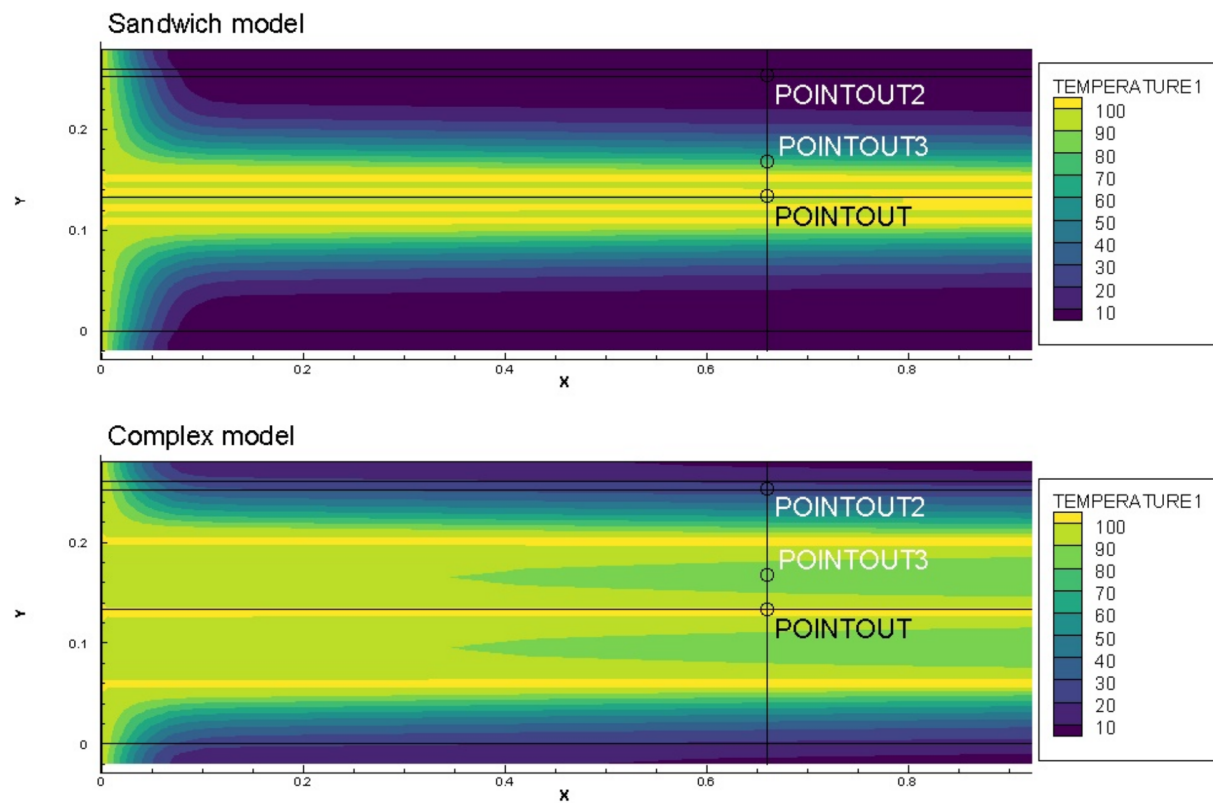


Figure A.10: Temperature distribution within the model complex and simplified "sandwich" model at  $t=1000s$

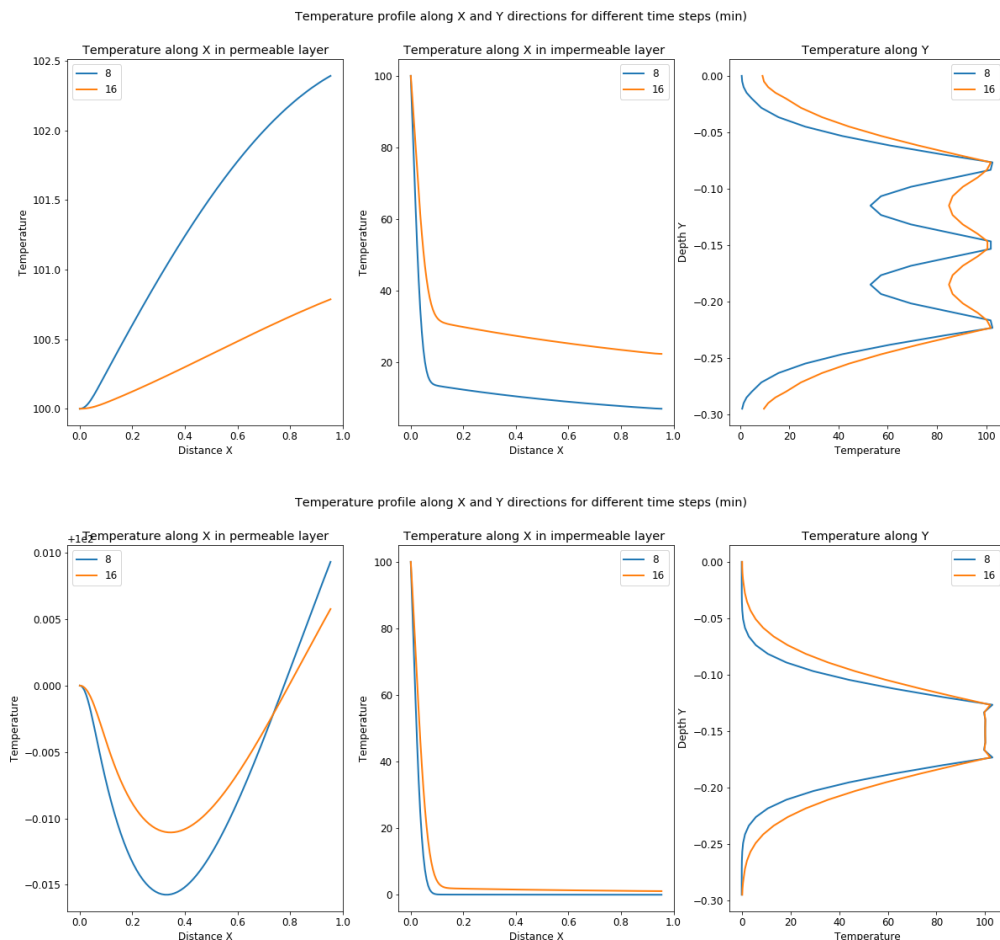


Figure A.11: Temperature profiles within the model complex and simplified "sandwich" model at t=1000s

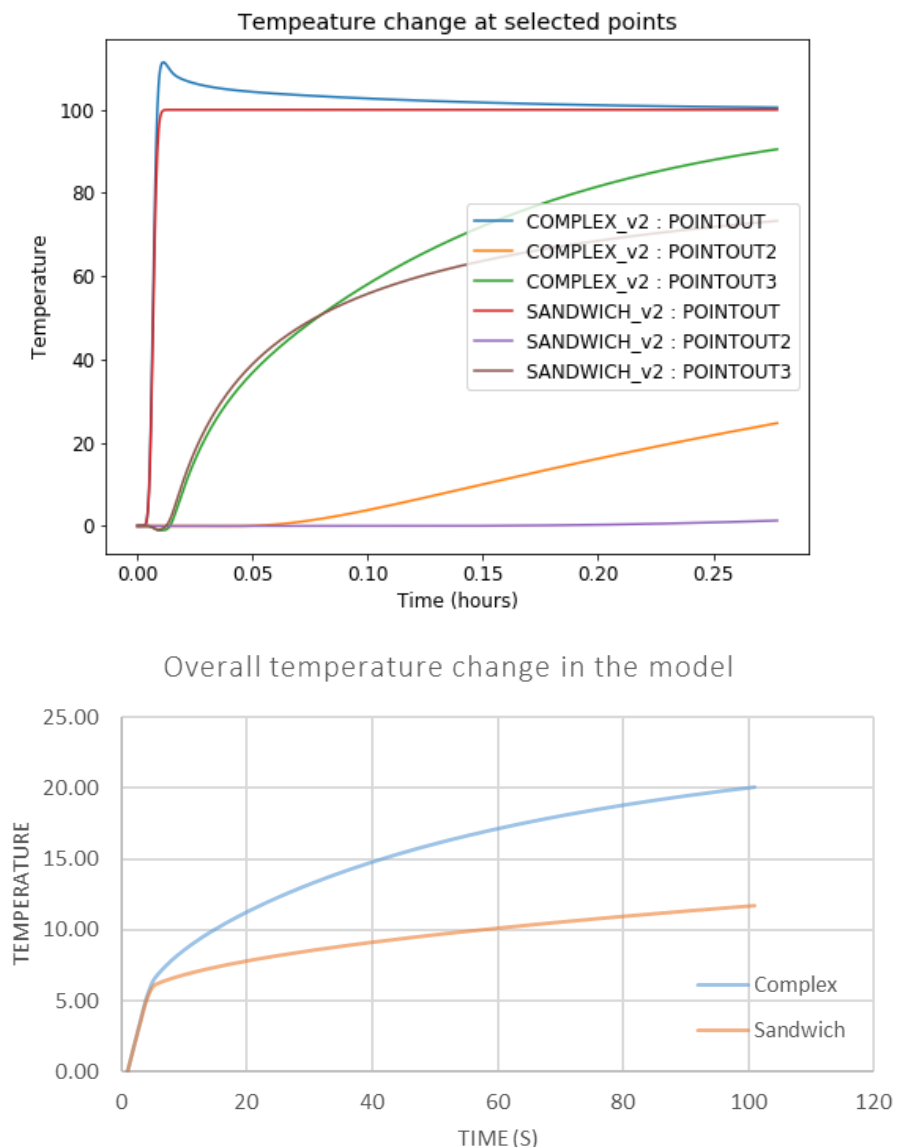


Figure A.12: a) Temperature change at the points shown in Fig. A.10 over time and b) Integrated temperature change over time for both models

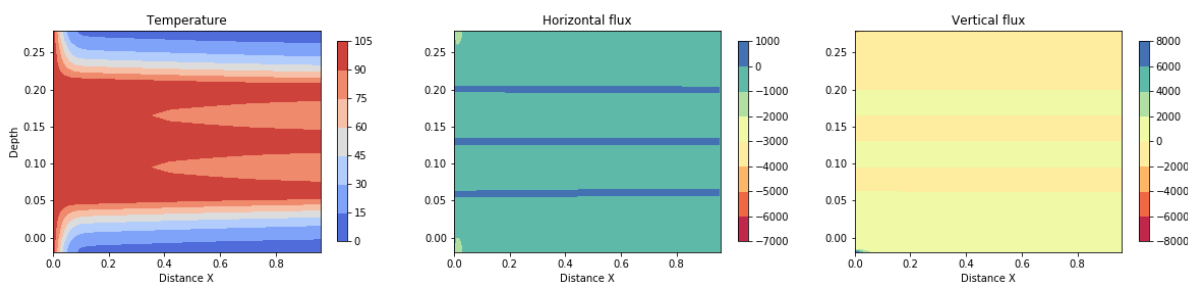


Figure A.13: Vertical and horizontal net heat fluxed within the complex model and temperature distribution at t=1000s

# References

- Adams, R. and Younger, P. (2001). A Strategy For Modeling Ground Water Rebound In Abandoned Deep Mine Systems. *Ground Water* [online]. 39.2, pp. 249–261. ISSN: 0017-467X, 1745-6584. DOI: 10.1111/j.1745-6584.2001.tb02306.x. [Accessed Nov. 26, 2019].
- Adams, R. and Parkin, G. (2002). Development of a coupled surface-groundwater-pipe network model for the sustainable management of karstic groundwater. *Environmental Geology*. 42.5, pp. 513–517.
- Allen, K., Backström, T. von, Kröger, D., and Kisters, A. (2014). Rock bed storage for solar thermal power plants: Rock characteristics, suitability, and availability. *Solar Energy Materials and Solar Cells* [online]. 126, pp. 170–183. ISSN: 09270248. DOI: 10.1016/j.solmat.2014.03.030. [Accessed Oct. 31, 2019].
- Anderson, E. (1951). *The dynamics of faulting and dyke formation with applications to Britain*.
- Anderson, R. and De Souza, E. (2017). Heat stress management in underground mines. *International Journal of Mining Science and Technology* [online]. 27.4, pp. 651–655. ISSN: 20952686. DOI: 10.1016/j.ijmst.2017.05.020. [Accessed Oct. 31, 2019].
- Andrés, C., Ordóñez, A., and Álvarez, R. (2017). Hydraulic and Thermal Modelling of an Underground Mining Reservoir. *Mine Water and the Environment* [online]. 36.1, pp. 24–33. ISSN: 1025-9112, 1616-1068. DOI: 10.1007/s10230-015-0365-1. [Accessed Oct. 31, 2019].
- Angelotti, A., Ly, F., and Zille, A. (2018). On the applicability of the moving line source theory to thermal response test under groundwater flow: considerations from real case studies. *Geothermal Energy* [online]. 6.1, p. 12. ISSN: 2195-9706. DOI: 10.1186/s40517-018-0098-z. [Accessed May 15, 2020].
- Bailey, M., Gandy, C., Watson, I., Wyatt, L., and Jarvis, A. (2016). Heat recovery potential of mine water treatment systems in Great Britain. *International Journal of Coal Geology* [online]. 164, pp. 77–84. ISSN: 01665162. DOI: 10.1016/j.coal.2016.03.007. [Accessed Oct. 31, 2019].
- Bamforth, S. (2014). *Bilston Glen: Scoping study*. URS Report.
- Banks, D., Fraga Pumar, A., and Watson, I. (2009). The operational performance of Scottish minewater-based ground source heat pump systems. *Quarterly Journal of Engineering Geology and Hydrogeology* [online]. 42.3, pp. 347–357. ISSN: 1470-9236, 2041-4803, 1470-9236. DOI: 10.1144/1470-9236/08-081. [Accessed Oct. 31, 2019].
- Banks, D. (2008). *An Introduction to Thermogeology: Ground Source Heating and Cooling*. Oxford, UK: Blackwell Publishing, Ltd. DOI: 10.1002/9781444302677. [Accessed Oct. 4, 2019].
- Banks, D. (2009). Thermogeological assessment of open-loop well-doublet schemes: a review and synthesis of analytical approaches. *Hydrogeology Journal*. 17.5, pp. 1149–1155.
- Banks, D., Skarphagen, H., Wiltshire, R., and Jessop, C. (2004). Heat pumps as a tool for energy recovery from mining wastes. *Geological Society, London, Special Publications* [online]. 236.1, pp. 499–513. ISSN: 0305-8719, 2041-4927. DOI: 10.1144/GSL.SP.2004.236.01.27. [Accessed Nov. 26, 2019].
- Banks, D., Skarphagen, H., Wiltshire, R., and Jessop, C. (2003). Mine water as a resource: space heating and cooling via use of heat pumps. *Land Contamination and Reclamation*. 11.2, pp. 191–198.

- Banks, D., Younger, P. L., Arnesen, R.-T., Iversen, E. R., and Banks, S. B. (1997). Mine-water chemistry: the good, the bad and the ugly. *Environmental Geology* [online]. 32.3, pp. 157–174. ISSN: 0943-0105, 1432-0495. DOI: 10.1007/s002540050204. [Accessed Nov. 26, 2019].
- Bao, T. and Liu, Z. (2019). Geothermal energy from flooded mines: Modeling of transient energy recovery with thermohaline stratification. *Energy Conversion and Management* [online]. 199, p. 111956. ISSN: 01968904. DOI: 10.1016/j.enconman.2019.111956. [Accessed Feb. 12, 2020].
- Barends, F. et al. (2010). “Complete solution for transient heat transport in porous media, following Lauwerier”. In: *SPE Annual Technical Conference and Exhibition*. Society of Petroleum Engineers.
- Barker, J., Downing, R., Gray, D., Findlay, J., Kellaway, G., Parker, R., and Rollin, K. (2000). Hydrogeothermal studies in the United Kingdom. *Quarterly Journal of Engineering Geology and Hydrogeology*. 33, pp. 41–58.
- Bauer, F., Michalowski, A., Kiedrowski, T., and Nolte, S. (2015). Heat accumulation in ultra-short pulsed scanning laser ablation of metals. *Optics Express* [online]. 23.2, p. 1035. ISSN: 1094-4087. DOI: 10.1364/OE.23.001035. [Accessed May 15, 2020].
- Beamish, D. and Busby, J. (2016). The Cornubian geothermal province: heat production and flow in SW England: estimates from boreholes and airborne gamma-ray measurements. *Geothermal Energy* [online]. 4.1, p. 4. ISSN: 2195-9706. DOI: 10.1186/s40517-016-0046-8. [Accessed Apr. 14, 2020].
- Beck, A. and Balling, N. (1988). Determination of virgin rock temperatures. In: *Handbook of terrestrial heat-flow density determination*. Springer, pp. 59–85.
- Beltrami, H., Matharoo, G. S., and Smerdon, J. E. (2015). Ground surface temperature and continental heat gain: uncertainties from underground. *Environmental Research Letters* [online]. 10.1, p. 014009. ISSN: 1748-9326. DOI: 10.1088/1748-9326/10/1/014009. [Accessed Dec. 2, 2019].
- Beltrami, H., Matharoo, G. S., Smerdon, J. E., Illanes, L., and Tarasov, L. (2017). Impacts of the Last Glacial Cycle on ground surface temperature reconstructions over the last millennium. *Geophysical Research Letters*. 44.1, pp. 355–364.
- Biglarian, H., Abbaspour, M., and Saidi, M. H. (2017). A numerical model for transient simulation of borehole heat exchangers. *Renewable Energy* [online]. 104, pp. 224–237. ISSN: 09601481. DOI: 10.1016/j.renene.2016.12.010. [Accessed May 15, 2020].
- Brereton, R., Browne, M., Cripps, A., Gebski, J., Bird, M., Halley, D., and McMillan, A. (1988). Glenrothes Borehole: Geological Well Completion Report. Investigation of the Geothermal Potential of the UK. *British Geological Survey, Keyworth*.
- Brown, G. and Mussett, A. (1995). Book Review: The inaccessible earth-and integrated view of its structure and composition/Chapman and Hall-1993. *Earth Moon and Planets*. 71, p. 175.
- Brown, M., Barley, B., and Wood, H. (2002). *Minewater treatment*. IWA publishing.
- Browne, M., Dean, M., Hall, H., McAdam, A., Monro, S., and Chisholm, J. (1999). *A lithostratigraphical framework for the Carboniferous rocks of the Midland Valley of Scotland*. Research report RR/99/07. British Geological Survey, p. 30.
- Burley, A., Edmunds M., W., and Gale, I. (1984). *Catalogue of geothermal data for the land area of the United Kingdom*. Second revision. British Geological Survey.

- Burnside, N., Banks, D., and Boyce, A. (2016). Sustainability of thermal energy production at the flooded mine workings of the former Caphouse Colliery, Yorkshire, United Kingdom. *International Journal of Coal Geology* [online]. 164, pp. 85–91. ISSN: 01665162. DOI: 10.1016/j.coal.2016.03.006. [Accessed Oct. 31, 2019].
- Busby, J., Kingdon, A., and Williams, J. (2011). The measured shallow temperature field in Britain. *Quarterly Journal of Engineering Geology and Hydrogeology* [online]. 44.3, pp. 373–387. ISSN: 1470-9236, 2041-4803. DOI: 10.1144/1470-9236/10-049. [Accessed May 15, 2020].
- Busby, J., Gillespie, M., and Kender, S. (2015). How hot are the Cairngorms? *Scottish Journal of Geology*. 51.2, pp. 105–115.
- Busby, J. (2019). Thermal conductivity and subsurface temperature data pertaining to the Glasgow Geothermal Energy Research Field Site (GGERFS).
- Cameron, I. and Stephenson, D. (1985). *British regional geology: The Midland Valley of Scotland*. Keyworth, Nottingham: British Geological Survey.
- Carslaw, H. S. and Jaeger, J. C. (1959). *Conduction of heat in solids*. Clarendon P.
- Cermak, J. (1990). Grain Boundary Diffusion of Co-60 in Nickel. *physica status solidi (a)* [online]. 117.2, pp. 387–393. DOI: 10.1002/pssa.2211170207.
- Chen, C., Shao, H., Naumov, D., Kong, Y., Tu, K., and Kolditz, O. (2019). Numerical investigation on the performance, sustainability, and efficiency of the deep borehole heat exchanger system for building heating. *Geothermal Energy* [online]. 7.1, p. 18. ISSN: 2195-9706. DOI: 10.1186/s40517-019-0133-8. [Accessed Apr. 14, 2020].
- Clean Growth - Transforming Heating* (2018). Department for Business, Energy & Industrial Strategy, p. 136.
- Dethlefsen, F., Beyer, C., Feeser, V., and Köber, R. (2016). Parameterizability of processes in subsurface energy and mass storage: Supported by a review of processes, codes, parameters, and a regional example: Schleswig-Holstein, Germany. *Environmental Earth Sciences* [online]. 75.10, p. 885. ISSN: 1866-6280, 1866-6299. DOI: 10.1007/s12665-016-5626-1. [Accessed Oct. 31, 2019].
- Diao, N., Li, Q., and Fang, Z. (2004). Heat transfer in ground heat exchangers with groundwater advection. *International Journal of Thermal Sciences* [online]. 43.12, pp. 1203–1211. ISSN: 12900729. DOI: 10.1016/j.ijthermalsci.2004.04.009. [Accessed May 15, 2020].
- Diersch, H.-J., Rühaak, W., Schätzl, P., Bauer, D., and Heidemann, W. (2010). “Numerical Modelling of Solar Heat Storage Using Large Arrays of Borehole Heat Exchangers”. In: Proceedings World Geothermal Congress 2010. Bali, Indonesia.
- Diersch, H.-J. (2005). *FEFLOW finite element subsurface flow and transport simulation system, reference manual*. WASY. Berlin: Institute for Water Resources Planning and Systems Research. 292 pp.
- Downing, R. and Gray, D. (1986). *Geothermal energy: the potential in the United Kingdom*. Vol. 143, pp. 499–507.
- Erol, S., Hashemi, M. A., and François, B. (2015). Analytical solution of discontinuous heat extraction for sustainability and recovery aspects of borehole heat exchangers. *International Journal of Thermal Sciences* [online]. 88, pp. 47–58. ISSN: 12900729. DOI: 10.1016/j.ijthermalsci.2014.09.007. [Accessed May 15, 2020].

- Esterhuizen, G. and Karacan, C. (2007). A METHODOLOGY FOR DETERMINING GOB PERMEABILITY DISTRIBUTIONS AND ITS APPLICATION TO RESERVOIR MODELING OF COAL MINE LONG-WALLS.
- Farr, G., Sadasivam, S., Manju, Watson, I., Thomas, H., and Tucker, D. (2016). Low enthalpy heat recovery potential from coal mine discharges in the South Wales Coalfield. *International Journal of Coal Geology* [online]. 164, pp. 92–103. ISSN: 01665162. DOI: 10.1016/j.coal.2016.05.008. [Accessed Oct. 31, 2019].
- Ferket, H., Laenen, B., and Van Tongeren, P. (2011). “Transforming flooded coal mines to large-scale geothermal and heat storage reservoirs: what can we expect?” In: *Mine water - Managing the Challenges*. IMWA Congress 2011. Aachen, Germany, pp. 171–175.
- Ghoreishi-Madiseh, S. A., Ghomshei, M. M., Hassani, F. P., and Abbasy, F. (2012). Sustainable heat extraction from abandoned mine tunnels: A numerical model. *J. Renewable Sustainable Energy*, p. 17.
- Ghoreishi-Madiseh, S., Hassani, F., and Abbasy, F. (2015). Numerical and experimental study of geothermal heat extraction from backfilled mine stopes. *Applied Thermal Engineering* [online]. 90, pp. 1119–1130. ISSN: 13594311. DOI: 10.1016/j.applthermaleng.2014.11.023. [Accessed Oct. 31, 2019].
- Gillespie, M., Crane, E., and Barron, H. (2013). *Study into the Potential for Deep Geothermal Energy in Scotland - Volume 2*. AEC/001/11. Scottish Government, p. 129.
- Gordon, D., Bolisetti, T., Ting, D. S.-K., and Reitsma, S. (2017). Short-term fluid temperature variations in either a coaxial or U-tube borehole heat exchanger. *Geothermics* [online]. 67, pp. 29–39. ISSN: 03756505. DOI: 10.1016/j.geothermics.2016.12.001. [Accessed Apr. 14, 2020].
- Gosnold, W., Majorowicz, J., Klenner, R., and Hauk, S. (2011). Implications of post-glacial warming for northern hemisphere heat flow. *Grc Transactions*. 35.GRC1029332.
- Guo, P., He, M., Zheng, L., and Zhang, N. (2017). A geothermal recycling system for cooling and heating in deep mines. *Applied Thermal Engineering* [online]. 116, pp. 833–839. ISSN: 13594311. DOI: 10.1016/j.applthermaleng.2017.01.116. [Accessed Oct. 31, 2019].
- Guo, P., Zheng, L., Sun, X., He, M., Wang, Y., and Shang, J. (2018). Sustainability evaluation model of geothermal resources in abandoned coal mine. *Applied Thermal Engineering* [online]. 144, pp. 804–811. ISSN: 13594311. DOI: 10.1016/j.applthermaleng.2018.06.070. [Accessed Oct. 31, 2019].
- Hall, A., Scott, J. A., and Shang, H. (2011). Geothermal energy recovery from underground mines. *Renewable and Sustainable Energy Reviews* [online]. 15.2, pp. 916–924. ISSN: 13640321. DOI: 10.1016/j.rser.2010.11.007. [Accessed Oct. 4, 2019].
- Hasterok, D., Gard, M., and Webb, J. (2018). On the radiogenic heat production of metamorphic, igneous, and sedimentary rocks. *Geoscience Frontiers* [online]. 9.6, pp. 1777–1794. ISSN: 16749871. DOI: 10.1016/j.gsf.2017.10.012. [Accessed Mar. 4, 2020].
- He, H., Dyck, M. F., Horton, R., Ren, T., Bristow, K. L., Lv, J., and Si, B. (2018). Development and Application of the Heat Pulse Method for Soil Physical Measurements. *Reviews of Geophysics* [online]. 56.4, pp. 567–620. ISSN: 87551209. DOI: 10.1029/2017RG000584. [Accessed May 15, 2020].
- Hein, P., Kolditz, O., Görke, U.-J., Bucher, A., and Shao, H. (2016). A numerical study on the sustainability and efficiency of borehole heat exchanger coupled ground source heat pump systems. *Applied Thermal En-*

- gineering [online]. 100, pp. 421–433. ISSN: 13594311. DOI: 10.1016/j.applthermaleng.2016.02.039. [Accessed May 15, 2020].
- Henton, M. (1974). HYDROGEOLOGICAL PROBLEMS ASSOCIATED WITH WASTE-DISPOSAL INTO ABANDONED COAL WORKINGS. *Water Services*. 78.944, pp. 349–352.
- Herrin, J. M. and Deming, D. (1996). Thermal conductivity of U.S. coals. *Journal of Geophysical Research: Solid Earth* [online]. 101.B11, pp. 25381–25386. DOI: 10.1029/96JB01884. eprint: <https://agupubs.onlinelibrary.wiley.com/doi/pdf/10.1029/96JB01884>.
- Hillis, R., Thomson, K., and Underhill, J. (1994). Quantification of Tertiary erosion in the Inner Moray Firth using sonic velocity data from the Chalk and the Kimmeridge Clay. *Marine and Petroleum Geology* [online]. 11.3, pp. 283–293. ISSN: 02648172. DOI: 10.1016/0264-8172(94)90050-7. [Accessed May 15, 2020].
- Jaupart, C. and Mareschal, J. (2005). Production from Heat Flow Data. *The Crust*. 3, pp. 65–84.
- Jessop (1995). Geothermal energy from old mines at Springhill Nova Scotia, Canada.
- Kolditz, O., Bauer, S., Bilke, L., Böttcher, N., Delfs, J. O., Fischer, T., Görke, U. J., Kalbacher, T., Kosakowski, G., McDermott, C. I., Park, C. H., Radu, F., Rink, K., Shao, H., Shao, H. B., Sun, F., Sun, Y. Y., Singh, A. K., Taron, J., Walther, M., Wang, W., Watanabe, N., Wu, Y., Xie, M., Xu, W., and Zehner, B. (2012). Open-GeoSys: an open-source initiative for numerical simulation of thermo-hydro-mechanical/chemical (THM/C) processes in porous media. *Environmental Earth Sciences* [online]. 67.2, pp. 589–599. ISSN: 1866-6280, 1866-6299. DOI: 10.1007/s12665-012-1546-x. [Accessed Oct. 31, 2019].
- Krige, L. J. (1939). Borehole temperatures in the Transvaal and Orange free state. *Proceedings of the Royal Society of London. Series A. Mathematical and Physical Sciences*. 173.955, pp. 450–474.
- Kruse, N. and Younger, P. (2009). Development of thermodynamically-based models for simulation of hydrogeochemical processes coupled to channel flow processes in abandoned underground mines. *Applied Geochemistry* [online]. 24.7, pp. 1301–1311. ISSN: 08832927. DOI: 10.1016/j.apgeochem.2009.04.003. [Accessed Oct. 31, 2019].
- Lauwerier, H. A. (1955). The transport of heat in an oil layer caused by the injection of hot fluid. *Applied Scientific Research, Section A* [online]. 5.2, pp. 145–150. ISSN: 1573-1987. DOI: 10.1007/BF03184614.
- Lazzari, S., Priarone, A., and Zanchini, E. (2010). Long-term performance of BHE (borehole heat exchanger) fields with negligible groundwater movement. *Energy*. 35.12, pp. 4966–4974.
- Le Brun, M., Hamm, V., Lopez, S., Ungemach, P., Antics, M., Ausseur, J. Y., Cordier, E., Giuglaris, E., Goblet, P., and Lalos, P. (2011). “Hydraulic and thermal impact modelling at the scale of the geothermal heating doublet in the Paris Basin, France”. In:
- Lee, M., Brown, G., Webb, P., Wheildon, J., and Rollin, K. (1987). Heat flow, heat production and thermo-tectonic setting in mainland UK. *Journal of the Geological Society, London*. 144, pp. 35–42.
- Lyu, Z., Song, X., Li, G., Hu, X., Shi, Y., and Xu, Z. (2017). Numerical analysis of characteristics of a single U-tube downhole heat exchanger in the borehole for geothermal wells. *Energy* [online]. 125, pp. 186–196. ISSN: 03605442. DOI: 10.1016/j.energy.2017.02.125. [Accessed Apr. 14, 2020].
- MacDonald M, A., Robins, N., Ball F, D., and O Dochartaigh E, B. (2005). An overview of groundwater in Scotland, p. 9.

- Majorowicz, J., Gosnold, W., Gray, D., Safanda, J., Klenner, R., and Unsworth, M. (2012). "Implications of Post-Glacial Warming for Northern Alberta Heat Flow— Correcting for the Underestimate of the Geothermal Potential". In: *Transactions - Geothermal Resources Council*. Vol. 36.
- Małolepszy, Z. (2003). "Low Temperature, Man-Made Geothermal Reservoirs in Abandoned Workings of Underground Mines". In: *Stanford Geothermal Workshop*. Standford.
- Marshall, D. (1958). Measurement of sap flow in conifers by heat transport. *Plant physiology*. 33.6, p. 385.
- Molina-Giraldo, N. (2011). "Heat transport modeling in shallow aquifers: The role of thermal dispersion in aquifers and heat conduction into confining layers". PhD thesis. Universität Tübingen.
- Monaghan, A. (2014). *The Carboniferous shales of the Midland Valley of Scotland: geology and resource estimation*. British Geological Survey for Department of Energy and Climate Change, London, UK. [Accessed Oct. 4, 2019].
- Monaghan, A. A. and Parrish, R. (Jan. 2006). Geochronology of Carboniferous–Permian magmatism in the Midland Valley of Scotland: implications for regional tectonomagmatic evolution and the numerical time scale. *Journal of the Geological Society* [online]. 163.1, pp. 15–28. ISSN: 0016-7649, 2041-479X. DOI: 10.1144/0016-764904-142. [Accessed May 15, 2020].
- Monzo, P. (2011). "Comparison of different Line Source Model approaches for analysis of Thermal Response Test in a U-pipe Borehole Heat Exchanger". PhD thesis. Stockholm. 113 pp.
- O'Dochartaigh, B., Macdonald, A., Fitzsimons, V., and Ward, R. (2015). *Scotland's aquifers and groundwater bodies*. Geological Survey Open Report OR/15/028. British Geological Survey, p. 76.
- O'Dochartaigh, B., Smedley, P., MacDonald, A., Darling, W., and Homoncik, S. (2011). Baseline Scotland: groundwater chemistry of the Carboniferous sedimentary aquifers of the Midland Valley.
- O'Neill, H. S. (2016). Heat-Producing Elements (HPEs). In: *Encyclopedia of Engineering Geology*. Ed. by P. Bobrowsky and B. Marker. Series Title: Encyclopedia of Earth Sciences Series. Cham: Springer International Publishing, pp. 1–6. ISBN: 978-3-319-12127-7. DOI: 10.1007/978-3-319-39193-9\_265-1. [Accessed Apr. 14, 2020].
- Ogata, A. and Banks, R. (1961). *A solution of the differential equation of longitudinal dispersion in porous media: fluid movement in earth materials*. US Government Printing Office.
- Owens, L. (2015). *Junckies Level*. The Coal Authority.
- Ozgener, O., Ozgener, L., and Tester, J. W. (2013). A practical approach to predict soil temperature variations for geothermal (ground) heat exchangers applications. *International Journal of Heat and Mass Transfer* [online]. 62, pp. 473–480. ISSN: 00179310. DOI: 10.1016/j.ijheatmasstransfer.2013.03.031. [Accessed May 15, 2020].
- Pruess, K. and Bodvarsson, G. (1983). *Thermal effects of reinjection in geothermal reservoirs with major vertical fractures*. Tech. rep. Lawrence Berkeley Lab., CA (USA).
- Radioti, G., Sartor, K., Charlier, R., Dewallef, P., and Nguyen, F. (2017). Effect of undisturbed ground temperature on the design of closed-loop geothermal systems: A case study in a semi-urban environment. *Applied Energy* [online]. 200, pp. 89–105. ISSN: 03062619. DOI: 10.1016/j.apenergy.2017.05.070. [Accessed May 15, 2020].

- Raymond, J. (2018). Colloquium 2016: Assessment of subsurface thermal conductivity for geothermal applications. *Canadian Geotechnical Journal* [online]. 55.9, pp. 1209–1229. ISSN: 0008-3674, 1208-6010. DOI: 10.1139/cgj-2017-0447. [Accessed Feb. 26, 2020].
- Raymond, J. and Therrien, R. (2008). Low-temperature geothermal potential of the flooded Gaspé Mines, Québec, Canada. *Geothermics* [online]. 37.2, pp. 189–210. ISSN: 03756505. DOI: 10.1016/j.geothermics.2007.10.001. [Accessed Oct. 4, 2019].
- Read, W., Browne, M., and Stephenson, B. (2002). The Geology of Scotland. *Geological Society*, pp. 251–300.
- Renz, A., Rühaak, W., Schätzl, P., and Diersch, H.-J. G. (2009). Numerical Modeling of Geothermal Use of Mine Water: Challenges and Examples. *Mine Water and the Environment* [online]. 28.1, pp. 2–14. ISSN: 1025-9112, 1616-1068. DOI: 10.1007/s10230-008-0063-3. [Accessed Oct. 31, 2019].
- Rippon, J., Read, W. A., and Park, R. G. (1996). The Ochil Fault and the Kincardine basin: key structures in the tectonic evolution of the Midland Valley of Scotland. *Journal of the Geological Society* [online]. 153.4, pp. 573–587. ISSN: 0016-7649, 2041-479X. DOI: 10.1144/gsjgs.153.4.0573. [Accessed May 15, 2020].
- Rivera, J. A., Blum, P., and Bayer, P. (2015). Analytical simulation of groundwater flow and land surface effects on thermal plumes of borehole heat exchangers. *Applied Energy* [online]. 146, pp. 421–433. ISSN: 03062619. DOI: 10.1016/j.apenergy.2015.02.035. [Accessed May 15, 2020].
- Robins, N. (1990). *Hydrogeology of Scotland*. *Hydrogeology of Scotland*. British Geological Survey. London. ISBN: 0 11 884468 7.
- Rollin, K. (1987). Catalogue of geothermal data for the land area of the United Kingdom. Third revision: April 1987. Investigation of the Geothermal Potential of the UK.
- Ruedas, T. (2017). Radioactive heat production of six geologically important nuclides: RADIOACTIVE HEAT PRODUCTION. *Geochemistry, Geophysics, Geosystems* [online]. 18.9, pp. 3530–3541. ISSN: 15252027. DOI: 10.1002/2017GC006997. [Accessed Apr. 14, 2020].
- Rybäck, K., Hokrick, R., and Eugster, W. (1988). Vertical Earth Heat Probe Measurements and Prospects in Switzerland. *Communication and Proceedings*, pp. 67–372.
- Rybäck, L., Megel, T., and Eugster, W. (2000). “AT WHAT TIME SCALE ARE GEOTHERMAL RESOURCES RENEWABLE?” In: World Geothermal Congress. Tohoku, Japan, pp. 867–872.
- Rybäck, L. (1986). Amount and significance of radioactive heat sources in sediments. In: *Thermal modelling in sedimentary basins*.
- Rybäck, L. and Eugster, W. J. (2010). Sustainability aspects of geothermal heat pump operation, with experience from Switzerland. *Geothermics* [online]. 39.4, pp. 365–369. ISSN: 03756505. DOI: 10.1016/j.geothermics.2010.08.002. [Accessed May 15, 2020].
- Saadi, M. S. and Gomri, R. (2017). Investigation of dynamic heat transfer process through coaxial heat exchangers in the ground. *International Journal of Hydrogen Energy* [online]. 42.28, pp. 18014–18027. ISSN: 03603199. DOI: 10.1016/j.ijhydene.2017.03.106. [Accessed Apr. 14, 2020].
- Saaltink, M., Domenech, C., Ayora, C., and Carrera, J. (2002). Modelling the oxidation of sulphides in an unsaturated soil. In: *Mine Water Hydrogeology and Geochemistry*. Youger, El & Robins, N.S. Vol. 198. Geological Society, London, Special Publications., pp. 187–204. ISBN: 61-73.0305-8719/02/15.00.

- Sandiford, M., McLaren, S., et al. (2006). *Thermo-mechanical controls on heat production distributions and the long-term evolution of the continents*. Citeseer.
- Sgambat, J. P., LaBella, E. A., and Roebuck, S. (1980). *Effects of Underground Coal Mining on Ground Water in the Eastern United States*. Vol. 1. Industrial Environmental Research Laboratory, Office of Research and ...
- Signorelli, S., Kohl, T., and Rybach, L. (2005). "Sustainability of Production from Borehole Heat Exchanger Fields". In: *Proceedings World Geothermal Congress*. World Geothermal Congress 2005. Antalya, Turkey.
- Singh, R. K. and Sharma, R. V. (2017). Numerical analysis for ground temperature variation. *Geothermal Energy* [online]. 5.1, p. 22. ISSN: 2195-9706. DOI: 10.1186/s40517-017-0082-z. [Accessed May 15, 2020].
- Stark, C. (2019). *Net Zero: The UK's contribution to stopping global warming*. Committee on Climate Change, p. 277.
- Stephenson, D., Loughlin, S., Millward, D., Waters, C., and Williamson, I. (2003). *Stephenson, D., Loughlin, S.C., Millward, D., Waters, C.N. & Williamson, I. T. 2003. Carboniferous and Permian Igneous Rocks of Great Britain North of the Variscan Front*. Vol. 27. : Geological Conservation Review Series. ISBN: 978-1-86107-497-3.
- Stylianou, I. I., Florides, G., Tassou, S., Tsoliakis, E., and Christodoulides, P. (2017). Methodology for estimating the ground heat absorption rate of Ground Heat Exchangers. *Energy* [online]. 127, pp. 258–270. ISSN: 03605442. DOI: 10.1016/j.energy.2017.03.070. [Accessed Apr. 14, 2020].
- Su, D., Diao, N., and Fang, Z. (2004). "An analytical solution of the temperature response in ground heat exchangers with groundwater advection". In: *6th International Symposium of Heat Transfer, Beijing*. Vol. 112. Citeseer.
- Sutton, M. G., Nutter, D. W., and Couvillion, R. J. (2003). A ground resistance for vertical bore heat exchangers with groundwater flow. *J. Energy Resour. Technol.* 125.3, pp. 183–189.
- Tammemagi, H. Y. and Wheildon, J. (1974). Terrestrial Heat Flow and Heat Generation in South-west England. *Geophysical Journal International* [online]. 38.1, pp. 83–94. ISSN: 0956-540X. DOI: 10.1111/j.1365-246X.1974.tb04110.x.
- Todd, F., McDermott, C., Harris, A. F., Bond, A., and Gilfillan, S. (2019). Coupled hydraulic and mechanical model of surface uplift due to mine water rebound: implications for mine water heating and cooling schemes. *Scottish Journal of Geology* [online], sjg2018-028. ISSN: 0036-9276, 2041-4951. DOI: 10.1144/sjg2018-028. [Accessed Oct. 13, 2019].
- Trewin, N. (2002). The Geology of Scotland, 4th edn, Geological Society, London.
- Turcotte, D. L. and Schubert, G. (2002). *Geodynamics*. Cambridge university press.
- Tye-Gingras, M. and Gosselin, L. (2014). Generic ground response functions for ground exchangers in the presence of groundwater flow. *Renewable energy*. 72, pp. 354–366.
- Underhill, J. R., Monaghan, A. A., and Browne, M. A. (2008). Controls on structural styles, basin development and petroleum prospectivity in the Midland Valley of Scotland. *Marine and Petroleum Geology* [online]. 25.10, pp. 1000–1022. ISSN: 02648172. DOI: 10.1016/j.marpetgeo.2007.12.002. [Accessed Oct. 4, 2019].

- Upton, B. G. J., Stephenson, D., Smedley, P. M., Wallis, S. M., and Fitton, J. G. (2004). Carboniferous and Permian magmatism in Scotland. *Geological Society, London, Special Publications* [online]. 223.1, pp. 195–218. ISSN: 0305-8719, 2041-4927. DOI: 10.1144/GSL.SP.2004.223.01.09. [Accessed May 15, 2020].
- Vandegehuchte, M. W. and Steppe, K. (2012). Use of the correct heat conduction–convection equation as basis for heat-pulse sap flow methods in anisotropic wood. *Journal of Experimental Botany* [online]. 63.8, pp. 2833–2839. ISSN: 1460-2431, 0022-0957. DOI: 10.1093/jxb/ers041. [Accessed May 15, 2020].
- Vilà, M., Fernández, M., and Jiménez-Munt, I. (2010). Radiogenic heat production variability of some common lithological groups and its significance to lithospheric thermal modeling. *Tectonophysics* [online]. 490.3, pp. 152–164. ISSN: 00401951. DOI: 10.1016/j.tecto.2010.05.003. [Accessed Apr. 14, 2020].
- Vincent, C. J., Rowley, W. J., and Monaghan, A. A. (2010). Thermal and burial history modelling in the Midlothian-Leven syncline in the Midland Valley of Scotland using BasinMod and HotPot. *Scottish Journal of Geology* [online]. 46.2, pp. 125–142. ISSN: 0036-9276, 2041-4951. DOI: 10.1144/0036-9276/01-376. [Accessed Apr. 14, 2020].
- Wang, H., Yang, B., Xie, J., and Qi, C. (2013). Thermal performance of borehole heat exchangers in different aquifers: a case study from Shouguang. *International Journal of Low-Carbon Technologies* [online]. 8.4, pp. 253–259. ISSN: 1748-1317. DOI: 10.1093/ijlct/cts043. [Accessed May 15, 2020].
- Webb, P., Lee, M., and Brown, G. (1987). HEAT FLOW - HEAT PRODUCTION RELATIONSHIPS IN THE UK AND THE VERTICAL DISTRIBUTION OF HEAT PRODUCTION IN GRANITE BATHOLITHS. *Geophysical Research Letters*. 14.3, pp. 279–282.
- Westaway, R. and Younger, P. L. (2013). Accounting for palaeoclimate and topography: A rigorous approach to correction of the British geothermal dataset. *Geothermics* [online]. 48, pp. 31–51. ISSN: 03756505. DOI: 10.1016/j.geothermics.2013.03.009. [Accessed Apr. 14, 2020].
- Wheildon, J. and Rollin, K. (1986). *Heat Flow. 8-20 in Geothermal Energy: the Potential in the United Kingdom*. London: British Geological Survey.
- Whitworth, K. (2002). The monitoring and modelling of mine water recovery in UK coalfields. In: *Mine Water Hydrogeology and Geochemistry*. Youger, El & Robins, N.S. Geological Society, London, Special Publications., p. 198. ISBN: 61-73.0305-8719/02/15.00.
- Wolkersdorfer, C. (2008). *Water Management at Abandoned Flooded Underground Mines*. 465 pp. ISBN: 978-3-540-77330-6.
- Younger, P. (2001). Mine water pollution in Scotland: nature, extent and preventative strategies. 265, pp. 309–326.
- Younger, P. L. (2004). ‘Making water’: the hydrogeological adventures of Britain’s early mining engineers. *Geological Society, London, Special Publications* [online]. 225.1, pp. 121–157. ISSN: 0305-8719, 2041-4927. DOI: 10.1144/GSL.SP.2004.225.01.09. [Accessed Nov. 26, 2019].
- Younger, P. L., Banwart, S. A., and Hedin, R. S. (2002). *Mine water: hydrology, pollution, remediation*. Vol. 5. Springer Science & Business Media.
- Younger, P. and Adams, R. (1999). Predicting mine water rebound.
- Zanchini, E., Lazzari, S., and Priarone, A. (2010). Improving the thermal performance of coaxial borehole heat exchangers. *Energy* [online]. 35, pp. 657–666. DOI: 10.1016/j.energy.2009.10.038.

- Zeng, H. Y., Diao, N. R., and Fang, Z. H. (2002). A finite line-source model for boreholes in geothermal heat exchangers. *Heat Transfer Asian Research* [online]. 31.7. 2D unsteady state analytical solution and a semi analytical solution: Establishes the transient response at any point in the ground for the radial and the axial coordinates subject to a constant line heat source (FLS) in the rod., pp. 558–567. ISSN: 1099-2871, 1523-1496. DOI: 10.1002/htj.10057. [Accessed Apr. 27, 2020].
- Zhai, X., Wang, G., Wu, J., and Bi, Y. (2019). Goaf Compaction Evaluation Based on Integrity and Permeability Measurement of the Overburden Strata. *Tehnickički vjesnik*. 26.2, pp. 510–517.
- Zhang, C., Tu, S., Zhang, L., Bai, Q., Yuan, Y., and Wang, F. (2016). A methodology for determining the evolution law of gob permeability and its distributions in longwall coal mines. *Journal of Geophysics and Engineering* [online]. 13.2, pp. 181–193. ISSN: 1742-2132, 1742-2140. DOI: 10.1088/1742-2132/13/2/181. [Accessed May 15, 2020].
- Zhao, Y., Ma, Z., and Pang, Z. (2020). A Fast Simulation Approach to the Thermal Recovery Characteristics of Deep Borehole Heat Exchanger after Heat Extraction. *Sustainability*. 12.5, p. 2021.